Universitat Autònoma de Barcelona

Interferometric Biosensors for Rapid Identification of Nosocomial infections

Jesús Manuel Maldonado Vázquez

Universitat Autònoma de Barcelona

Doctorat en Biotecnologia

Departament de Genètica i Microbiologia-Facultat de Biociéncies

Interferometric Biosensors for Rapid Identification of Nosocomial infections

Doctoral thesis-2017

Jesús Manuel Maldonado Vázquez

Author

Prof. Laura M. Lechuga

Director

Dr. Ana Bélen González Guerrero

Co-Director

Prof. Antoni Villaverde

Tutor

CSIC Consejo Superior de Investigaciones Científicas

ICN2 Institut Català de Nanociència i Nanotecnologia — Excelencia Severo Ochoa

To my mom,

Abstract

This doctoral Thesis is focusing on the development of a novel optical biosensor as an alternative technique for the identification of nosocomial infections in a faster way. This new tool will also facilitate the finding of the most effective treatment for each patient, reduce the nonspecific use of broad-spectrum antimicrobial drugs, and facilitate new antibiotic treatments. We propose the use of a novel nanophotonic sensor based on an interferometric transducer device, the Bimodal Waveguide device (BiMW) for the rapid, specific, highly sensitive and direct analysis of different pathogens associated to nosocomial infections and their multidrug resistant. First, we assessed and optimized different biofunctionalization strategies for an efficient immobilization of the required biorecognition receptors, which ensure a highly sensitive bacterial detection with enough selectivity and reproducibility, particularly suitable for the direct detection in complex matrices, such as urine and ascitic fluid. The optimized strategies were employed for the identification of various nosocomial pathogens such as *Bacillus cereus, Escherichia coli,* and *Pseudomonas aeruginosa* using antibodies as biorecognition elements. The detection of *Escherichia coli* was done in human ascitic fluid. Finally, the BiMW biosensor was employed to identify the multidrug-resistant bacteria such as: i) the identification of methicillin-resistant *Staphylococcus aureus* (MRSA) using a specific aptamer, which is able to discriminate among a susceptible one to antibiotic and a multidrug-resistant Staphylococcus, and (ii) the ultra-sensitive detection of multidrug-resistant *E. coli* genes without PCR amplification.

This Thesis takes advantage of the knowledge in photonics biosensors and bioanalytical methods in our Group in order to develop a powerful tool for the direct and effective identification of nosocomial pathogens and their antibiotic-resistance in a rapid and label-free scheme.

RESUMEN

Esta tesis doctoral se centra en el desarrollo de un nuevo biosensor óptico como una técnica alternativa para la identificación de infecciones nosocomiales con el fin de determinar el tratamiento más eficaz y reducir el uso inespecífico de fármacos antimicrobianos de amplio espectro. Proponemos el uso de un nuevo sensor nanofótonico basado en un dispositivo interferométrico, el biosensor de guías de onda bimodales (BiMW) para un análisis rápido, específico, directo y altamente sensible de los diferentes patógenos asociados a infecciones nosocomiales y su resistencia a múltiples fármacos. En primer lugar, se evaluaron y optimizaron diferentes estrategias de biofuncionalización para conseguir una inmovilización eficiente de los elementos de bioreconocimiento que aseguran una detección bacteriana altamente sensible con suficiente selectividad y reproducibilidad, particularmente para la detección directa en matrices complejas tales como orina y líquido ascítico. Posteriormente, las estrategias optimizadas se utilizaron para la identificación de diversos patógenos nosocomiales como *Bacillus cereus*, *Escherichia coli* y *Pseudomonas aeruginosa* utilizando anticuerpos como elementos de bioreconocimiento. La detección de *Escherichia coli* se realizó en una matriz compleja como es el líquido ascítico humano. Finalmente, el biosensor BiMW se empleó para identificar bacterias resistentes a múltiples fármacos como: i) la identificación de S*taphylococcus aureus* resistente a meticilina (MRSA) usando un aptámero, que es capaz de discriminar entre un *Staphylococcus* susceptible a antibióticos y un *Staphylococcus* multirresistente y (ii) la detección ultra sensible de genes de *E. coli* resistentes a múltiples fármacos, sin la necesidad de una previa amplificación por PCR.

En general, esta tesis aprovecha los conocimientos en biosensores fotónicos y en métodos bioanalíticos de nuestro Grupo de investigación para desarrollar una poderosa herramienta que permita la identificación directa y efectiva de patógenos nosocomiales y su resistencia a antibióticos.

Agradecimientos

Quisiera expresar mi agradecimiento a todos los que con su ayuda han hecho posible logar la culminación de este trabajo. Donde lo más valioso de esta etapa mi vida fue conocer y coincidir con muchos de ustedes.

Primero me gustaría agradecer sinceramente a mi Directora de Tesis, Prof. Laura Lechuga, sus conocimientos, su manera de trabajar, su motivación y su paciencia han sido fundamentales para mi formación como investigador. También agradecer la confianza que depositó en mí para la realización de este proyecto. Asimismo a mi Co-directora Ana Belén por el ímpetu que brindó al trabajo con su asesoría y consejos. A mi Tutor Toni Villaverde que cada seguimiento me daba una gran motivación para continuar.

A todos los miembros del nanoB2A que han sido grandes y maravilloso conmigo, y l verdad no sé por dónde empezar. A David Fari y Bert que fueron unos grandes colegas de despacho. A mi chavas preferidas Stefania y Rebeca por la gran amistad que me han dado desde que las conocí y que me llevo para siempre. También quiero agradecer a Mar, Maricarmen, Carlos, Joel, María, Sam, Sonia, Nuria, Jessica, Toni y Silvia por cada conversación y momentos que viví durante estos años. Cristina (parce), Patri y Cristina Kurachi fueron grandes momentos los que viví con ustedes en el doctorado desde tomar el café hasta cada divertida conversación que teníamos en los labs, muchas gracias por su amistad y apoyo. A Borja y Ester por esa confianza y amistad que mostraron desde mí llegada a Barcelona. A family Ros (Xavi, Pol y la Ana amiga) por su gran muestra de amistad y cariño durante estos años. Blanca!!!!!!!!, muchas gracias por ser una gran amiga todo este tiempo y dejarme conocer a la Blanca pambolera que me sacaba cada risa, siempre recordaré las visitas al camp nou.

Por otro parte, este proyecto no hubiera alcanzado estas metras sin la colaboración de las personas del grupo de Microbiología del Vall d'Hebron. Gracias a JuanJo y Nuria, quienes apoyaron para la evolución de este trabajo.

Marisol, Rafael, Aldo y Lalo fueron unos grandes amigos y me ha dado mucho gusto conocerlos, compartir muchas experiencias, viajes, cenas y salidas. Fueron un pilar importante en mi adaptación en Barcelona y muchas gracias por estar ahí en esos momentos tantos buenos como complicados. Seguro que en algún momento nos reuniremos. Los quiero mucho, amigos.

A los que considero mis *"Brotha from anotha motha"*: Chia!!!!!!!!to (Daniel), Adrián (astu), Jhonattan (no te metas a lo hondo), Santos, Alex (chamo), Firehun, Jens, Crispin, Jerry, Oscar suchi, y Luis (portuga). Conocerlos fue una de las cosas más importante que me pudo haber sucedido durante estos años de doctorado. Cada risa, cada momento, viaje, fiestas y sobre todo esa amistad que me llevaré para siempre. A las chicas de Cerdanyola Crew (Momo, Tucky y Rubia), son lo más grande que pudo haber dado Cerdanyola y conocerlas fue de lo mejor, por cada momento vivido durante este tiempo.

A mi comunidad latina: Abraham, Hidalgo, Paola, Gaby!!!!!!, Paty Oscar (parcero), Melissa y Adrián, por la gran suerte que tuve de coincidir con ustedes estos años, han sido grandes compañeros y amigos. La peña del fútbol en el SAF: Marcos, Fran, Carlos, Daniel, Nano, Cristóbal y Jo, son unos cracks, me la pase de maravilla en cada partido con ustedes. Mis roommies preferidas: Cristina y Laura fue un gran temporada por ese ático en el cual reíamos a morir, las echaré de menos.

Gracias a todos los chico del ICN y visitantes de nuestro grupo, todos de alguna manera han compartido un momento conmigo: Giulia, Carlita, Lulia, Aron, Albert (Paco) y Rémi.

Y finalmente quiero dedicar este trabajo a mi familia, en especial a mi Madre Rosa, quien me ha brindado todo su apoyo en todos los aspectos posibles. Gracias También a mis hermanos David y Pepe, por apoyarme y recibirme con cariño. Y cada miembro de mi familia mi abue Mane, tía Magui, mi peque Adriel, Suany y cada uno de ellos que de alguna u otra manera he recibido su apoyo y confianza, por su paciencia en mis momentos de estrés, por escucharme cuando tenía tantas cosas que contar y mil gracias por soportarme en toda esta locura en la cual me dedico, los amo.

Gracias a todos.

Contents

List of Figures

List of tables

Abbreviations and Acronyms

1-ethyl-3(3-dimethylaminopropyl) carbodiimide hydrochloride	EDC
2-N-morpholino ethanesulfonic acid	MES
3-aminopropyltriehoxy silane	APTES
3-glycidyloxypropyltrimethoxysilane	GOPTS
(3-mercaptopropyl) trimethoxysilane	MPTMS
β-Lactamase	bla
Antimicrobial Peptide	AMPs
Atomic Force Microscope	AFM
Bimodal waveguide interferometer	BiMW
Bovine serum albumin	BSA
Caboxyethylsilanetriol sodium salt	CTES
Colony-forming units	CFU
Copolymer poly-(L-lysine) graft-PEG	PLL-PEG
Deoxyribonucleic acid	DNA
Enzyme-linked immunosorbent assay	ELISA
Ethylenediaminetetra acetic acid	EDTA
Fluorescein isothiocyanate bovine serum albumin	FICT-BSA
Healthcare-associated infections	HAI
Human Growth Hormone	hGH
Isocyanatepropyltriethoxysilane	ICPTS
Limit of detection	LOD
Methicillin-resistant Staphylococcus aureus	MRSA
N-hydroxysuccinimide	NHS
N, N-Dimethylformamide	DMF
Penicillin-binding proteins	PBPs

Phosphate buffer saline	PBS
Polydimethylsiloxane	PDMS
Polymerase chain reaction	PCR
P-phenylenediisothiocynate	PDITC
Ribonucleic acid	RNA
Quartz crystal microbalance	QCM
Spontaneous bacterial peritonitis	SBP
Standard Deviation	SD
Surface plasmon resonance	SPR
Thyroid stimulating hormone	hTSH
Urinary tract infections	UTI
X-ray photoelectron spectroscopy	XPS

Chapter 1

General Introduction

Chapter I

Abstract: this chapter provides a background of nosocomial infections and their multidrug resistant. After a brief review of conventional methods and their limitations to detect bacteria, biosensor technologies in general and interferometric biosensors in particular, are described. Finally, we discuss the function of biorecognition elements in biosensor devices.

1. Introduction

1.1. Nosocomial infections

The term nosocomial infection (From Greek meaning: nosos=disease and komien= to care for) refers to an infection that develops at least 48 hours after the patient is admitted to a hospital. They are also known as hospital-acquired or healthcare-associated infections (HAI) [1], referring to the type of infections caused by a prolonged stay at the hospital and it accounts for a major risk factor for serious health issues leading to death [2]. Studies show that in Europe, 5-10% of all hospitalizations results in nosocomial infections, with the highest rates in surgical and intensive care units [3]. This is approximately 4.1 million patients and that 37 000 of these patients die as a direct consequence of their infection. In Spain, the numbers of patients that acquire HAI is 300 000 patients per year. These infections contribute to serious events including increased length stay at the hospital, additional treatment with antibiotics and susceptibility to further infections, developing sepsis, the requirement of advanced medical interventions and disability. Death nosocomial infections also entail a strong economic impact, and are estimated $ 9 billion worldwide [4]. These costs are mainly due to the prolonged stay of infected patients at the hospital and the lack of efficient diagnostics tools and treatment.

Nosocomial infection are classified in 9 types including the ones related to urinary tract infections (UTI), surgical and soft tissue infections, gastroenteritis, meningitis, chest infections, hospital-acquired tuberculosis and legionnaire's disease,

nosocomial viral infections, and diarrhea [5]. Despite most of the infections are superficial and easily treatable, the deeper infections may be fatal, particularly when they affect bones, brain, prosthesis or a transplanted organ. *Staphylococci* (*S. aureus*, including MRSA) causes almost 50% of infections; most of the remainder infections are caused by Gram-negative bacteria, including *E. coli* and *Pseudomonas*.

1.1.1. Agents of nosocomial infection

Most hospital-acquired infections are caused by pathogens common in general population. Bacteria are responsible for about 90% infections, whereas viruses, fungi and parasites are less contributing [6]. The bacteria that are often involved in nosocomial infections include *Streptococcus spp.*, *Acinetobacter spp.*, enterococci, coagulase-negative staphylococci, *Legionella Pseudomonas aeruginosa, Bacillus cereus, Staphylococcus aureus* and Enterobacteriaceae family members including *Serratia marcescens Escherichia coli* and *Klebsiella pneumonia.* Out of these, *P. aeruginosa*, *S. aureus* and *E. coli* have a major role in nosocomial infections [7].

E. coli is an emerging nosocomial pathogen causing problems in health care settings [8]. It can colonize in gastrointestinal tract of human beings. *E. coli* is responsible for several diseases including UTI, pneumonia, meningitis, peritonitis and gastroenteritis [8]. *S. aureus* is considered one of the most important pathogens responsible for nosocomial infections. It is not only a disease-causing organism but also plays its role as commensal. Hospitalized patients with decrease immunity and immunocompetent people in community are more prone to *S. aureus* infections [9,

10]. *P. aeruginosa* contributes to 11% of all nosocomial infections resulting in high mortality rates. The usual sites of colonization are kidney, urinary tract and upper respiratory tract. It is a cause of surgical and wound infections, UTI, pneumonia and cystic fibrosis [10]. These infections can be regarded as a significant when the levels of bacteria is b of 100 000 bacteria per milliliter of sample, especially if found together with blood cells.

The most employed real samples analyzed in nosocomial infections are urine, peritoneal fluid (ascitic fluid), blood, and salivary gland. Urine samples are used for testing for the presence of UTI-causing bacteria. In the case of ascitic fluid is employed for the detection of bacterial infections in cirrhotic patients. A large proportion of cirrhotic patients has ascites [11], i.e. an accumulation of fluid in the abdominal cavity. The infection of this ascitic fluid is called spontaneous bacterial peritonitis (SBP), is a common complication in these patients and the most frequent bacterial infection in cirrhosis.

1.1.2. Antibiotic-resistant nosocomial pathogens

After the discovery of the first therapeutic use of penicillin as an antibiotic in the early 1940s, the human beings though that life-threatening bacterial infections were discarded. However, by 1950 almost half of all hospital samples of patients infected by bacteria were resistant to penicillin, which forced to investigate in new antibiotics. Drug-resistant bacteria have been mostly kept under control since then because of progress in the development of other antibiotics.

However, the excessive and improper uses of broad-spectrum antibiotics, especially in healthcare settings, are elevating the number of nosocomial infections

due to the continuous appearance of drug-resistance bacteria. Penicillin-resistant pneumococci, multidrug resistant tuberculosis and methicillin-resistant *S. aureus* (MRSA), are examples of drug resistant bacteria. The distribution of the different type of bacteria is changing over time. For examples, *Escherichia spp, Klebsiella spp* and *Proteus spp* were responsible nosocomial infections in the 1960s, but in the 1980s, *P. aeruginosa* created clinical difficulties [12].

B-lactamase antibiotics including penicillin along with other antimicrobials became firstly resistant in 1940s. This resistance appeared because the Staphylococcal species developed penicillinase enzyme that destroys the β-lactam ring of the antibiotic, making the penicillin ineffective. This issue was solved by the introduction of penicillinase-resistant antibiotics, cephalosporins. In the 1960s, methicillin-resistant species of *S. aureus* were reported. This resistance was due to the modification of penicillin-binding proteins (PBPs) [13]. The PBPs are susceptible to modification by β-lactam antibiotics; an event that leads to bacterial death, PBP2a type is resistant to the action of all available β-lactam antibiotics.

During recent years, the problem of multidrug resistance is currently most acute in Gram-negative bacteria, where the treatment options can be severely limited. Moreover there are few promising new antibiotics with activity against Gram-negative bacteria under advanced development [14]. The spread of resistant strains and horizontal transfer of resistance genes, both contribute to raising the global prevalence of multiresistant Gram-negative bacteria [15].

1.2. Bacterial Detection Methods

1.2.1. Structure of a bacterial cell

Bacteria are normally between 0.5 and 5 μm in size with different morphologies such as spherical cocci, rod-shape bacilli, and spiral-shape spirilla or spirochetes. Unlike eukaryotic cells, most bacteria are encapsulated by a cell wall that is present on the outside of the cytoplasmic membrane (Fig. 1.1). The cell wall contains peptidoglycan, a negatively charge polymer matrix comprising of cross-linking chains of amino sugar, namely N-acetylglucosamine, and N-acetylmuratic acid. Bacteria are classified as either Gram positive or Gram negative depending upon the architecture and thickness of the cell wall [16].

The cell wall of Gram-positive bacteria comprises a thick layer of peptidoglycan, which also contains lipids and other protein components, surrounding a lipid membrane. In contrast, Gram-negative bacteria possess a much thinner peptidoglycan layer sandwiched in between two cell membranes. The outer membrane contains proteins, such as porins, as well as lipopolysaccharides (LPS), also known as endotoxin. The inner membranes of both types of bacteria contain various proteins. Both types of bacteria may have flagella.

A variety of surface antigens presented on the cell envelops of whole bacteria, including proteins, glycoproteins, lipopolysaccharides, and peptidoglycan, can act as targets for biorecognition.

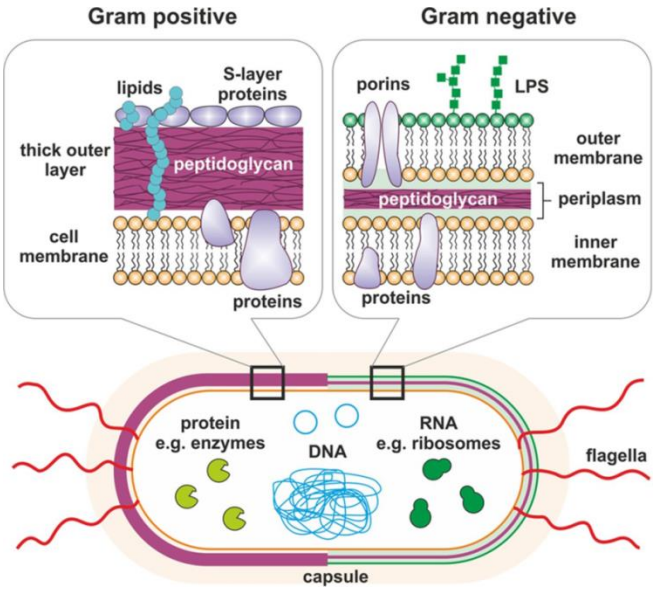

Fig. 1.1. Bacterial architecture and targets for biosensing [16].

1.2.2. Conventional bacteria detection methods

Conventional methods for bacteria detection are mainly based on culture and visual inspections taking advantage of that bacterium in a sample can grow into visible colonies on a defined medium. A colony can be derived from a single bacterial cell providing the identification due to the colony's morphology and metabolic capabilities. However, culture-based methods are often slow (up to 72 hours are required to obtain confirmed results) and may vary in time since the development of a colony containing 10^6 organisms will take between 18 and 24 hours or 5 to 7 days depending on the organisms [17]. Generally, traditional methods involve the following basic steps: preenrichment, selective enrichment, biochemical screening and serological confirmation [18]. Most of the methods currently employed by clinical diagnostic laboratory as the VITEK (bioMérieux, France) or MicroScan (Siemens, UK) systems (Fig. 1.2), which exploit colorimetric technique. But, require

susceptibility testing following bacterial culture, and can take from 9 to 20 h to obtain results.

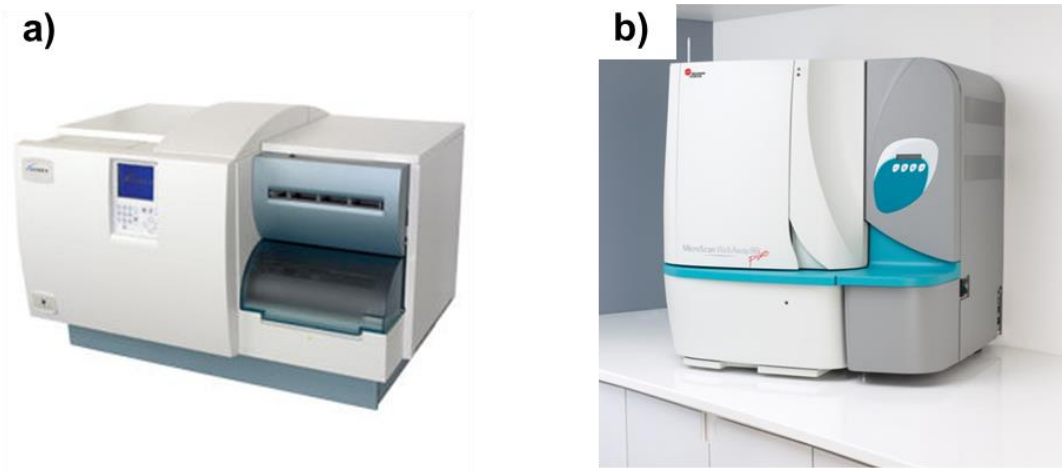

Fig. 1.2. a) VITEK® system and b) MicroScan system (Siemens) for microbial identification and antibiotic susceptibility testing [19, 20].

Molecular methods as the polymerase chain reaction (PCR) technique are faster but present their own challenges. PCR amplifies small quantities of genetic material to identify the presence of bacteria [21]. The PCR is extremely sensitive and is faster than culture growth, but it has several disadvantages as: i) the analysis requires pure samples since this technique is prone to contamination due to its high sensitivity, ii) the processing of the samples takes several hours, iii) the process is complex involving multiple steps and a high expertise in molecular biology, and iv) its high cost hinders their implementation for all the microbiological analysis required in hospital settings [22]. The recent advances in PCR technologies, such as digital PCR, quantitative PCR, and microfluidic PCR (Fig. 1.3), can provide better performance since they reduce the assay time, and the reagent and sample volumes. However, these alternative PCR variants require the use of dyes or fluorescent label probes, resulting in an increase in the total cost and complexity of

the assay [23-25]. PCR based methods have been employed for the detection of a broad range of pathogens like *Staphylococcus aureus*, *Bacillus cereus, Salmonella spp* [26-28].

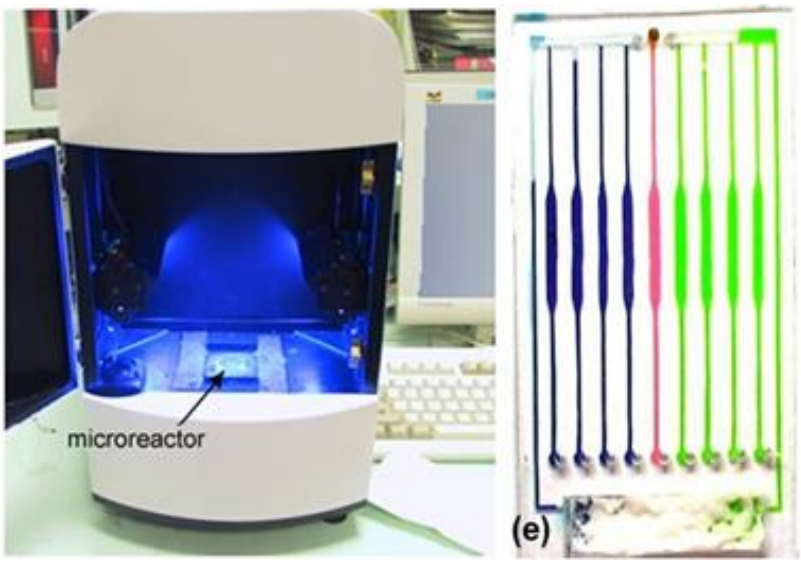

Fig. 1.3. Photograph of the prototype of a microfluidic PCR [29].

The recent progress in bacteria detection technology includes the microarray technology. Microarrays were originally used for the study of gene expression, but DNA microarray has been widely used in the field of pathogen detection. Microarrays are made up of glass slides or chips coated with up to hundreds of specific oligonucleotide probes [30]. In this method, the samples are labeled with fluorescent dye and binding to their corresponding probes. The results are obtained through the visualization of the fluorescence signal produced from the probe-target interaction [31]. Many works have reported to detect bacteria such as *Shigella* and *E. coli* serotypes by oligonucleotide DNA microarray [32]. In addition, microarrays with multiple probes per target are included for higher sensitivity, specificity and accuracy. These microarrays require special manufacturing and they are relatively high in cost.

In general, a microarray allows simultaneously identification of multiple bacterial pathogens. Therefore, it is capable of high-throughput analysis and it also has the potential to be automated [33].

Immunodetection techniques such as enzyme-linked immunosorbent assay (ELISA) have become a broadly used method for enteric bacteria detection because they permit a sensitive and specific detection. Methods based on antigen-antibody interaction are normally used for the identification of pathogens [18, 34]. Although the immunological detection methods are not as specific and sensitive as the nucleic acid detection, they have the ability to detect the microorganisms and their toxins that may not be expressed in the organism's genome.

The Immunodetection techniques use an antibody or antigen associated with a detectable label which can be an enzyme, a fluorescent or phosphorescent dye, and the detection strategy which are criterion to divide the immunoassay in:

Direct competitive immunoassay strategies, where the antibodies are immobilized over the surface and the sample containing the antigen is mixed with a solution containing a fixed quantity of labeled antigen that both compete for the active sites at the antibodies. In this case the signal is inversely proportional to the analyte concentration. Another strategy is the **indirect competitive**, where the analyte is immobilized over surface. The sample contain the antigen and the antibody, and the both antigens (immobilized and the sample) compete for the antibody. After the interaction, the antibodies on the surface are determined by a secondary labeled antibody.

Sandwich immunoassay, where the antibodies are immobilized on the surface and the interaction with the antigen is reached. After the interaction, a second antibody with a label also binds with the analyte.

The use the labels is no required in a label-free techniques which result in a great simplification of the detection strategies in comparison with labeled immunoassays. These can be classified into direct, competitive, and sandwich immunoassays.

In the **direct immunoassay**, the antibody is immobilized over the surface and the antigen is directly detected. This assay is fast and needs low quantity of sample. The **competitive immunoassay**, the antigens are immobilized on the surface and a sample with the antigen and the antibody is adding to compete with immobilized antigen. The signal is obtained by the interaction of the remaining free antibody of the solution with bioreceptor layer. Finally, the **sandwich immunoassay**, this strategy is similar to employed in the case of labeled immunoassays, but without using a label. This strategy is less employed in label-free techniques.

Table 1 summarizes the advantages and limitations of the conventional methods for pathogen detection.

Table 1. Summary of advantages and limitations of conventional methods

Detection method	Advantages	Limitations
Simple and Real-time PCR	• High sensitivity • High specificity • Reproducible • Not require post-amplification of products processing • Real-time monitoring of PCR amplification products	• High cost • Difficult for multiplexed real-time PCR assay • Affected by PCR inhibitors • Requires trained personnel • Prone to cross contamination

Microarrays	• High sensitivity • High specificity • High throughput • Enable detections of multiple pathogens • Allow detection of specific serotypes • Labor-saving	• High cost • Require trained personnel • Labeling of target genes
ELISA	• Specific • Can be automated being more time efficient and labor-saving • Allow the detection of bacterial toxins	• Low sensitivity • Prone to false negative • May result in cross-reactivity with closely related antigens

1.2.3. Overview of Biosensor Devices

A biosensor is an analytical device which is able to transform a biological response into a signal. Biosensors include a bioreceptor element such as antibodies, nucleic acid, bacteriophages, antigen or cells (section 1.2.5), which recognizes the target analyte and a transducer based on optical, acoustical, mechanic or electrochemical signal detection, for converting the recognition event into a measurable signal (Fig. 1.4). Biosensors are well-developed devices for the direct and efficient detection of analytes since many years ago. The most representative example is the glucose biosensor, which is employed by millions of diabetic patients around the world.

Biosensors have been developed for many different analytes, ranging in size from small molecules to nucleic acid and proteins up to whole bacteria and viruses [35]. Biosensors offer several advantages over conventional methods, including low

limit of detection, real-time analysis, label-free detection, and low sample consumption.

A key point in the development of a biosensor is the immobilization strategy employed for the attachment of the specific bioreceptor on the transducer surface. Many methods of immobilization of biological molecules have been used for biosensing [36]. These include physical adsorption, where the biological molecule is directly adsorbed onto a suitable surface, entrapment, where the molecules are trapped within a matrix, covalent attachment involving direct immobilization via a series of chemical bonds between the surface and the biological molecules, and cross-linking, where the biological molecules are chemically bonded to the sensor surface via the use of a biofunctional agent.

One fundamental parameter for the performance of a biosensor is the ***sensitivity****,* which is related to the magnitude of the transducer response to the change in the analyte concentration. Other fundamental parameter is the ***resolution*** which indicates the ability to detect the sensor signal variation induced by a sample, and corresponds to the smallest variation that can be measured. The resolution depends on the noise of the employed set-up (thermal, detector noise, etc.) and is normally estimated as three times the standard deviation of the total system noise. Finally, the combination of the resolution and the sensitivity define the ***limit of detection*** *(LOD)*, the minimum amount of the analyte which can be accurately quantified, which enables to compare different sensor configuration.

In the particular case of microorganism detection, biosensors can offer a rapid and cost-effective method for bacteria detection which can be performed at the point

of care without the need of a trained technician. They could provide a more rapid diagnosis of bacteria allowing a faster and more effective therapeutic intervention, thereby preventing full-blow infections and mortality [16]. In the case of the bacteria sensing, two types of biosensors have been developed: a) those which require a previous sample processing (bacteria lysis) to liberate the target bacterial molecule and b) those which detect the whole bacteria. For example, there are developments showing biosensors for the detection of bacterial components such as DNA [37, 38], RNA [39, 40], enzymes [41], or exotoxins [42]. However, the major disadvantage of these biosensors is the requirement of a previous sample processing and the use of extra reagents, which increase the time and cost of the tests. Hence, biosensors for the direct detection of whole bacteria are much more desirable for rapid and cost-effecting testing at the point of care. Therefore, biosensors hold great promise to addressing the analytical needs in nosocomial infection diagnostic.

Here, we review recent advances in biosensor for bacteria diagnosis, especially electrochemical, piezoelectric and optical biosensor, and introduce strategies that constitute those biosensors with such sensing performance.

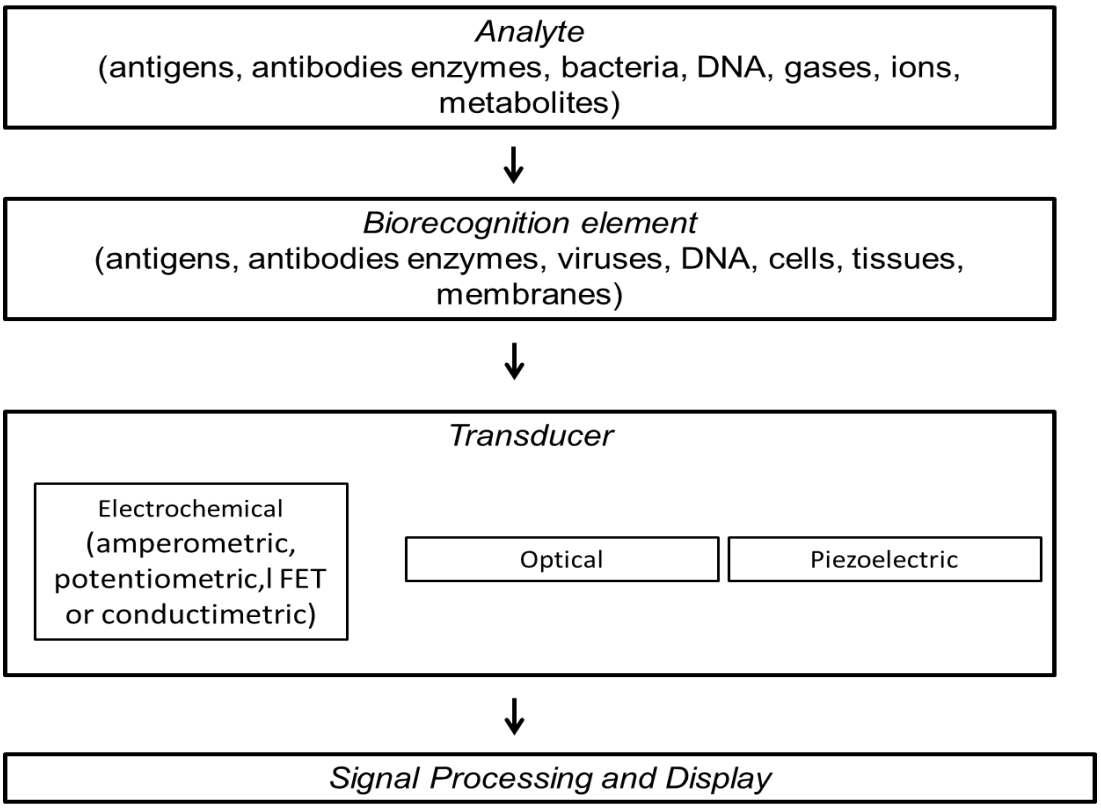

Fig. 1.4. General Scheme of a biosensor device.

Electrochemical biosensors

Electrochemical biosensors are the most employed transducers in the biosensor field. These sensors include amperometric, potentiometric, conductometric and impedimetric techniques [43-45]. Electrochemical biosensors work by eliciting a measurable current (amperometric), a measurable charge accumulation or potential (potentiometric), modifying conductive properties of a medium (conductometric) or impedimetric, by measuring resistance and reactance which combine to form impedance. [46, 47].

Electrochemical biosensors have been employed for the detection of various bacteria, including *Staphylococcus aureus* using a potentiometric sensor, obtaining a LOD of 8×10^{2} CFU.mL^{-1} when the aptamer was covalently bound to surface. An

amperometric detection of *Staphylococcus aureus* was achieved using a competitive immunoassay with magnetic amplification resulting in a LOD of only 1 CFU.mL^{-1} [48]. Although the limit of detection is very good, the system requires labels and enhancement of the signal which hinder its use as a point-of-care device.

Impedimetric sensors are the most commonly employed for the detection of whole bacteria due to low cost of the materials employed during their fabrication. An impedimetric biosensor was reported for *E. coli* detection, which allowed a detection limit of 8×10^2 CFU mL^{-1} with a detection time lower than 15 min. Although a variety of electrochemical biosensor are being employed to detect whole bacteria [49], the main disadvantages of impedance biosensors are the low reproducibility, high limit of detection, and problems with nonspecific signal [50, 51].

Piezoelectric biosensors

Various piezoelectric-based sensors have been developed for the detection of whole bacteria. Quartz crystal microbalance (QCM) biosensors are a kind of piezoelectric sensors that detect the resonance frequency change that results from increasing the mass on the sensor surface due to the analyte binding. QCM biosensors have been used for the detection of bacteria, including *E. coli* (LOD=10^6 CFU.mL^{-1}) [52, 53], *Salmonella enterica serovar Typhimurium* (LOD=10 CFU.mL^{-1}) [54], and *bacillus anthracis* (LOD=10^3 CFU.mL^{-1}) [55]. The main limitations of QCM sensors are the high values of the LOD. Two main approaches have been used for overcoming this disadvantage: nanoparticle preconcentration and amplification. The development of sandwich-type assays employing nanoparticles for signal

amplification has been used for the detection of very few bacterial cells, down to 10 CFU.mL^{-1} [54]. However, the use of nanoparticles implies an additional step that is not easy to automatize, losing the advantages of a label-free technique, which implies a drawback to use it as a point-of-care device.

Optical biosensors

Optical biosensors operate by employing the electromagnetic radiation that interacts with the analyte. There are a large variety of labeled or label-free techniques which has been used in optical biosensors such as spectrometry (e.g., luminescence, phosphorescence, fluorescence and Raman), guided modes in optical waveguide structures and Surface Plasmon Resonance. Label-free optical biosensors are operated by means of the principle of detection of the evanescent field, which is easy to perform and allows quantitative and kinetic measurements. In label-free detection, the target is not labeled and its functionality is not altered so that it can interact naturally. Label-free biosensing is commonly based on a refractive index (RI) change instead of the sample mass.

1.2.4. Evanescent wave sensing

When using a waveguide as a sensor, part of the electromagnetic field of the light traveling in a waveguide is spread outside the waveguide surface interrogating a volume of several hundred of nanometers over its surface. Any bimolecular event taking place on the sensor surface (e.g. the interaction of an immobilized bioreceptor with its specific analyte) will change the surface

refractive index modifying the characteristics of the light. This change can be quantitatively related to the concentration of the analyte in the sample.

Examples of evanescent wave sensor technology include surface plasmon resonance (SPR), ring resonators, photonic crystal structures, and waveguide interferometers.

Surface Plasmon Resonance (SPR) based sensor

SPR sensor is based on the oscillating charges at the interface of two media with dielectric constants of opposite signs such as a metal (e.g. gold or silver) and a dielectric [56]. When a polarized light containing a range of incident angles, falls on an electrically conducting metallic film, the incident light is no totally reflected but generates an evanescent field which penetrates into the metal layer. At a certain resonance angle and wavelength the propagation constant of the evanescent field matches with the oscillating charge wave at the metal dielectric interface. The evanescent field interacts with and is absorbed by the free electron cloud in the metal generating surface plasmon resonance that results in a reduction in the intensity of the reflected light at the resonant incident angle and wavelength (Fig. 1.5).

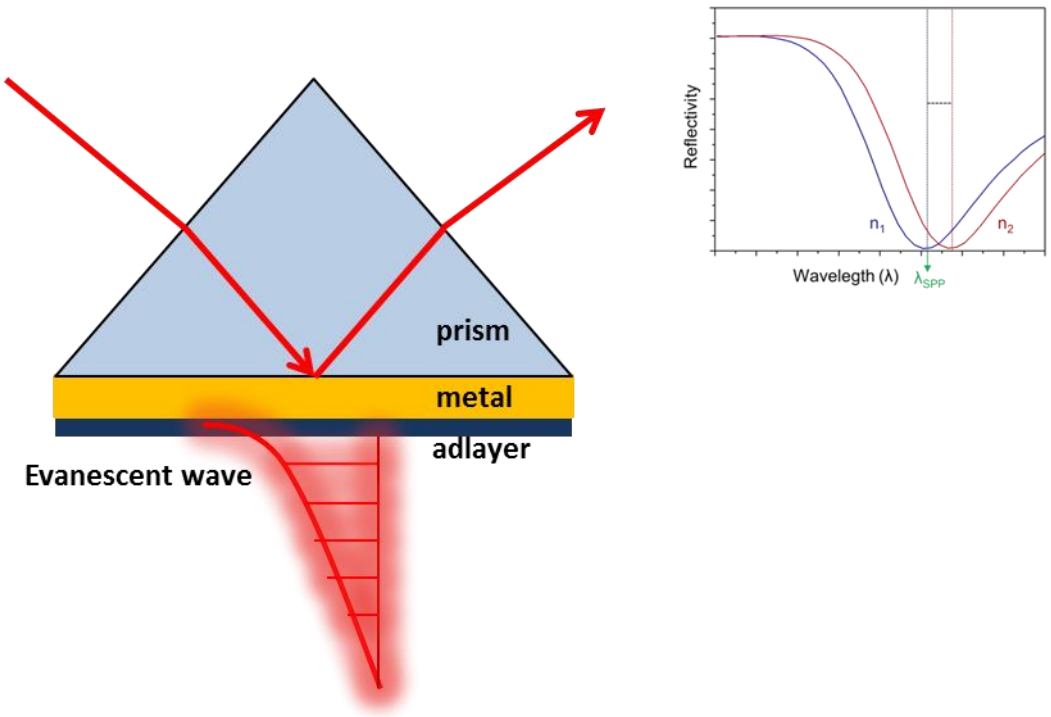

Fig. 1.5. Schematic of the operational principle of prism coupled SPR.

Various SPR-based biosensors have been developed for the detection of whole bacteria resulting in devices with poor performances (LOD = 1×10^3 CFU.mL^{-1}) due to the low penetration depth of the evanescent field (around 100 nm) in comparison with the bacteria size (microns) and the similarity in refractive indexes between the bacterial cytoplasm and the aqueous medium [57-60]. Recently, SPR combined with a magnetic separation method using Au-coated magnetic nanoparticles (NPs) resulted in a LOD of only 3 CFU.mL^{-1} [58]. A SPR based on Au NP-capped nanostructures allowed simultaneous identification of three different bacterial cells achieving LOD of 30 CFU.mL^{-1} [61]. A SPR combined with silver NPs allowed the detection of *E. coli, Staph,* and *B. subtilis* with a LOD of 50 CFU.mL^{-1}[62]. Given that SPR biosensors still require relatively large equipment for a laboratory-based test, much effort has recently been dedicated to reduce the

equipment size and the complexity of the sensor by integrating microfluidics which is useful for a point-of-care diagnostic.

Sensors based on integrated optics

The main limitations of SPR for detection bacteria could be overcome by optical biosensors based on integrated optics (IO) since they can be easily miniaturized; they offer high potential for lab-on-a-chip (LOC) integration, high sensitivities.

Among the different integrated optical biosensors, the most employed for biosensing are ring resonators, and interferometric sensors. Being the interferometric ones the most attractive due to their high sensitivity and broad dynamic range (Fig. 1.5).

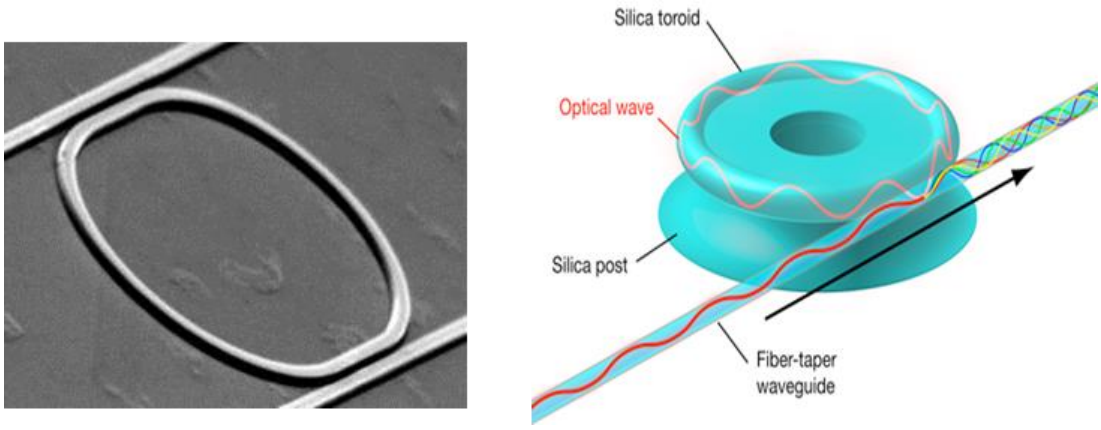

Fig.1.5. Scanning electron microscope (SEM) photograph (left) and working principle (right) of a ring resonator biosensor [63].

Ring Resonators are two dimensional structures which allow confinement of the light within a ring cavity, creating resonances due to total internal reflection. A byproduct of total internal reflection is the evanescent wave, which penetrates several tens of nanometer within of the boundary of the ring resonator into the

surrounding medium. Ring resonators are versatile structures that have been used in optical telecommunication circuits as wavelength filters, switches and frequency converters. Ring resonators comprise ring-shaped waveguide structures optically coupled to one or more linear waveguide, patterned on a planar surface [63]. Ring resonators have been employed for example in the detection of *E. coli* using a direct immunoassay achieving a LOD of 10^5 CFU.mL^{-1} [64].

Interferometric biosensors are one of the most label-free sensitive biosensors even reported. Their working principle relies on the interference of two light waves which are experience different optical path lengths. In this configuration, one of the light waves is interacting with the sample whilst the other one acts as a reference. When both light waves interfere, the intensity of the resulting light is a periodic function of the phase variation of the beams. This phase variation can be related to a bulk refractive index change or to a biomolecular interaction if a previous receptor layer was included in the path of the sensing beam. In interferometry, phase variation is proportional to the interaction length of the light with the sample within the evanescent field. As a consequence, the sensitivity of a particular interferometric configuration can be increased by enlarging the length of the sensor area. In addition, the reference arm of the interferometric devices can be employed to compensate external fluctuations, as for example, the dependence of the refractive index with the temperature.

There are two possible configurations for a waveguide interferometric biosensor. The first option is when light waves of the same wavelength and polarization (sensing and reference) propagate by different paths having the same

effective refractive index (Neff). This is the most employed configuration; the Mach-Zehnder (MZI) [65] (see Fig. 1.6), Hartman (HI) [66] and Young interferometers (YI) [67] and the dual polarization interferometry (DPI) [68] fall into this category. The second option is that light waves of the same wavelength and polarization propagate by the same path having different Neff, as in the case of the Bimodal Waveguide Interferometer (BiMW).

Several interferometer sensors have been used for the detection of bacteria as for example, the HI was employed to detect *Salmonella typhmurium* in the range of 5×10^{8} to 5×10^{10} CFU.mL^{-1} with a detection time of 5 min [69]. A YI was employed to detect tuberculosis bacterium using antibody specific for this bacterium. Although the LOD was not calculated, they demonstrated that it was possible to diagnose tuberculosis bacterium using YI [70].

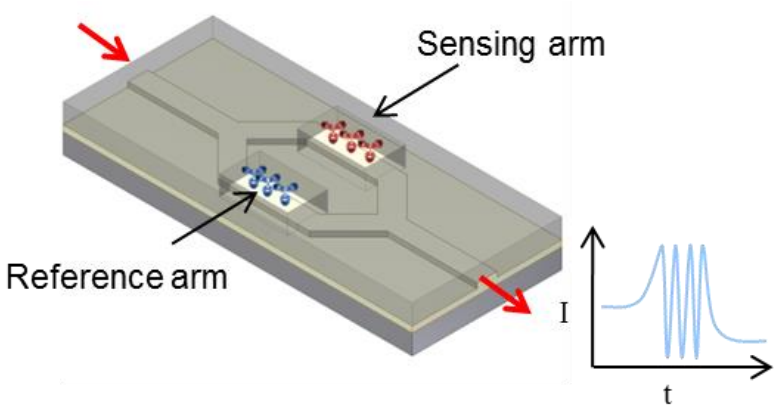

Fig. 1.6. Scheme of an interferometer biosensor based on a Mach-Zhender configuration.

The MZI is the most common interferometric configuration and has demonstrated high sensitivity detection of proteins and DNA. Also the MZI have been employed to detect bacteria with a LOD of 10^{6} CFU.mL^{-1} [71].

The **Bimodal waveguide interferometer (BiMW) biosensor** employed in this Thesis (Fig.1.7) is based on a first waveguide, which supports a single mode. The light is confined and travels in this waveguide till a step junction where the fundamental and the first order modes are excited and propagated until the end of the device, resulting in an intensity distribution that depends on the phase difference between the two modes due to the interaction with the sample along the optical propagation pathway. Then, when the interaction between two biomolecules occurs on the sensor area of the device, both modes interfere producing a phase variation according with:

$$\Delta\boldsymbol{\varphi} = \frac{2\pi}{\lambda}\boldsymbol{L\Delta N_{eff}} = \frac{2\pi}{\lambda}\boldsymbol{L(N_{eff}(TE_1) - N_{eff}(TE_0))} \quad (1.3)$$

Where L is the length of the sensor area and λ is the wavelength. In this device, light exiting is captured on a two-section photodetector generating currents I_{up} and I_{down} in the upper and lower sections, respectively. The phase shift induced by a biomolecular interaction taking place on the sensor surface is calculated by the signal S, which is proportional to the$\boldsymbol{\Delta\phi}$, according with the expression:

$$\boldsymbol{S} = \frac{\boldsymbol{I_{up} - I_{down}}}{\boldsymbol{I_{up} + I_{down}}}\ \boldsymbol{\alpha}\ \mathbf{cos}[\boldsymbol{\Delta\phi(t)}] \quad (1.4)$$

From this equation it can be deduced that the phase variation is independent of the light intensity and the output signal is not sensitive to fluctuations in the coupling efficiency. Furthermore, the signal will not vary by fluctuations in the input light. This configuration has demonstrated a LOD of

5×10^{-8} RIU for bulk changes of the refractive index and a value of $fg.mm^{-2}$ for surface sensitivity which are the lowest reported for an optical biosensor. As the MZI device [65], the BiMW biosensors present the drawbacks of phase ambiguity and sensitivity fading, but solve the misinterpretation of the signal by normalizing the output signals.

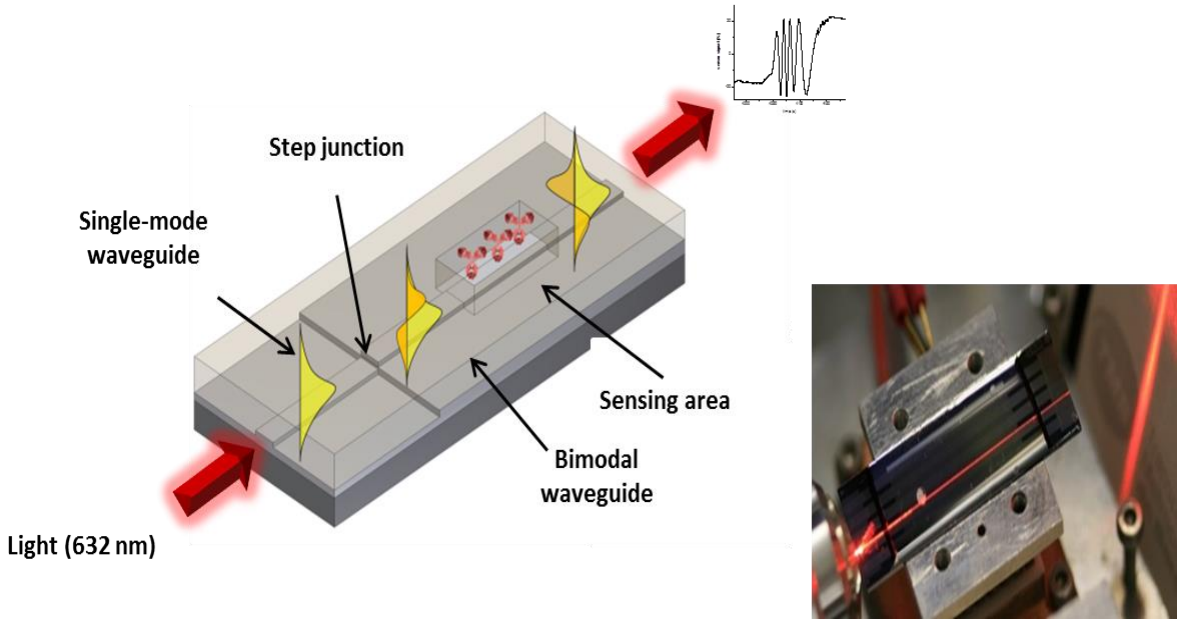

Fig.1.7. Scheme of the BiMW interferometric biosensor (left) and photograph of a BiMW chip (right).

1.2.5. Bioreceptors and type of bioassays for bacteria detection

The biorecognition layer is a key element in a biosensor device. It consists in the covering of the biosensor surface with selective biomolecules which recognize a target through specific interactions. They need to be specific and sensitive against their target in order to induce a positive signal and prevent cross-reactivity with other substances from the sample. The biomolecules commonly used for bacterial biosensors are antibodies, aptamers, phages, sugars and peptides. Fig. 1.8 gives an outline of the main types of bioreceptors used in bacterial biosensors.

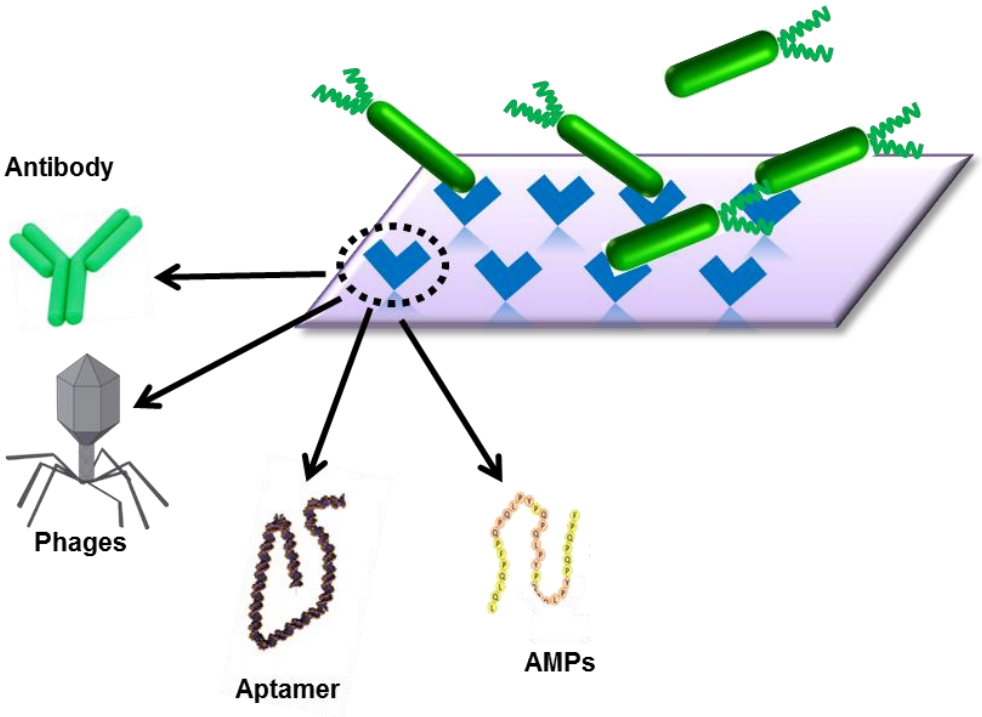

Fig. 1.8. Different bioreceptors which can be employed in a biosensor device for bacteria detection

Antibodies: antibodies are proteins produced by the immune system in order to neutralize and eliminate pathogens. These Y shape proteins are composed of four chains, two large heavy chains and two small light chains. Antibodies have an antigen-binding region that recognizes and binds to antigenic agents, which is called epitope (Fig. 1.9). Several biosensors using antibodies have been developed for the detection of bacteria. A SPRi with antibodies as bioreceptor was used for the detection of *Salmonellas enterica* and *E. coli* achieving a LOD of 3 $CFU.mL^{-1}$ [72, 73]. Although, this system has a good LOD, it needs a long time between each experiment. Also, a SPR using antibodies was employed to detect *E. coli*, resulting in a LOD of 3 $CFU.mL^{-1}$. This extraordinary LOD is due to the amplification of the signal using magnetic NPs [58].

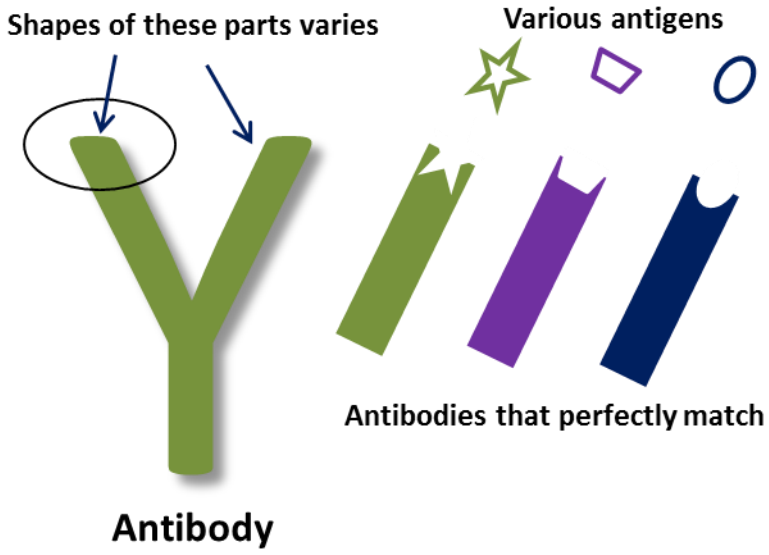

Fig.1.9. Schematic representation of antibody-antigen selective recognition.

Aptamers: aptamers are single-stranded oligonucleotides that can be artificially generated by a method called systematic evolution of ligands by exponential enrichment (SELEX) [74, 75]. Aptamers sequences can be applied to whole bacteria detection in comparison to DNA probes need a bacterial lysis step to extract the nucleic acid. Aptamers have several advantages over natural antibodies such as; i) the production of antibodies require the manipulation of whole cells while aptamer synthesis is entirely chemical, ii) aptamers are chemically modifiable, giving them additional properties, including nuclease resistance that is essential for the applications in complex media such as serum, and iii) the aptamers can be exposed to elevated temperatures without being irreversibly denatured and simply refold when the temperature goes down. Aptasensors have been reported to detect whole bacteria. An electrochemical aptasensor was employed to detect *S. Typhimurium*

with a LOD of 10^3 CFU.mL^{-1} [76, 77], an optical biosensor based on SPR was used for the detection of *P. aeruginosa,* obtaining a LOD of 10^4 CFU.mL^{-1} [78].

Bacteriophages: Virulent bacteriophages (or phages) are viruses that bind to specific receptors on the bacterial surface to inject their genetic material inside the bacteria. These entities are of 20-200 nm in size. The injection of the phage nucleic acid into the bacteria allows the phages to propagate inside the bacteria using the bacteria's own replication machinery. Phages identify the bacterial receptor through its tail spike proteins [79]. An important characteristic of phages is that they can only recognize and infect alive bacteria. The high levels of specificity and selectivity have allowed the development of pathogen detection technologies. But, an incorrect orientation of phages can negatively influence the sensor sensitivity. SPR biosensor was used to detect *E. coli* using phage T4 immobilized on a SAM with a bond involving phage protein amines reaching a LOD in PBS of 7×10^2 CFU.mL^{-1} [80]. Also the detection of *S. aureus* was done with the covalent immobilization of phage head on a SPR device, giving a LOD of 10^{-3} CFU.mL^{-1} in PBS [81].

Antimicrobial Peptide (AMPs): AMPs are a part of the innate immune system from many organisms. They provide a line of defense against a broad range of pathogens [82]. Many AMPs act on bacterial membranes or other generalized targets, and have been used for pathogen detection [83]. AMPs are small (less than 40 amino-acid residues), charged, amphipathic molecules. With these characteristics, the AMPs enable to attach to membrane, form pores and induce cell lysis [84]. Because of their high stability, their ease and low cost of synthesis and their broad range of activities

toward various microorganisms, AMPs offer a promising alternative approach for biodetection devices. Several sensors have used AMPs over gold surface, the peptide was attached on microelectrode through C-terminal cysteine residue and its binding capacity was measured using electrical impedance spectroscopy. The results showed a LOD of about 10^3 CFU.mL^{-1} of heat killed bacteria [85]. Also, a SPR was employed to detect *P. aeruginosa* and *S. aureus* using AMPs, obtaining a LOD of 10^3 CFU.mL^{-1} [86].

1.2.6. Immobilization of biorecognition elements

To achieve a specific and sensitive response towards the analyte of interest, a recognition element must be previously immobilized on the sensor surface (Fig. 1.10). The immobilization procedure will be determined by the material of the sensor surface and the reactive functional groups available in the bioreceptor, and it must preserve the bioreceptor activity, allowing the recognition of analytes while avoiding structural damage. In general, three different approaches have been used to immobilize bioreceptors onto solid supports. One is physical adsorption where a noncovalent immobilization of the biomolecule on solid surface is achieved, making use of van der Waals forces, hydrophobic and electrostatic interaction, and ionic bonds [87]. The main advantage of this strategy is that additional steps are not required, and it is applicable to any protein. However, physical interactions are weak and sensitive to changes on experimental conditions, giving low control over the orientation of the bioreceptor [88] and a poor stability and reproducibility.

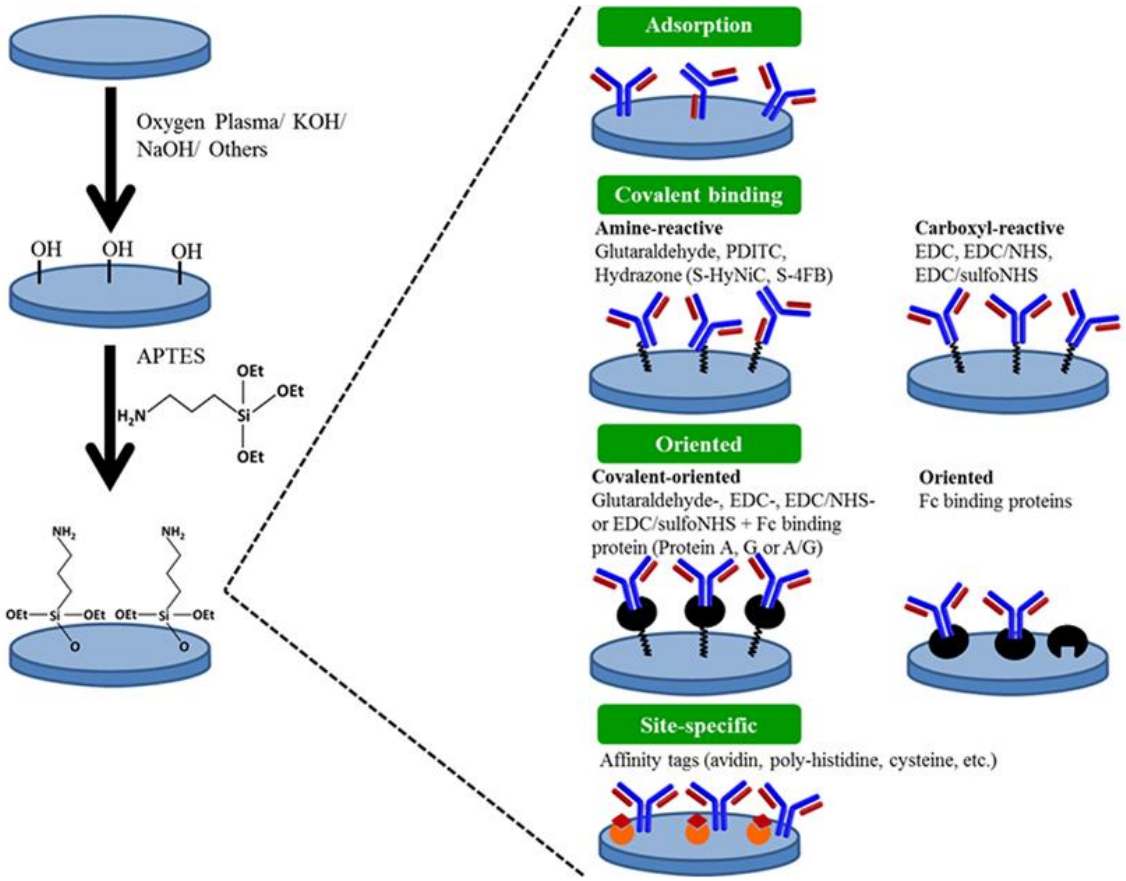

Fig.1.10. Scheme of the Immobilization of antibodies onto silicon surfaces [89].

A second strategy is biochemical affinity; this is based on the strong interaction between biotin and avidin (or streptavidin) [90]. This strategy requires a prior step of biomolecule conjugation with biotin, followed by linkage with avidin which is attached to the surface or vice versa. Biotinylation can also be site directed, enabling oriented immobilization of the bioreceptor. Another option is based on the high affinity and binding specific of proteins A and G, which allows capture of antibodies in an oriented manner [91]. Finally, the covalent immobilization provides the best approach to combine the longevity of the biofunctionalized surface with high sensitivity due to specific orientation of bioreceptor [92-94]. The covalent immobilization is highly reproducible, can direct the bioreceptor, can control the yield

of immobilization, and can achieve high interaction efficiency. The most typical approach for silicon based-materials is based on the use of organosilanes to covalently attach biomolecules onto silicon materials [95]. A summary of these strategies are presented in Table 2.

Table 2. Main Immobilization strategies for biosensors.

Immobilization strategies	Description	Advantages	Disadvantages
Physical adsorption	Immobilization based on weak interactions	Single-step immobilization; no coupling reagents required.	Random orientation; no control over distribution.
Biochemical affinity	Immobilization via noncovalent interactions (biotin-avidin)	Oriented immobilization	Possible loss of bioactivity; coupling reagents required
Covalent	Chemical bond formation between protein and surface groups	Possible oriented immobilization; homogenously oriented layer; spatial surface patterning; stable immobilization	Modification required; coupling reagents required

Immobilization of DNA probe can take place mainly by means of three of methods, physisorption, covalent immobilization, and immobilization through avidin-biotin interactions. DNA physisorption is the simplest attachment method given that no DNA modification is required. But, the DNA is immobilized by weak interactions. This immobilization can be efficient with high percentage of surface coverage. As this immobilization does not permit controlling DNA coverage, results in a disadvantage as high immobilization densities do not imply high hybridization efficiencies.

Using avidin-biotin interaction strategy, which is based on strong noncovalent interactions, DNA is usually attached directly or via a flexible spacer to the small biotin moiety which forms a strong bond with surface-bound avidin. Despite, the use of this interaction for immobilization of DNA requiring use of oligonucleotides modified with biotin and no permitting the recycle of the device.

Covalent attachment is the preferred immobilization because of its high reproducibility, probe directionality, and high hybridization efficiency. However, for this immobilization, oligonucleotide must be chemically modified with a functional group in order to induce covalent attachment on the surface.

1.3. Motivation and outline of the thesis

Nosocomial infections and the emergence of antibiotic-resistant pathogens are a major health problem with millions of reported cases every year. Nosocomial infections incur in significant socioeconomic burden arising from prolonged hospital stays, lasting disability, and increasing the demand for new antibiotics. Advanced diagnostic would allow clinicians to more quickly determine the most effective treatment, reduce the nonspecific use of broad-spectrum antimicrobials, and facilitate the enrollment in new antibiotic treatments. Although microbial methods for pathogens detection such as bacterial culture, immunoassay, and PCR are the clinical gold standard, they suffer from have several drawbacks including pre-analytical sample preparation, which generally needs sample collection, isolation of bacteria, increasing the pathogen concentration, and achieving a desired analysis

volume from a large amount of samples before detection. Besides that, they also require trained personal and adequate facilities.

The new generation of biosensors offers several advantages over conventional methods, including rapid and real-time analysis, label-free detection, low limit of detection, user-friendly, and low-cost. As the biotechnology advances rapidly, several biorecognition molecules have been designed, creating novel strategies for better detection performance. In this line, the research goal of our group is focused on the development of ultra-sensitive photonic biosensors for point-of-care analysis. Integrated optics biosensors have demonstrated better performance with respect to electro-chemical or piezoelectric biosensors. The main advantage is the possibility to integrate a label-free methodology, which results in compact and portable platforms, reduced sample volumes, and higher stable. In particular, the bimodal waveguide biosensor is the most promising solution for the achievement of an integrated platform for nosocomial detections due to an improved performance and good limits of detection with respect to the photonic biosensors resulted up to date.

In this context, the main goal of this Thesis is the designed evaluation of a novel interferometric biosensor for the identification of bacteria and their drug resistance as a powerful tool for rapid nosocomial infection testing. To achieve this goal, the following objectives have been pursued:

- The assessment and optimization of appropriate biofunctionalization strategies to immobilize the bioreceptor onto the BiMW surface for the identification of several bacteria related to nosocomial infections.

- The optimization of a methodology for the detection of bacteria with BiMW, minimizing the cross-reactivity coming from a complex matrix such as ascitic fluid from cirrhotic patients.
- The implementation of a novel analytical methodology with the BiMW biosensor for the multidrug resistant bacteria detection.

This Thesis explores the high potential of the bimodal waveguide interferometer for being used in label-free, rapid, and real-time biosensing of bacteria with a high level of sensitivity and operating in complex matrix as ascitic fluid which it finds in cirrhotic patients.

This chapter has provided the motivation and context of the Thesis work. It contains a brief background of nosocomial infections and the conventional methods for detecting them, discussing the advantages and limitations. In addition, this chapter has included an overview of the biosensors and interferometric devices. Chapter 2 will detail the methodologies and the chemical protocols implemented in this Thesis. In chapter 3, the evaluation of the most suitable covalent biofunctionalization strategies is provided. The capability of BiMW to directly detect proteins in a complex matrix as urine is demonstrated. Chapter 4, we investigate the ability of BiMW biosensors for the detection of different bacteria, and their limit of detection directly in ascitic fluid.

In chapter 5, we investigate the capability of the BiMW sensor for the rapid identification of the multidrug resistant of bacteria using aptamer as biorecognition element, and DNA oligonucleotides for the detection of genes without PCR

amplification. Finally, in the Conclusions section, the achievements and experiences will be summed up and the future research will be set out.

Chapter 2

Materials and methods

Abstract: In this chapter we describe the materials and methods used during this work including the BiMW device fabrication and its optical characterization and the experimental set-up employed for the evaluation. The list of all the chemical reagents and biological compounds employed is also included. Finally, there is a description of the biofunctionalization strategies and the different bioassays employed throughout this work.

2. Materials and methods

2.1. Design and fabrication of the BiMW sensors.

The BiMW chips were previously designed in our group (nanoB2A) and fabricated at the ICTS Clean Room facilities of the Microelectronic National Center (IMB-CNM-CSIC) in Barcelona. The design of the BiMW chip includes four different sections: section 1 (single mode waveguide), section 2 (the bimodal zone with SiO_2 cladding), section 3 (the bimodal zone with an opened window for the biosensing), and section 4 (bimodal zone with SiO_2 cladding) [96]. The main parameters for the design of the BiMW sensors are; a) Si_3N_4/SiO_2 materials have been chosen due to their high refractive index contrast, b) the depth values for the rib are of few nanometers and the values for the width are around 2.5-3 μm to obtain a single mode behaviour in the *y* coordinate, and c) the thickness of the core in the single-mode section must be 150 nm to obtain the best yield of the light at the output of the devices.

To define the BiMW device, a lithographic mask (CNM-763) was employed. The complete mask for the patterning of 12 BiMW chips in a wafer is shown in Fig. 2.1. The chips contain 20 sensors, 6 BiMW reference (without sensor area) and 6 single-mode waveguides, distributed in 2 groups of 8 and 1 group with 4 devices, all

groups contains 4 reference devices. There is a distance of 250 µm center-to-center in order to permit the integration with more components such as microfluidics.

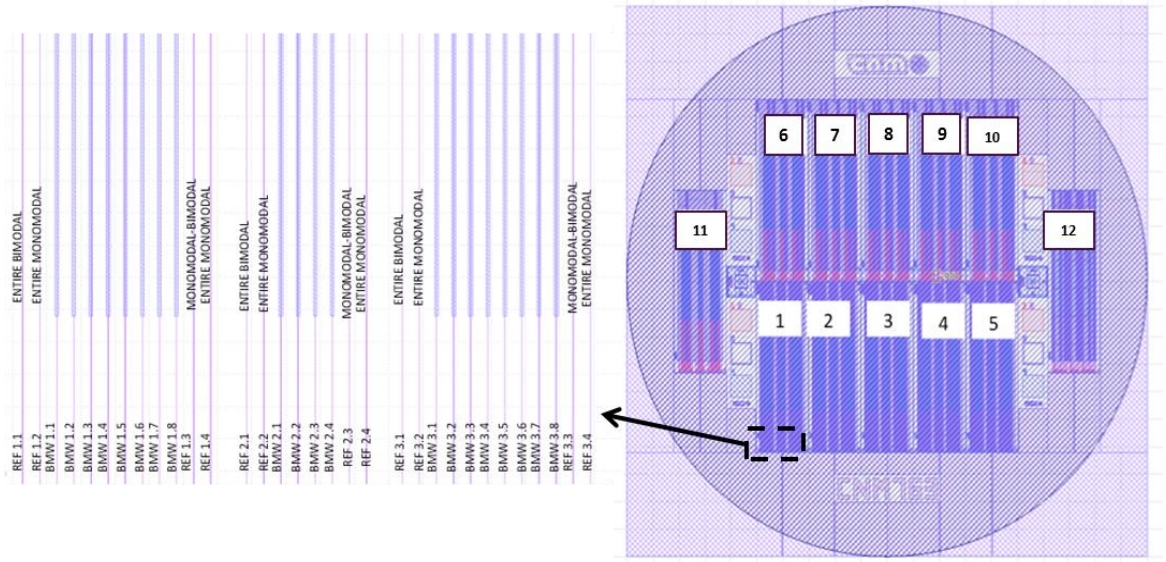

Fig. 2.1. BiMW mask layout for 12 BiMW chips. Each sensor chip contains 20 BiMW sensors and 12 reference waveguides.

The fabrication of the devices begins with a p-doped silicon wafer, where a 2 µm thick layer of thermal oxide is grown. Then a 0.34 µm thick core layer of silicon nitride is deposited by low pressure chemical vapor deposition (LPCVD). The single mode section is reduced to 0.15 µm with hot phosphoric acid (wet etching process). When the both modal section are defined, the rib structure (3 µm width and 1.5 nm height) is defined by buffer hydrofluoric acid (BHF) etching. A 100 nm thick layer of poly-crystalline silicon is employed as absorbing material which eliminates light scattering. This layer defines lateral bands along the waveguide.

A silicon dioxide layer (top cladding) of 1.5 µm is deposited by plasma enhanced chemical vapour deposition (PECVD) and the sensor area (15 mm × 50 µm) is opened by etching the silicon oxide cladding layer. Finally, the wafers were cover with a photoresist layer to protect the devices during the dicing process of the

chips. A schematic representation of the BiMW fabrication process is shown in Fig. 2.2.

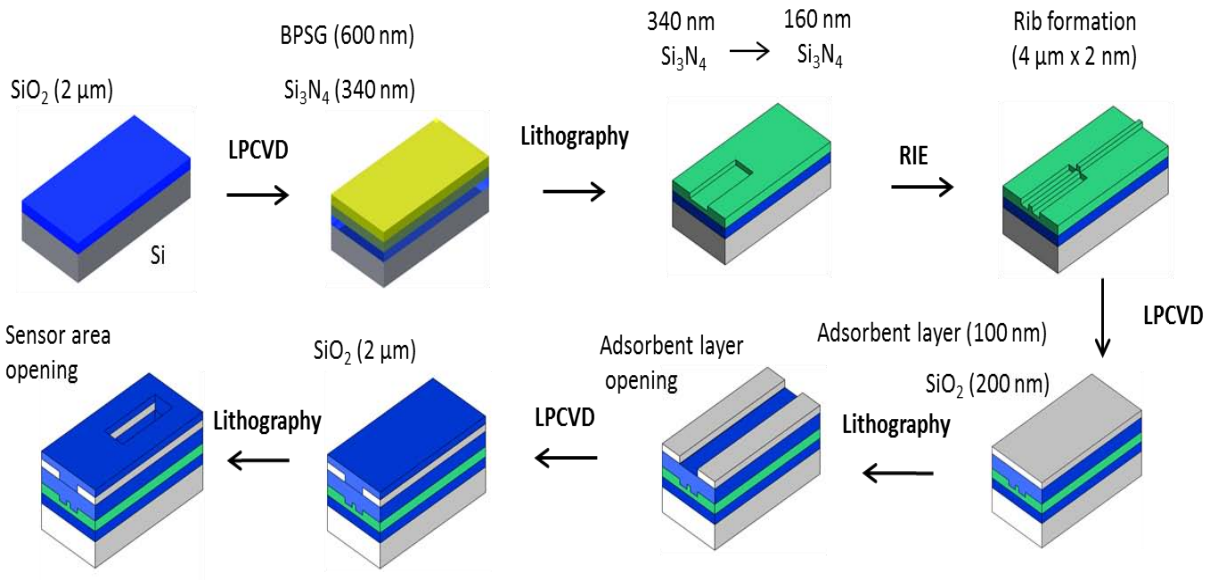

Fig. 2.2. Scheme of the different steps of the fabrication of the BiMW devices.

The fabrication of the rib is a critical step during the fabrication since the rib size is very close to the fabrication resolution. Hence, if the waveguide is not fabricated in the range between 2.5-3 µm, the BiMW performance could be affected by the creation of more two modes of the light. Topography of the rib is obtained by atomic force microscopy (AFM) and shown in Fig. 2.3a. A picture of the BIMW chip after the fabrication process is shown in Fig. 2.3b.

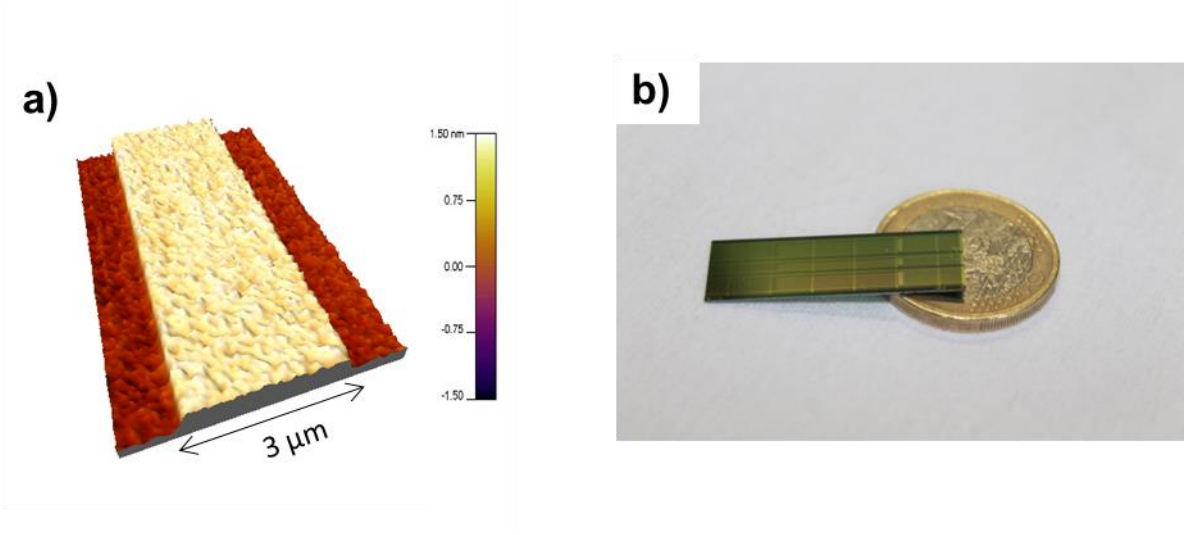

Fig. 2.3. a) AFM topography of the waveguide rib and a) Picture of the BiMW chip after the fabrication process.

2.2 Experimental set-up

For the optical and biological characterization of the BiMW biosensors, a bench-top set-up has been built (Fig. 2.4). A He/Ne laser (λ= 632.8 nm) was used as light source (using TE polarization). Visible light was coupled into the waveguide using a 40x microscope objective. The interferometric bimodal pattern at the output of the bimodal waveguide was captured by a two-sectional Si photodiode, which is placed much closed to the chip output edge for a minimum light dispersion at the exit. Each section of the photodiode was connected to a current amplifier as the currents I_{up} and I_{down} are amplified before being processed. The values of the currents are used to calculate the parameter S (signal), according to eq. 1.4.

The intrinsic sensitivity of the BiMW device to external temperature fluctuations was compensated by incorporating a Peltier element behind the sensor chip and a temperature controller, providing temperature stabilization with an

accuracy of 0.01 degrees. Data acquisition and analysis was performed using LabVIEW (National Instruments, USA) software.

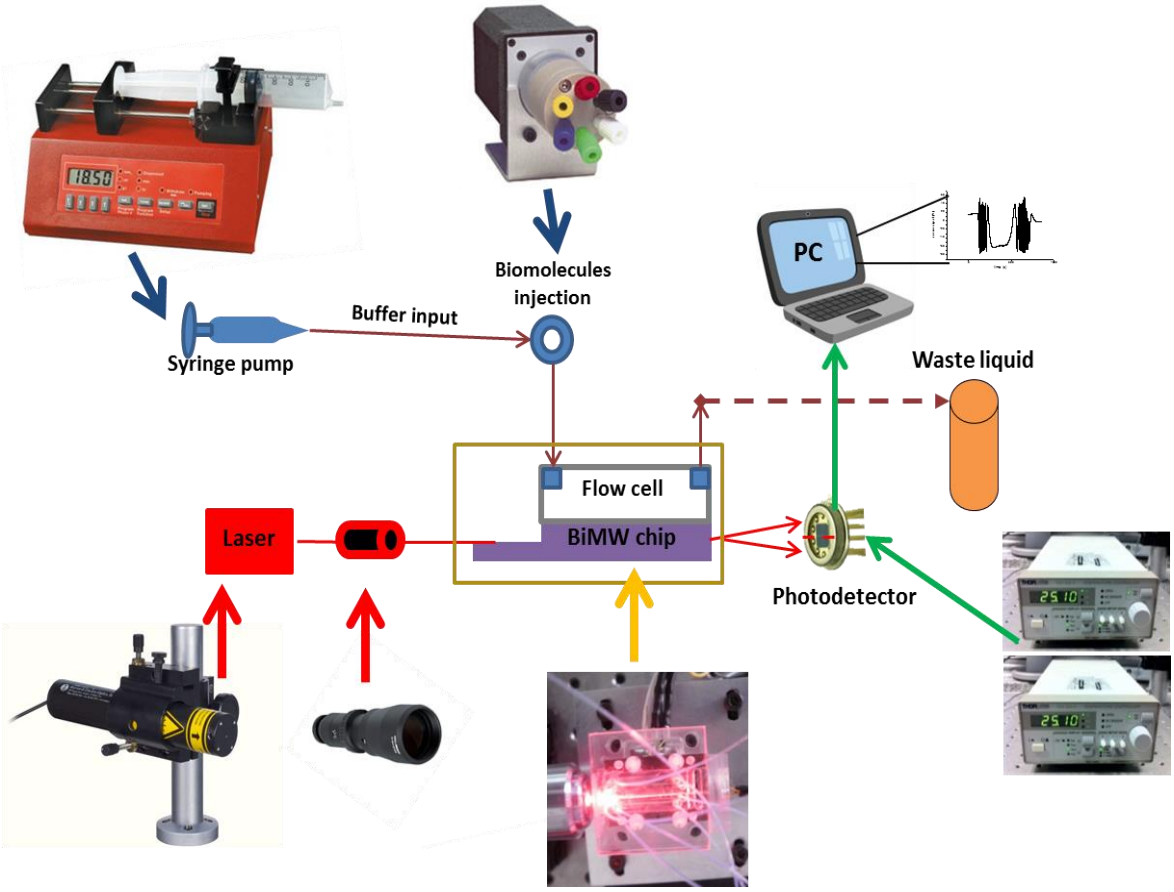

Fig. 2.4. Schematic representation of the experimental set-up for the evaluation of the BiMW biosensors system. The set-up comprised three mainly components: a flow cell and flow delivery system, optical system for in coupling of the light and the read-out and data acquisition system.

For sensing evaluation, we need to incorporate a microfluidic cell and a flow delivery system. The microfluidic cell was fabricated in polydimethylsiloxane (PDMS) polymer. The fabrication of the PDMS fluidic cell was done in three steps: i) fabrication of a SU-8 master mold, ii) fabrication of a PDMS replica and iii) the alignment of the PDMS flow channels with the BiMW sensor. The SU-8 master mold was fabricated over silicon wafers using a standard photolithography protocol in

Clean Room facilities. The PDMS microfluidic cell has eight channels with a distance of 250 µm center to center between them. Each microchannel has a length of 15 mm, a height of 50 µm and width of 100 µm that covers one waveguide sensor (Fig. 2.5). The alignment of the microfluidic system over the bimodal waveguide sensor was performed using a home-made aligner with three 3-axis micromanipulators and a vacuum pump. The microfluidic cell was connected to a syringe pump and an injection valve for fluid delivery. The velocity of the flow was modified according to the bioassay requirement, at a range from 5 to 30 µL min^{-1}.

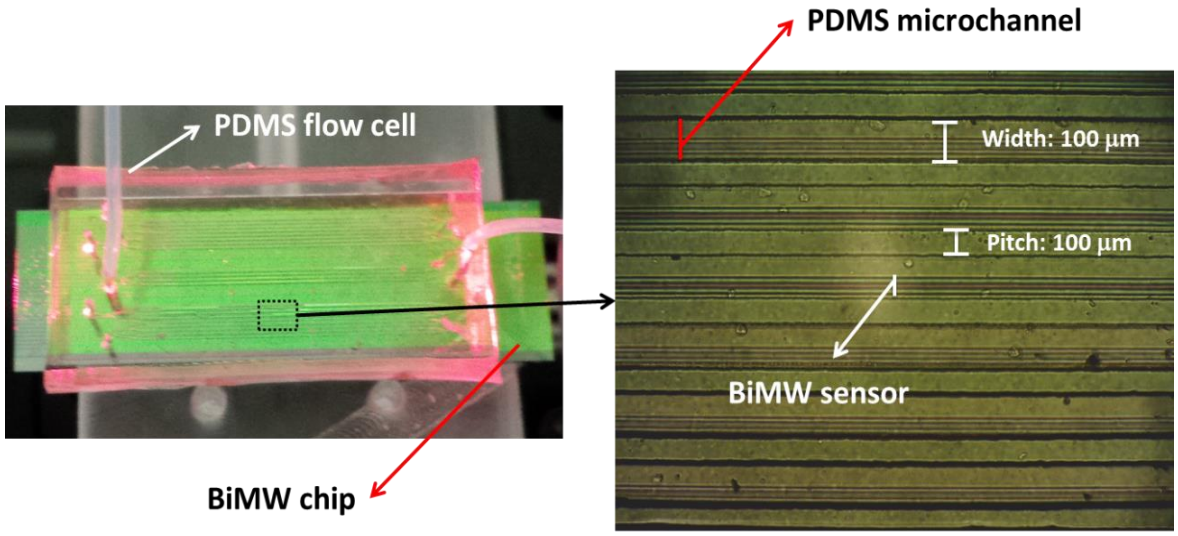

Fig. 2.5. Picture of the PDMS microfluidic cell over the BiMW sensor

2. 3. Calibration of the BiMW sensor

To demonstrate the sensitivity of the BiMW sensor, we perform a calibration curve by injectioning successive solutions with different refractive indexes. For that, we employ different concentrations of HCl (0.024 M, 0.049 M, 0.097 M, 0.242 M and 0.483 M). A previous refractive index evaluation of the employed HCl solutions was done with an ABBE Refractometer (Optic Ivymen System, Spain). We have used

HCl since it will not produce residues over the sensor area neither will affect the surface. HCl serial dilutions were injected in order to produce a variation of the refractive index (Table 3). The variation of the refractive index induce a phase variation ($\Delta\varphi$) in the BiMW sensor which is evaluated taking into account that a complete oscillation in the S_R signal corresponds to a 2π phase variation. We evaluate the phase variation *versus* the refractive index variation (Δn) (see Figure 2.6).

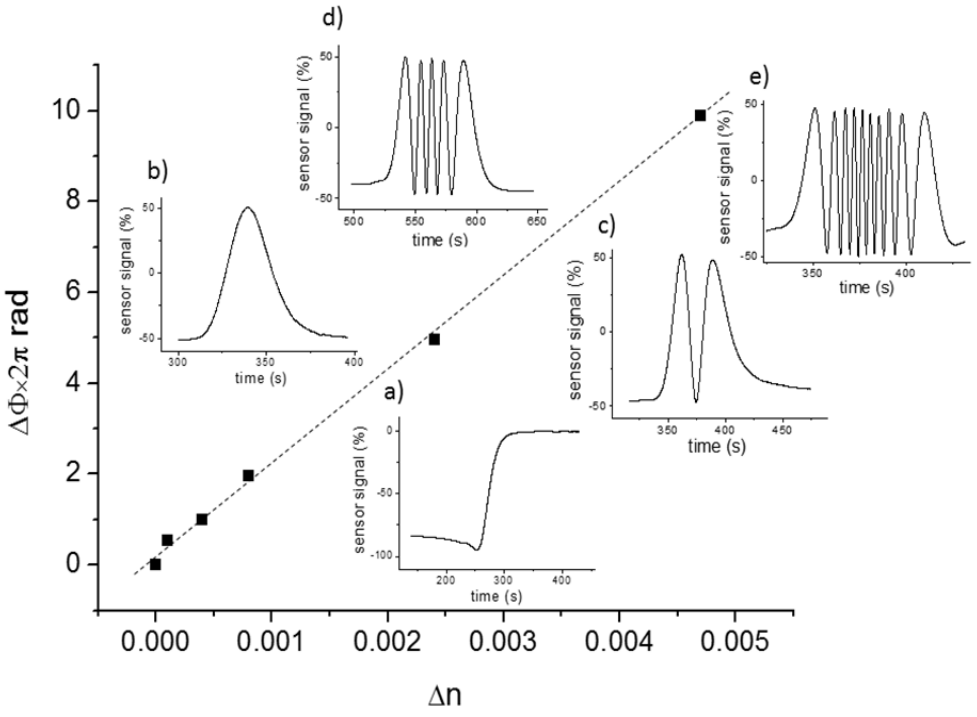

Fig. 2.6. Calibration curve of the BiMW sensor obtained by evaluating the phase change as a function of the variation of the refractive index due to the injection of HCl concentrations. Inset: a) output signal for the detection of HCl 0.024 M corresponding to a phase change of 0.53×2π rad, b) output signal for the detection of 0.049 M corresponding to a phase change of 1×2π rad, c) output signal for the detection of 0.097 M corresponding to a phase change of 1.97×2π rad, d) output signal for the detection of 0.242 M corresponding to a phase change of 4.96×2π rad and e) output signal for the detection of 0.483 M corresponding to a phase change of 9.90×2π rad.

Table 3: Values of the refractive index (η) of HCl concentrations and change in refractive index (Δη)

HCl concentration (M)	η	Δη	Δφ×2πrad
0.024	1.3329	4E-4	0.53×2π rad
0.049	1.3336	6E-4	1×2π rad
0.097	1.3340	1.3E-3	1.97×2π rad
0.242	1.3350	2.6E-3	4.96×2π rad
0.483	1.3372	5E-3	9.90×2π rad

The LOD ($\Delta\eta_{min}$) is calculated using Eq. (2.1). The phase resolution is evaluated from the measured S_R resolution, which is estimated as three times the standard deviation on the baseline noise, σ_{S_R}, giving the expression:

$$\Delta\eta_{min} = \frac{3\times\sigma_{S_R}}{S_{bulk}} \frac{\pi}{2V} \qquad (2.1)$$

For the calibration curve shown in Fig. 2.6, we have an experimental sensitivity of S_{bulk}=2056×2π rad/RIU (R^2=0.998). The noise of the system (σ= 0.007%) has been taken as the signal deviation of the average during a baseline acquisition of n=100 points. The phase resolution is considered to be three times the S/N ration which is $1\times10^{-4}\times2\pi$ rad, corresponding to a refractive index resolution ($\Delta\eta_{min}$) of the BiMW of only **5×10^{-8} RIU**.

2. 4. Chemical reagents and Biological compounds

2.4.1. Chemical reagents

Solvents for the sensor cleaning process: dry toluene, acetone, ethanol, hydrochloric acid (HCl, 35-38%), and methanol (MeOH) were supplied by Panreac (Spain). Carboxyethysilanetriol sodium salt (CTES) was purchased from ABCR (Germany). 2-[methoxy(polyethyleneoxy)propyl] trimethoxysilane (600 Da) (PEG-

silane) was purchased from nanocs (USA). (3-Aminopropyl)triethoxysilane (APTES), p-phenylenediisothiocynate (PDITC), N,N-Dimethylformamide (DMF), pyridine, 1-ethyl-3(3-dimethylaminopropyl) carbodiimide hydrochloride (EDC), N-hydroxysuccinimide (NHS), ethylenediaminetetra acetic acid (EDTA) and the components for phosphate buffer saline tween (PBST; 10 mM phosphate, 2.9 mM KCl, 137 mM NaCl, 0.005% tween-20, pH 7.4), 2-N-morpholino ethanesulfonic acid (0.1 M MES, 0.5 M NaCl, pH 5.5-6), 4-(2-hydroxyethyl)-1-piperazineethanesulfonic acid (10 mM HEPES pH 7.4) and carbonate buffer (0.1 M Na_2CO_3, pH 9), Glutaraldehyde solution grade I were purchased from Sigma-Aldrich (Spain). Copolymer poly-(L-lysine) graft-PEG (PLL-PEG, MW 75.000 $g.mol^{-1}$) was purchased from SuSoS (Switzerland), nylon membrane filter was purchase from VWR international (USA) and Polymers for flow cell fabrication SU-8 2025 was purchased from Microchem (USA) and Polydimethylsiloxane (PDMS) was purchased from Sylgard® (USA). Milli-Q water from Millipore (USA) was always employed.

2.4.2. Biological compound and samples.

Recombinant human Growth Hormone (rhGH) composed exclusively of the 22 kDa isoform and thyroid stimulating hormone (hTSH) were provided by Dr. Parlow, National Hormone and Peptide Program (NHPP), National Institute of Diabetes and Digestive and Kidney Diseases (NIDDK, CA, USA). The monoclonal antibody (anti-hGH) which recognizes the 22K and 20K hGH isoforms was obtained from and characterized by the Department of Immunology and Oncology from the National Center of Biotechnology (CNB-CSIC, Madrid, Spain). The anti-hGH was additionally purified by a HiTrap™ NHS-activated HP Column purchased from GE Healthcare (Uppsala, Sweden) previously prepared with rhGH and dialyzed by a PD-

10 Desalting Column, both obtained from GE Healthcare (Uppsala, Sweden). The anti-hGH was injected into the column at a concentration of 4 $mg.mL^{-1}$, obtaining 2.7 mL of purified antibody. This antibody solution was dialyzed; the resulting purified antibody was obtained at a concentration of 395 $\mu g.mL^{-1}$. Bovine serum albumin (BSA) and albumin fluorescein isothiocyanate conjugate bovine (FTIC-BSA) were purchased from Sigma-Aldrich (Steinheim, Germany).

Polyclonal antibodies for *E. coli, B. cereus*, and *P. aeruginosa* were purchased from abcam® (Spain). The anti-*E.coli* is a polyclonal antibody against O antigen or the somatic which corresponds to terminal sugar on the cell surface lipopolysaccharide, and the capsular or K antigen. With this characteristic the antibody has the capability to capture all *E. coli* serotypes. In the case the anti-bacillus cereus is polyclonal antibody which reacts with spores and vegetative cells of Bacillus cereus and subtilis. And anti-Pseudomonas is also a polyclonal antibody against pseudomonas in bacterial sample.

MRSA Aptamer with amino modification and recombinant *S. aureus PBP2a* protein were purchased from Base Pair technologies (USA). Lyophilized bacterial pellets of *E. coli* (ATCC 8739) and *B. cereus* (ATCC 11778) were provided by ielab (Spain). The ascitic fluid sample from the therapeutic paracentesis of a cirrhotic patient was provided and characterized by the Medicine Liver Unit, Hospital Vall d'Hebron (Barcelona, Spain). The ascitic fluid employed in this work contained a protein concentration of 1.9 $g.dL^{-1}$, 135 $UI.L^{-1}$ concentration of lactate dehydrogenase, 0.13×10^9 $cells.L^{-1}$ of total cells and 1×10^6 $cells.L^{-1}$ of red blood cells. The microbiological culture was negative. Sample was obtained after the

patient provided his/her informed consent and with the approval of the relevant Ethics Committee.

2.4.3. Bacterial culture conditions, lysis, and purification

The bacterial pellets were reconstituted in DI water employing the volume indicated by the manufacturer. Therefore, the concentration of the stock solutions was 7.41×10^5 cfu.mL^{-1} for *B. cereus* and 4.31×10^4 cfu.mL^{-1} for *E. coli*, respectively. It is relevant to note that the values for bacteria concentration were certificated by different accredited laboratories conforming to internationally recognized standards. The bacterial solutions were aliquoted and stored at -20 °C until use. Purification of bacteria was carried out by centrifugation at 3000 rpm for 15 min at 4º C. The supernatant was removed and the pellet was suspended in PBST for *B. cereus* and in ascitic fluid for *E. coli*. Each bacterial suspension was then mixed thoroughly using a pipette. Different concentrations of bacteria were prepared by diluting the stock solutions with the appropriate medium. For *B. cereus*, 1 mL of the stock solution was filtered with a 0.2 µm nylon membrane filter.

P. aeruginosa, *E. coli, S. aureus* and *MRSA* strains from Vall d'Hebron hospital (Barcelona, Spain) were prepared for bacterial capture assays and antimicrobial experiments. The bacteria were streaked onto Luria broth (LB) and incubated overnight at 37ºC. Purification of bacteria was carried out by centrifugation at 3000 rpm for 15 min at 4º C. Bacteria were then suspended in PBST for *P. aeruginosa* and *E.coli* and PBS for *S. aureus* and *MRSA*. Bacteria concentrations were confirmed by employing a nanophotometer from bioNovacientífica, S.L. (Spain) at 660 nm with an optical density (O.D.) of 0.7 corresponding to a value of 1×10^7 cfu.mL^{-1}

2.4.4. Design of DNA probes, immobilization and pre-treatment

Probes were designed by the free software OligoArchitect™ and evaluated in NCBI database by Primer-blast. This in-silico evaluation can be applied to select highly performing probe for optical biosensing applications. In this study the *bla*$_{CTX\text{-}M\text{-}15}$ and *bla*$_{NDM\text{-}5}$ genes were the DNA target. For the *bla*$_{CTX\text{-}M\text{-}15}$ detection, forward *bla*$_{CTX\text{-}M\text{-}15}$ probe and reverse *bla*$_{CTX\text{-}M\text{-}15}$ probe were used to detect both DNA strands. In the case of bla$_{NDM\text{-}5}$ gene, forward probe was used with a polyT (10 mer) spacer. All the probes were modified with amine terminal group for react with PEG-silane chemistry. Finally, synthetic DNA was used as positive and negative control. All DNA material was purchased from Ibian technology, S.L. after high-performance liquid chromatography purification. Detailed information about probes is reported in Table 4.

All DNA from the bacteria were extracted by using Quiagen DNA extraction kit according to the manufacturer's instruction. The extracted DNA samples were analysed by gel electrophoresis and the concentration of the total DNA (all bacteria DNA) in extractions were quantified using a nanophotometer at 260 nm. The concentrations of the 10-fold diluted extracted DNA solution were 12.5 µg.mL^{-1} for CTX-M-15 sample, 13.8 µg.mL^{-1} for NDM-5, 80 µg.mL^{-1} *E. coli*, and 47.5 µg.mL^{-1} *P. aeruginosa*. Before the analysis with the BiMW biosensor, the concentrations of DNA solution were converted to molarity.

Table 4. Probes and target sequences employed in this Thesis.

CTX-M-15 synthetic target	**5' TTT GCG CAT ACA GCG GCA CAC TTC CTA ACA ACA GCG TGA CGG TTG CCG TCG CCA TCA GCG TGA ACT GGC GCA GTG ATT TTT TAA CCA T 3'**
Negative synthetic control	**5' ACGCUGUCGGUGAGU 3'**
CTX-M-15 forward probe	**5' NH_2-$(CH_2)_6$-TTG TTA GGA AGT GTG CCG 3'**
CTX-M-15 reverse probe	**5' NH_2-$(CH_2)_6$-TAA GTG ACC AGA ATC AGC GG 3'**
NDM-5 probe	**5' NH_2-$(CH_2)_6$-TTT TTT TTT TGC CCA ATA TTA TGC ACC CG 3'**

The immobilizations of the DNA probes were carried out using PEG-silane surface. First, the carboxyl groups on the sensor surface were activated with a solution of 0.4 M EDC/0.1 M sulfo-NHS in MES buffer for 3 hours. Amine probe solutions in 1mM $MgCl_2$ and 10 mM PBS at a concentration of 20 µM were incubated over the surface sensor overnight at room temperature. Before BiMW analysis all samples were fragmented by applying ultrasonic bath and vortex 1 min at 3000 rpm. After fragmentation, all double-strand DNA containing samples were heated to 95ºC for 5 min in order to separate the two DNA strands. Strands re-association was prevented by 1 min cooling on ice of the samples before their injection into the BiMW biosensor.

In order to validate the presence of the $bla_{CTX\text{-}M\text{-}15}$ and $bla_{NDM\text{-}5}$ genes, PCR of the samples were carried out as previously described [97-100]. The following thermal conditions were used: denaturation at 94ºC for 5 min; 35 cycles of 94ºC for 1 min, 55ºC for 1 min and 72ºC for 1 min; a final extension period of 72ºC for 7 min. The PCR products were analysis by agarose electrophoretic gel.

2. 5. Biofunctionalization protocols

Prior to surface functionalization, a prior cleaning was carried out to remove contamination that can affect the reaction of the silanes. The BiMW chips were cleaned with acetone, ethanol and water, followed by sonication in methanol/hydrochloric acid 1:1 for 10 min, rinsing with water and drying with a stream of nitrogen. Then, a layer of the active hydroxyl group was generated by oxidation using UV/O_3 cleaner (BioForce Nanosciences, USA) for 1 h and with the exposition in a 10% HNO_3 solution at 75° C for 25 min. Here, different functionalizations were carried out depending on the sample matrix and the selected bioassay.

2.5.1. Immobilization of antibodies using CTES functionalization

We have employed a caboxyethylsilanetriol sodium salt (CTES) silane functionalization in Chapter 3 and Chapter 4 of this Thesis following the protocol detailed by our Group [101]. CTES is an organosilane stable in water that is a very important property in order to avoid organic solvent handling. Moreover, CTES permits the immobilization of biomolecules inside the fluidic cell (*in-situ*) and the carboxylic group is stable during long periods, once attached on the sensor surface.

The BiMW chips were immersed in 1% of CTES silane in water for 1 h, and then cleaned with water and placed for 1 h in an oven at 110 °C for a thermal curing step. The silane coated chip was placed on the experimental set-up and the next functionalization steps were done *in-situ* employing water as running buffer at a flow rate of 20 µL.min^{-1}. The carboxylic groups on the sensor surface were activated by injecting a solution of 0.2 M EDC/0.05 M NHS in MES buffer. Antibody solution in 10

mM PBST at a concentration of 50 µg.mL^{-1} was immediately injected over the freshly activated surface. Finally, the surface was blocked using PLL-PEG at a concentration of 0.5 mg.mL^{-1} in HEPES buffer to avoid non-specific adsorptions. Figure 2.7 shows a representative scheme of the CTES silanization procedure.

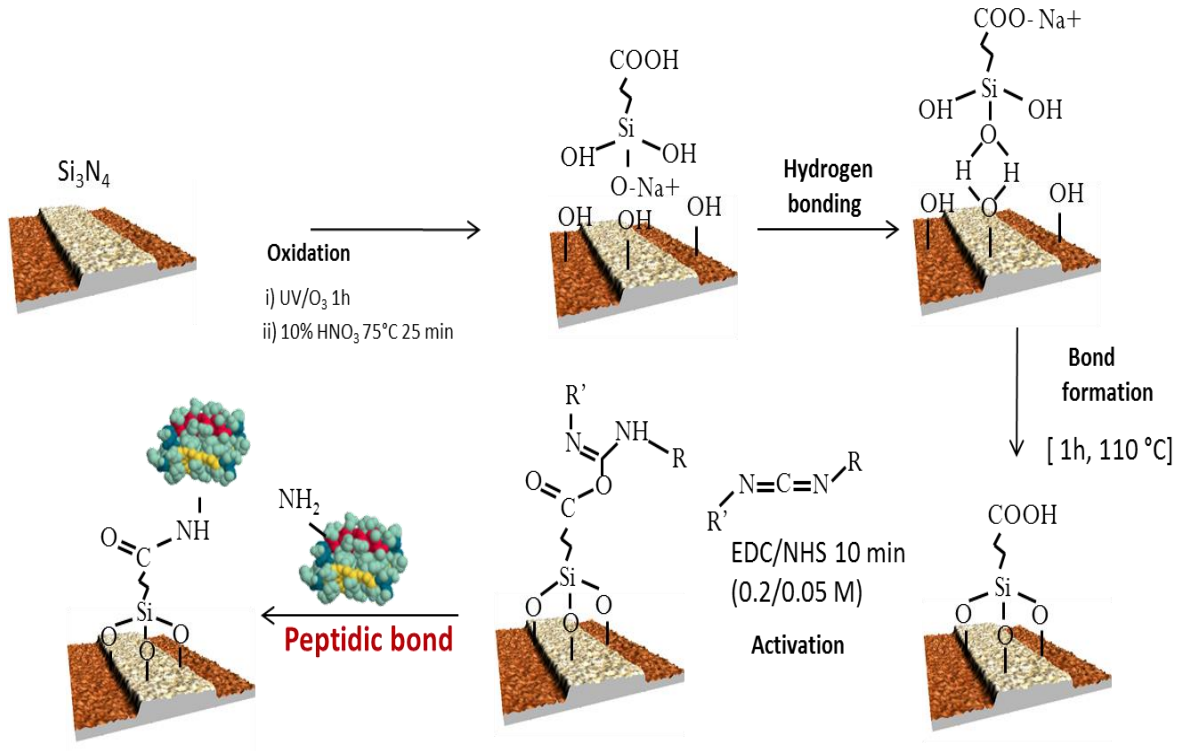

Fig. 2.7. Scheme of the CTES silanization procedure.

2.5.2. Immobilization of antibodies using APTES functionalization

We have employed a 3-aminopropyltriehoxy silane (APTES) functionalization procedure optimized for working with complex matrices such as urine or ascitic fluid. We have decided to study an APTES silanization due to its stability, high surface density, and good fouling property. APTES silane provides ended amino groups that after the reaction with a proper crosslinker can react with bioreceptors carrying a specific linker group [102-104]. Figure 2.6a shows a general scheme of the APTES functionalization protocol.

We optimized a protocol for the assembly of APTES monolayer onto Si_3N_4 test surfaces. Specifically, we focused on the development of an efficient protocol antibody immobilization for the detection of bacteria and proteins. We placed those test samples in 0.5%, 1%, 2%, 3% and 5% of APTES solution, respectively, maintaining the silanization time fixed to 1 h. Then, the silanized surfaces were sonicated for 2 min in ethanol to remove unbounded silane molecules, rinsed with water, and dried with N_2. Finally, the silane layers were cured in an oven at 110°C for 1 h.

To tether the biomolecules over the APTES surface, we employed p-Phenylene diisithiocynate (PDITC) crosslinker. PDTIC is a small homobifunctional crosslinker that is used in bioconjugation chemistry. PDITC is very stable in solution and reactive to primary amine groups. The silanized surfaces were activated by immersing them in 10 mM of PDITC in DMF and 1% of pyridine for two hours. After this time, the surfaces were cleaned using acetone, ethanol, and water, respectively. To evaluate the yield of the biointeraction when using this protocol, a fluorescent labelled protein like fluorescein isothiocyanate bovine serum albumin (FICT-BSA) was used as model. Then, the surfaces were incubated overnight with 50 µg/mL of FTIC-BSA in carbonate buffer (pH=9). Basic pH leads to the reactive of the APTES primary amine, promoting the reaction with isothiocyanate group.

After of the optimization of APTES with different concentration which resulted in 1%, we decided to find the optimal time for this concentration and avoiding agglomeration. Then, samples were incubated in a 1% solution of APTES for 15 min, 30 min, 1 h and 5 h, respectively, in order to optimize the incubation time of the surface with the silane solution. Then, the silanized

surfaces were sonicated for 2 min in ethanol to remove unbounded silane molecules, rinsed with water, and dried with N_2. The resulting silanized surfaces were activated by immersing the samples in 10 mM of PDITC in DMF and 1% of pyridine for two hours. Then, they were cleaned using acetone, ethanol, and water. The surfaces were incubated overnight with 50 $\mu g.mL^{-1}$ of BSA in carbonate buffer (pH=9). The optimization of the activation of the amino groups by the use of PDITC was performed by immersing the samples previously silanized in 0.1, 1, 10 and 20 mM, respectively, of the crosslinker in DMF and 1% of pyridine for two hours. Next, they were cleaned using acetone, ethanol and water. The samples were then incubated overnight in a solution of FTIC-BSA 50 $\mu g.mL^{-1}$ in carbonate buffer.

The optimization of APTES concentration was found and The fluorescent analysis (see Figure 2.8b) showed that 2% and 3% of APTES resulted in the formation of bundles and organized structures typical of amphipathic molecules when high concentration are employed. When the concentration of was increased to 5%, the formation of APTES agglomeration was found. The APTES concentration of 1% generated the best surface density avoiding the agglomeration of APTES silane.

To evaluate the influence of the deposition time, samples were incubated with 1% APTES in ethanol for different times, 15 min, 30 min, 1 h, and 5 h, and after that, they were evaluated by AFM. The immersion time that showed the best covering and minimized the formation of silane clusters was 1 h (Figure 2.8c). Finally, the concentration of PDITC crosslinker was also optimized with concentration of 0.1 mM, 1 mM, 10 mM and 20 mM, and analyzed by fluorescent microscopy, obtaining the best performance for 20

mM (Figure 2.9d). This PDTIC concentration showed a homogeneous signal, which is an indication of the assembly of the silane monolayer without agglomerations.

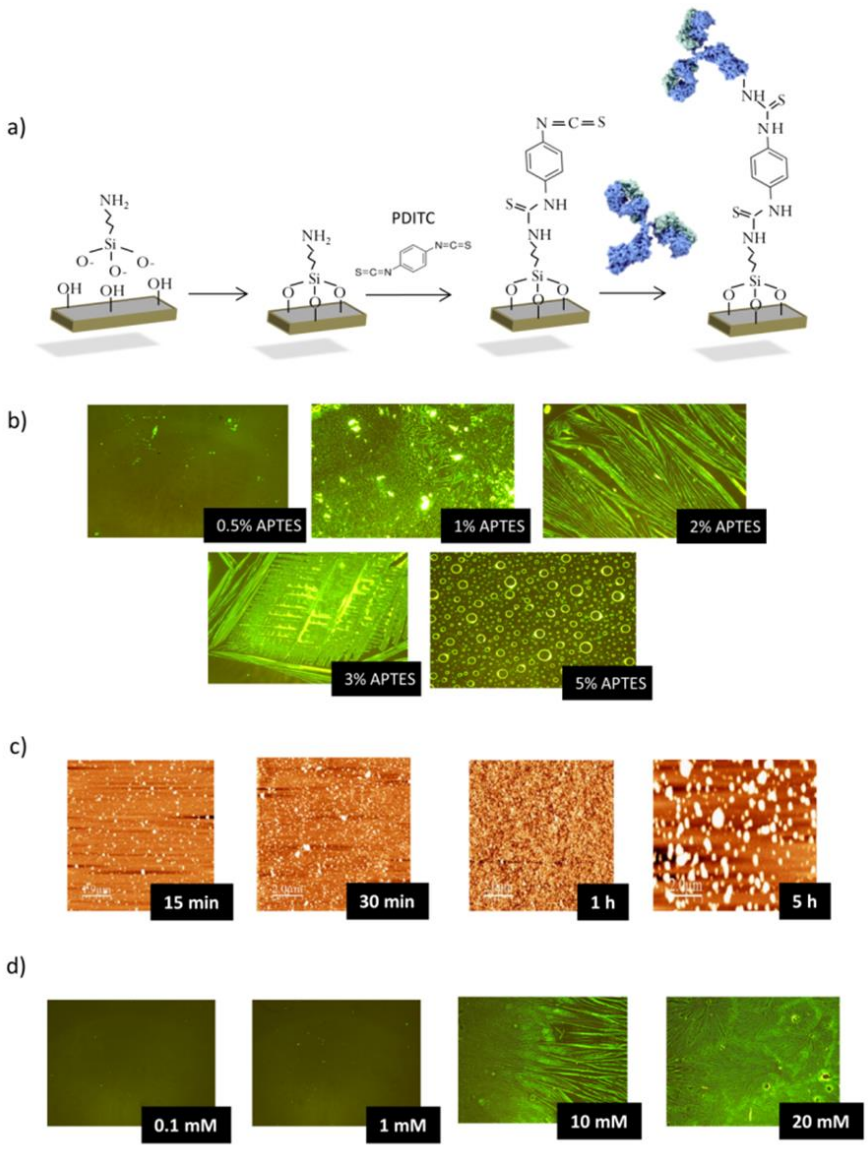

Fig. 2.8. APTES Silanization procedure for Si_3N_4 surfaces functionalization; a) sketch of the APTES silanization procedure. Optimization of the parameters affecting the silanization procedure: b) optimization of the silane concentration, c) optimization of the silanization time, and d) optimization of the PDITC crosslinker concentration.

2.5.3. Optimization of the surface functionalization using PEG silane

Substrates and chips were incubated with PEG-silane solution in an ethanol/water 95:5 (v/v) solution for 2 hours at 4 ºC, they were then rinsed with ethanol and water, and dried with a nitrogen stream. The curing step was performed by placing the chips into a bottle glass in an autoclave for 90 min at 120 ºC and a pressure of 1.5 bars.

Characterization of the PEG-silane concentration by Atomic force microscopy

Several substrates were functionalized using different concentrations of PEG-silane (10, 25 and 50 $mg.mL^{-1}$), but using the same conditions of time, temperature, solution, and overpressure and find the most compact coverage surface. The substrates were evaluated by atomic force microscopy in tapping mode (MFP3D AFM, Asylum Research,USA) using a silicon probe (force constant 50 N/m). The AFM images were acquired by scanning the samples at room temperature and all the scans were 1.5 µm and 200 nm in size. WSxM software (Nanotec, Spain) [101] was used for image analysis. Surface roughness was obtained by assessing the diagonal deviation from the average value of three different regions of the sample.

X-ray photoelectron spectroscopy (XPS)

We decided to employ X-ray photoelectron spectroscopy, also known as electron spectroscopy for chemical analysis (ESCA), for studying the antibody immobilization on the functionalised silicon nitride surface information on the structural organization of the bioreceptor layer The XPS experiments were

performed using a Phoibos 150 analyzer (SPECS GmbH, Berlin, Germany) in ultra-high vacuum condition (base pressure 1×10^{-10} mbar). A monochromatic $Al_{K\alpha}$ X-ray source (1486.74 eV) operating at 400 W was employed. Survey spectra were collected from 0 to 1380 eV with a pass energy of 50 eV, and high-resolution spectra were collected for each element (e.g. C, N and O) with a pass energy of 20 eV. Survey and high-resolution spectra were collected at 0º take off angle, defined as the angle spanned by the electron path to the analyser and the sample surface. The spectra were obtained at room temperature. The calibration was made by referencing to aliphatic C1s (BE for C-C=284.7 eV).

Scanning electron microscopy (SEM)

The images of bacterial adhesion to the sensor surface were examined by a 400L field-emission scanning microscope (FE-SEM; FEI Magellan) operated at an acceleration voltage of 2 kV and with a working distance of 4.5 mm. The validation of the specificity of the aptamer against MRSA and the MRSA morphology was carried out by SEM images (Quanta Quanta 650F; Field Emission Inc., USA) at an acceleration voltage of 2 kV with a working distance of 9 mm. All samples were attached to double-sided adhesive tape and mounted on an aluminium support.

Bacterial Adhesion experiment

Bacteria (*P. aeruginosa, S. aureus and E. coli*) were suspended in PBST buffer. Then, Si_3N_4 surfaces were functionalised with the PEG-silane by the above mentioned protocol. Silicon nitride surfaces with untreated PEG-silane were placed in 1 mL of 1×10^7 cfu of each bacterium for 1 hour, then the PBST buffer was replaced with a fixation buffer (glutaraldehyde 5% in HEPES buffer) and incubated

for 1 hour. The samples were washed with PBST and dried with nitrogen stream before examination by SEM.

Chapter 3

Biofunctionalization of the bimodal waveguide interferometer sensor

Abstract: this chapter focuses on the optimization study done to find the most efficient strategies for the antibody immobilization on the BiMW sensor surface using silanization strategies. The silanization procedures are assessed in terms of stability and sensitivity. A model immunoassay using the pair human growth hormone (hGH) and its specific monoclonal antibody was employed for the performance study of two types of silanization procedures (CTES and APTES silanization) in terms of their capability of detection and of avoiding unspecific adsorption; we also studied a PEG-silane silanization procedure to overcome the problem of biofouling and non-specific interactions. Finally, we assess the extreme sensitivity of the BiMW biosensor for the direct evaluation of hGH in undiluted urine matrix when we employ the high quality bioreceptor layer previously immobilized by the optimised procedure.

3. Biofunctionalization of the bimodal waveguide interferometer.

In biosensor devices, one of the main limitations is related to the correct functionalization of the sensor surface due to silicon surfaces are not regarded as an optimal material for interfacing with biological medium. This is because silicon-based surfaces demonstrate biofouling, the strong tendency of biomolecules to physically adsorb to the surfaces when contacted with complex matrices [105-107]. Different biofunctionalization procedures have been studied in the area of silicon-based biosensors. The most employed procedure is the assembly of chemisorbed monolayer of a silane compound, a class of self-assembled monolayer (SAM), on silicon surfaces with terminal amino, epoxy, carboxyl or chloro groups [108]. Such silane derivatives also provide a means to tailor adhesion, biocompatibility, charge, hydrophilicity, and hydrophobicity, when properly assembled on the sensor surface.

An important factor in controlling the functionalized surface properties is the length of the linker between the receptor and the transducer surface. The possibility of maintaining the receptor close to the substrate is key in silicon photonic

biosensors since the evanescence field exponentially decays with the distance from the surface [109]. For that, the typical silane molecules used for functionalizing silicon surfaces have a length around three carbon atoms. That the case of the amino-ended silanes APTES. Other short alkyl chain organosilanes used for biofunctionalization are CTES (carboxylic acid-ended surface) [110], 3-glycidyloxypropyltrimethoxysilane (GOPTS, epoxy-ended surface) [111, 112], isocyanatepropyltriethoxysilane (ICPTS, isocyanate-ended surface) [113, 114] or (3-mercaptopropyl)trimethoxysilane (MPTMS, thiol-ended surface) [115]. However, the use of very short alkyl chain silanes place the biomolecule too close to the surface, increasing the risk of bioreceptor denaturalization and of unspecific signals due to adsorption on the sensor surface.

After the silanization of the surface, the immobilization of the receptor is usually done by covalent binding. The strategy employed will depend on the ended functional group present on the silanized surface and the functional group available on the bioreceptor for the bioconjugation, being amino groups the most frequently employed for both.

The most common chemistries for covalently immobilizing bioreceptors onto amine-ended surfaces are based on N-hydroxysuccinimide (NHS) esters (which can react with primary and secondary amines to create stable amide and imide linkages, respectively [108]) and *p*-phenylene diisothiocyanate (PDITC), able to activate amino-modified supports with isothiocyanate functional groups. PDITC has the potential to form well-organized assemblies driven by π-π stacking, significantly decreasing non-specific binding [116]. Glutaraldehyde has been also widely employed as a crosslinker between

amino surfaces and biomolecules, but it has some undesirable effects, such as the formation of several layers that could break during the biorecognition process. In the case of carboxylate-ended surfaces, they can be functionalised with bioreceptors having available amine residues after the reaction of the carboxylic acid with NHS in the presence of *N*-Ethyl-*N*′-(3-dimethylaminopropyl)carbodiimide (EDC) [101].

For the bioconjugation to epoxide rings-ended surfaces, nucleophilic primary amines, sulfhydryls groups, or hydroxyl groups are required to be present on the biomolecules [117] to create secondary amine, thioether, or ether bond, respectively. Finally, thiol-modified surfaces have also been described in the literature for attachment of thiolated oligonucleotides by disulfide bond, or aminated biomolecules (antibodies), previously using heterobifunctional cross-linker m-maleimidobenzoyl-N-hydroxysuccinimide ester (MBS) [115]. All these bioconjugation methods are represented in Figure 3.1.

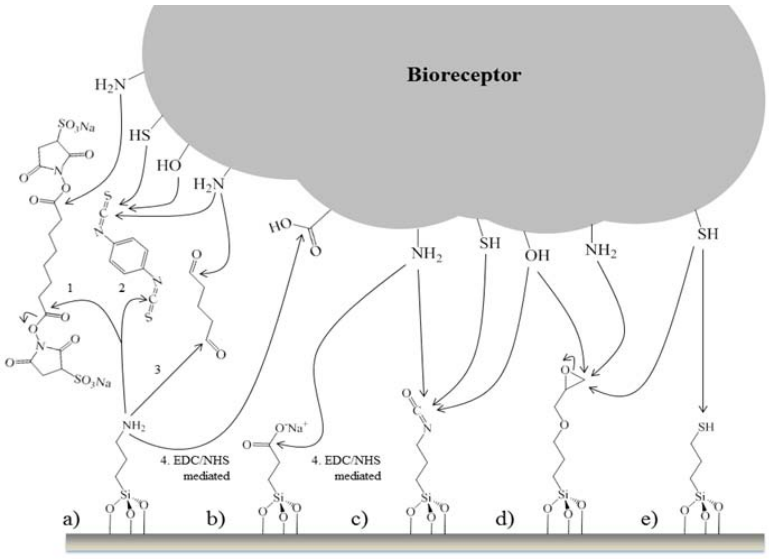

Fig. 3.1. Bioconjugation procedures employed for: a) amine-, b) carboxy-, c) isocyanate-, d) epoxy-, and e) thiol-ended surfaces. 1) BS3-crosslinking, 2) PDITC-crosslinking, 3) glutaraldehyde-crosslinking, and 4) EDC/NHS-mediated approaches, respectively

Direct BiMW immunosensor for the detection of hGH hormone using CTES silanization

The CTES silanization method, described in the previous Chapter, was used to immobilize specific antibodies for the detection of the hormone hGH (22kDa) onto the silicon nitride surface of a BiMW sensor as a model of the methodology standardization. The hGH is an essential hormone for normal growth and development, the most secreted by the anterior pituitary gland. The secretion of hGH is finding in a high range of concentrations in blood, in levels of 40 to 60000 $pg.mL^{-1}$ in a 24 h period [118]. The secretion of hGH is regulated by many factors and conditions such as age, sleep, diet, and stress [119, 120].

The overproduction of hGH causes acromegaly that triggers systematic respiratory, cardiovascular diseases, damages in the brain structure, and the neoplastic complication. The determination of hGH in hospital or health clinics is a routinely test to treat a hormone disorder. We present a label-free immunoassay for the detection hGH using the BiMW devices as a rapid evaluation of hGH hormone.

To check the antibody immobilization, the BiMW chip was placed in the set-up after silanization with CTES and covered with the fluidic cell. Then, the carboxyl groups were activated by flowing 250 µL of EDC/NHS (0.2/0.05 M), immediately followed by an injection of 250 µL of the anti-hGH antibody (50 $\mu g.mL^{-1}$). The immobilization response of the antibody was 7.25 $\times 2\pi$ rad in average, which indicates that the antibody immobilization in the sensor area reached high antibody coverage due to the covalent attachment. During all the experiment milli-Q water was flowed at a constant rate of 20 $\mu L.min^{-1}$. The interferometric signals corresponding to activation and to the binding process were monitored in real time

and can be observed in Figure 3.2. The capability of our system to monitor in the sensor response in real-time is very useful in order to assess the successes after each step of functionalization, biointeraction and regeneration.

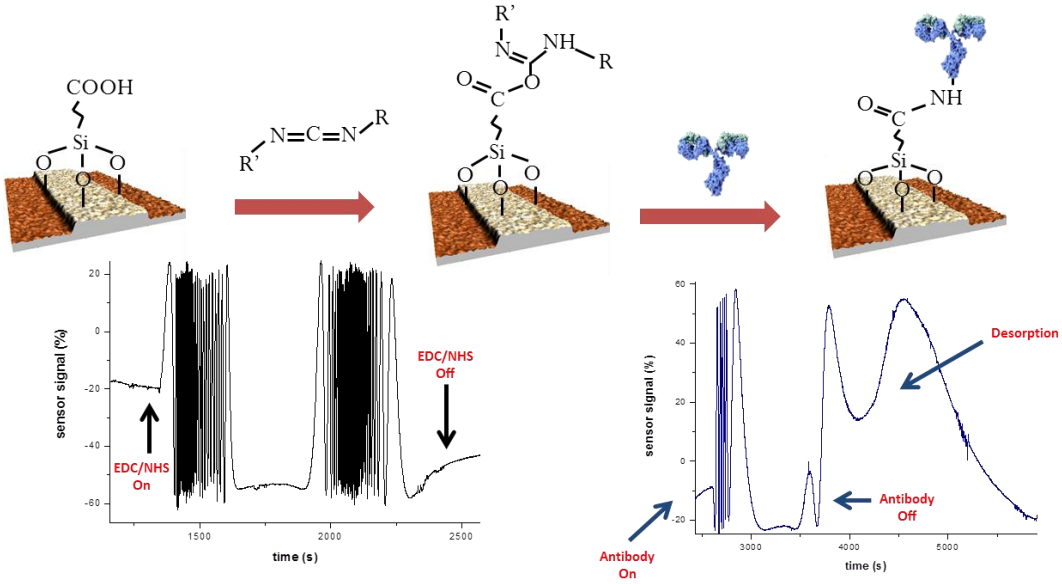

Fig. 3.2. Real-time monitoring of the sensor surface activation with EDC/NHS chemistry and antibody immobilization by covalent bonding

After the bioreceptor immobilization, a solution of BSA 2 mg mL^{-1} was flowed over the sensor surface as a blocking step to prevent nonspecific adsorptions of others proteins in the tubing, sensor surface. Then, hGH solutions ranging from 10 to 50 $pg.mL^{-1}$ were prepared in triplicate in PBS by serial dilution starting from an original 1 $mg.mL^{-1}$ stock solution. PBS was used as running buffer during all the experiments. The volume of sample introduced was 250 µL in each case flowed at 30 $µL.min^{-1}$ over the sensor surface. A regeneration solution of HCl 100 mM was employed at 40 $µL.min^{-1}$ to recover the original bioreceptor surface after each measurement.

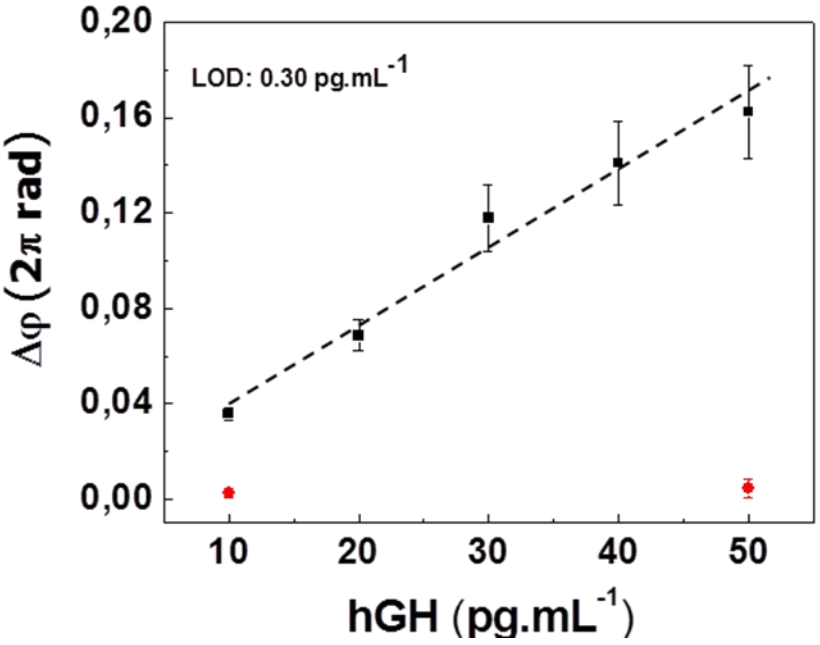

Fig.3.3. Calibration curve of the biodetection of the hormone hGH in PBS (*black, squares*) in comparison with non-specific hTSH target (*red, circles*)

We performed triplicate measurements of the hGH concentrations ranging from 10 to 50 pg.mL^{-1} and we adjusted the data to a fit model covering all the range of concentrations, as shown in Figure 3.3. The interaction between the antibody and the antigen was disrupted by the flow of a regeneration solution of HCl 0.1M which allows reusing the same biosensor up to eight times measurements with a good reproducibility. After that, the signal decrease 50% compared with the first measurements. The LOD was determined from the linear regression, as the concentration corresponding to the minimum measurable signal, set as three times the standard deviation of the blank signal. In this case, the LOD was found to be of only **0.30 pg.mL^{-1}**. The specificity of the bioreceptor layer was demonstrated by injecting a non-target but related Thyroid stimulating hormone (hTSH) at different concentrations (see Figure 3.3, *red circles*).

We can compare the good LOD obtained using the BiMW devices with a label-free detection bioassay developed by our group using SPR [121]. The immunoassay demonstrated a LOD of 0.9 ng.mL^{-1} which is higher than obtained with the BiMW devices. In view of this result, we moved the silanization strategy for the detection of the hGH in complex matrix as urine. However, the detection of hGH in urine was not possible because of unspecific adsorptions. The interferometric signal corresponding to the unspecific adsorption of urine is shown in Figure 3.4 with a phase variation of 0.7×2π rad. The signal obtained for the urine when using CTES silane could be explained by the non-homogenous covering on the surface, which produces protein clusters and creates silicon nitride holes that can induce biofouling during the biomolecule interactions.

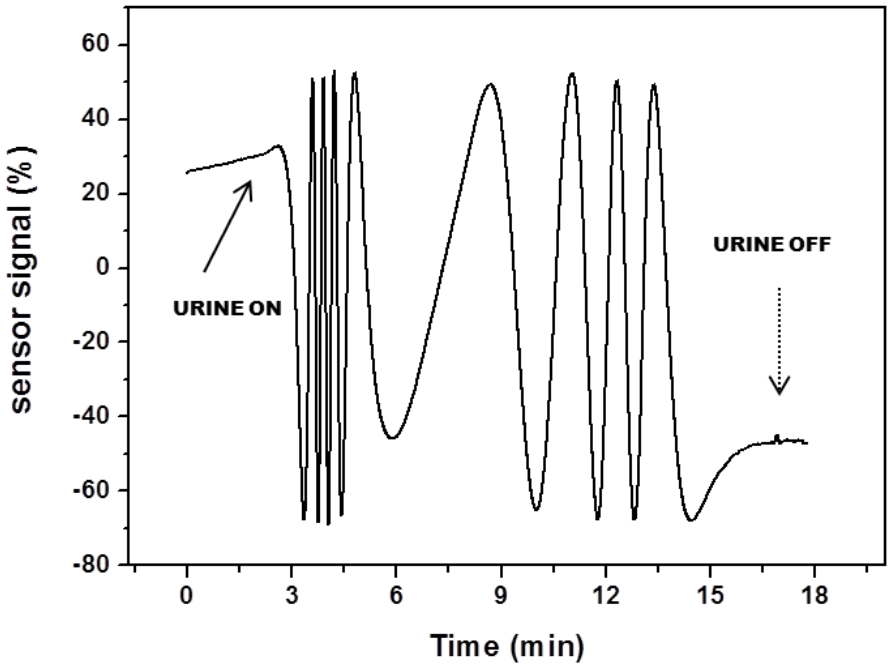

Fig. 3.4. The evaluation of unspecific adsorption of pure urine on the functionalized surface with CTES silane.

Direct and label-free detection of the human Growth Hormone in urine using APTES silanization

Due to the few possibility to detect hGH using CTES silanization strategy such as is shown in results described above. We decided to explore the APTES silanization as an alternative to solve the problem of the non-specific adsorptions in urine using the BiMW devices.

The activation of the sensor surface with the PDTIC chemistry and the subsequent antibody immobilization were done ex-situ at room temperature in absence of light. The BiMW chip was placed in the set-up after the immobilization process. A solution of BSA 2 $mg.mL^{-1}$ was also flowed over the sensor surface to prevent nonspecific adsorption and a non-spiked urine sample was injected to estimate the non-specific interactions coming from urine, while maintaining PBST in a continuous flow (see Figure 3.5). The signal of urine in the case of APTES silanization was negligible while using the CTES silanization the unspecific adsorption signal (Fig.3.4) was $0.7 \times 2\pi$ rad. Demonstrating the good non-fouling properties of the bioreceptor surface when using APTES silanization.

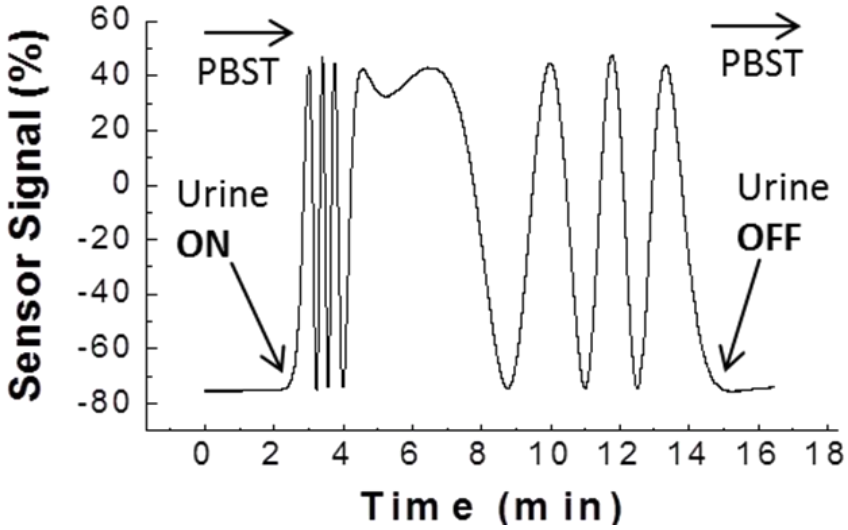

Fig.3.5. Evaluation of the non-specific adsorption of non-spiked urine on the biofunctionalized surface with APTES silane.

After the demonstration of the antifouling properties of the sensor surface, PBST was replaced by non-spiked urine as running buffer to avoid a complex interferometric signal due to the abrupt change of the refractive index of the solution when switching from buffer to urine in bulk. Spiked urine samples with different concentrations of hGH ranging from 0.1 to 1 ng.mL^{-1} were evaluated (Fig. 3.6). A regeneration solution of HCl 100 mM flowed at 40 µL.min^{-1} was employed at 40 µL.min^{-1} to recover the original surface.

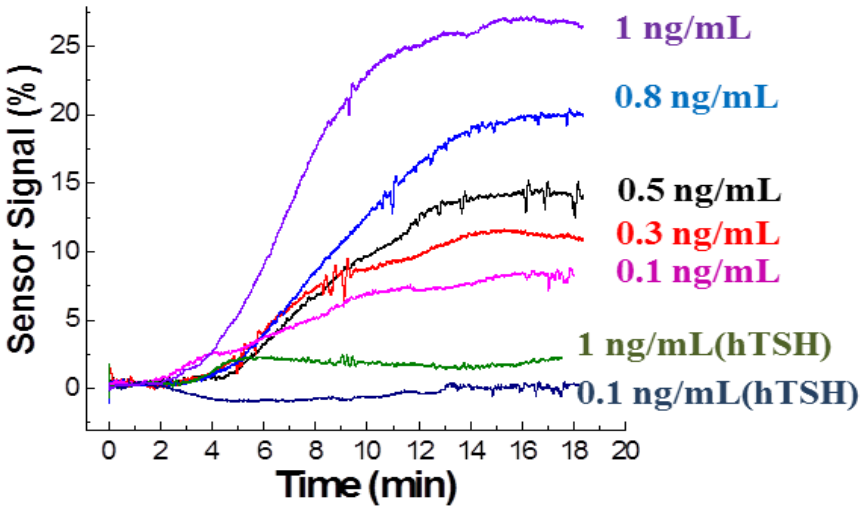

Fig. 3.6 Real-time sensorgram of urine samples spiked with different hGH concentrations and comparison with unspecific hTSH hormone.

In Figure 3.7, we show the phase variation *versus* the hGH concentration in urine. A linear response was obtained for all the range of concentrations evaluated. The LOD was calculated by linear fitting of the data, obtaining a value of only **3 pg mL^{-1}**; this valued is one order of magnitude higher than the one obtained in buffer most likely caused by the partial denaturalization of the antibodies due to the urea present in the urine. The limit of quantification (LOQ), considered as the concentration of target that causes a signal that corresponds to 10 times the N/S of the system, is the lowest concentration that can be experimentally quantified corresponding to **10 pg.mL^{-1}**.

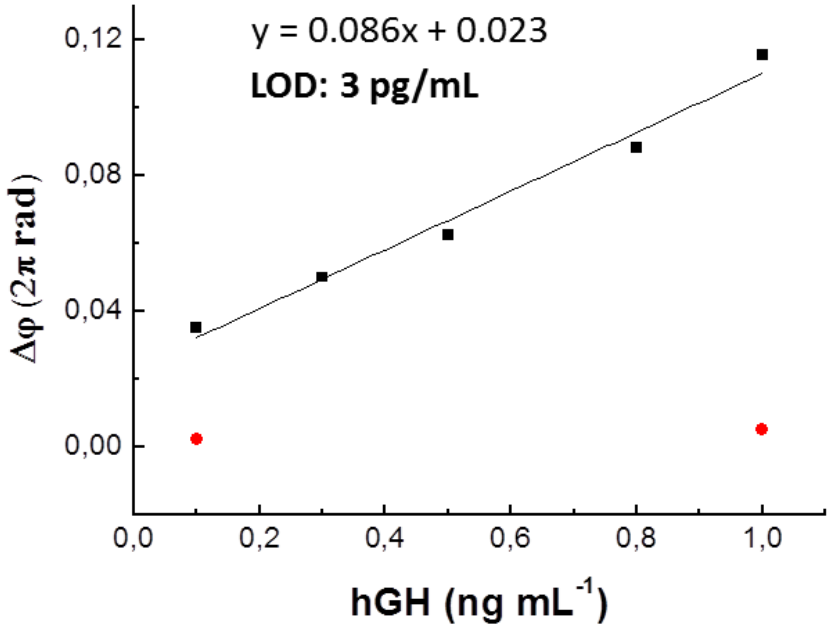

Fig.3.7. Calibration curve of hGH in urine (*black, squares*) in comparison with non-specific hTSH target (*red, circles*).

In addition, we studied the stability of the immobilized antibody during several regeneration process employed for the reusability of the biosensor. After the study of different regeneration buffers such as NaOH, HCL and salts ($MgCl_2$ and NaCl) in different concentrations and flow rates, it was found that HCl 100 mM at 40 µL. min^{-1} disrupted completely the protein-protein interaction. Using this regeneration conditions, we observed that the biosensor response decreases almost 50% after four regeneration cycles (see Fig. 3.8)

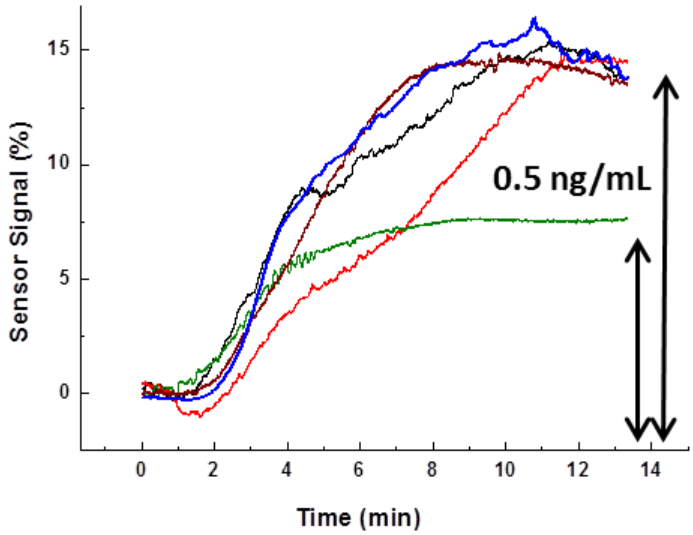

Fig.3.8. Sensorgram of 0.5 ng.mL^{-1} of hGH in urine after the regeneration step with HCl 100 mM. We can observed that the signal decrease 50% after four regeneration cycles.

Optimization of the surface functionalization using PEG silane

An alternative strategy to overcome the problem of biofouling is creating a biocompatible interface with the capability to immobilize biomolecules and avoiding blocking steps. We have studied a new biofunctionalization strategy based on PEG-silane in order to improve the antifouling properties of our receptor monolayer and discover the possibility to immobilize different biorecognition molecules. The first stage involved the study and characterization of a PEG_{600}silane layer which enables the covalent immobilization of antibodies.

PEG-silane Surface Characterization

Surface topography and roughness of the samples functionalised using different PEG-silane concentrations were evaluated using AFM to provide information about the best conditions to obtain a well-packaged silane layer. XPS was carried out in order to corroborate the coupling of the PEG-silane to the silicon

nitride surface and the subsequent immobilization of the bioreceptors over the PEG-silane surface. Finally, the specific adsorption of bacteria in silicon nitride surfaces coated with PEG-silane was analysed with FE-SEM.

Atomic force microscope analysis

Atomic force microscopy is a useful tool for studying the modified surfaces as it provides real-space film morphology and nanostructure. It also provides detailed topographical information about surface features in terms of roughness values of the interfaces. Therefore, various PEG-silane coated substrates resulting from various concentrations (10, 25 and 50 mg mL^{-1}) were evaluated by AFM.

AFM images (2D and 3D) are shown in Fig. 3.9. In a PEG surface obtained for a PEG concentration of 10 mg mL^{-1} (Fig. 3.9b) the roughness increases compared to unmodified silicon nitride (Fig. 3.9a). This may be due to insufficient coverage of the silicon nitride with PEG-silane. Therefore, a PEG-silane concentration of 10 $mg.mL^{-1}$ appears to be low to provide uniform and complete coverage of the silicon nitride surface.

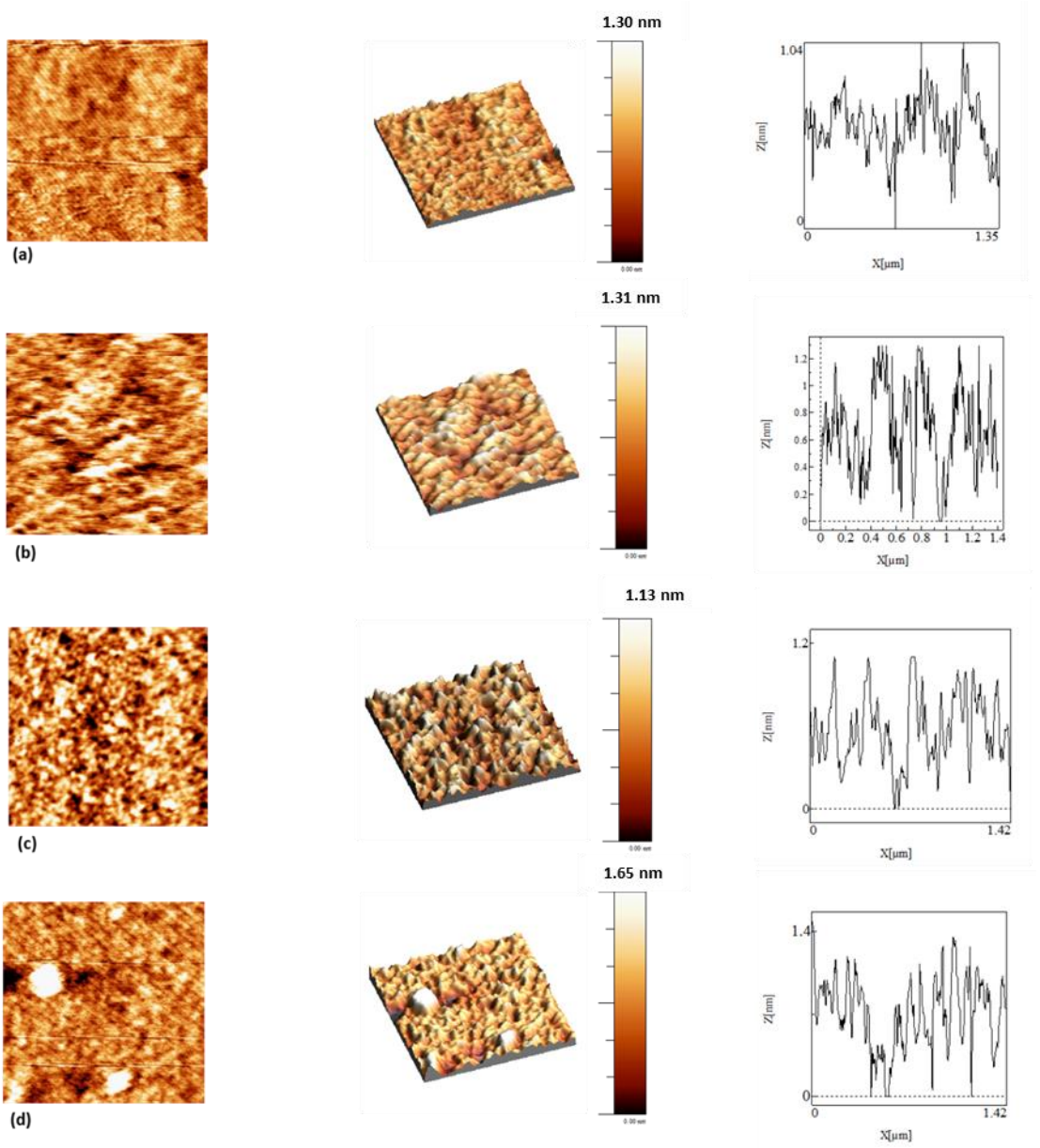

Fig. 3.9. 2D and 3D images of 200 nm scan and section plots of 1.5 µm scans for different PEG-silane concentrations: (a) clean silicon nitride; (b) 10 mg.mL^{-1}; (c) 25 mgmL^{-1}; (d) 50 mg.mL^{-1}.

The homogeneity of the surface in terms of distribution of features and feature size was improved by using 25 mg.mL^{-1} (Fig. 3.9c). A further increase in the PEG-silane concentration to 50 mg.mL^{-1} resulted in larger, agglomerated features (Fig. 3.9d). A comparison between triplicate RMS roughnesses values for substrates coated with PEG-silane at different concentrations can be seen in Fig. 3.10. Surface

roughness increased in substrates coated with PEG-silane in 10 mg.mL^{-1} and 50 mg.mL^{-1}. However, the RMS roughness of 25 mg.mL^{-1} was the most homogeneous.

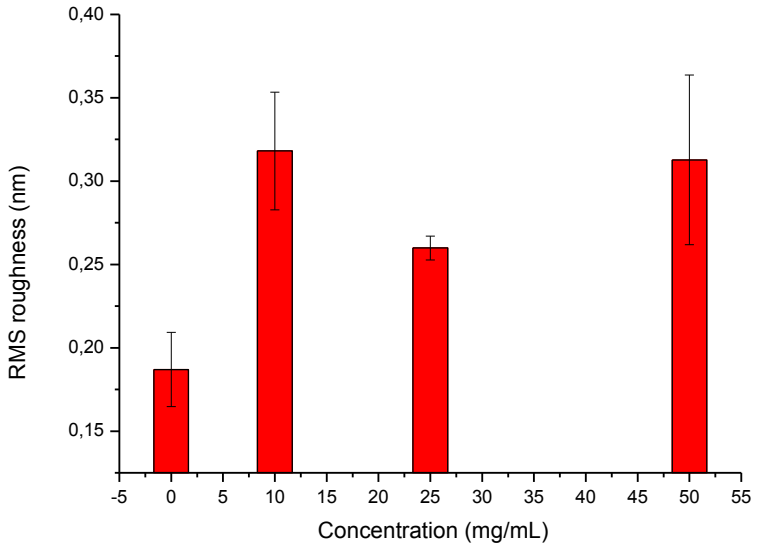

Fig. 3.10. RMS roughness values for clean and PEG-silane silicon nitride surfaces covered with various PEG-silane concentrations.

XPS characterization

A comparison of the survey spectra for untreated Si_3N_4, PEG-silane and antibody modified surfaces illustrated significant changes in carbon, silicon, oxygen and nitrogen peaks, due to the addition of the different molecular layers (Fig. 3.11) [122].

Upon immersion in antibody solutions, the Si_3N_4 is clearly coated with PEG-silane and antibodies, as evidenced by the significant increase of carbon and the decrease of the oxygen and nitrogen contributions from the Si_3N_4 substrate and SiO_2 oxidation layer. These results clearly indicate a complete coverage of the surface with PEG-silane and antibody adsorption.

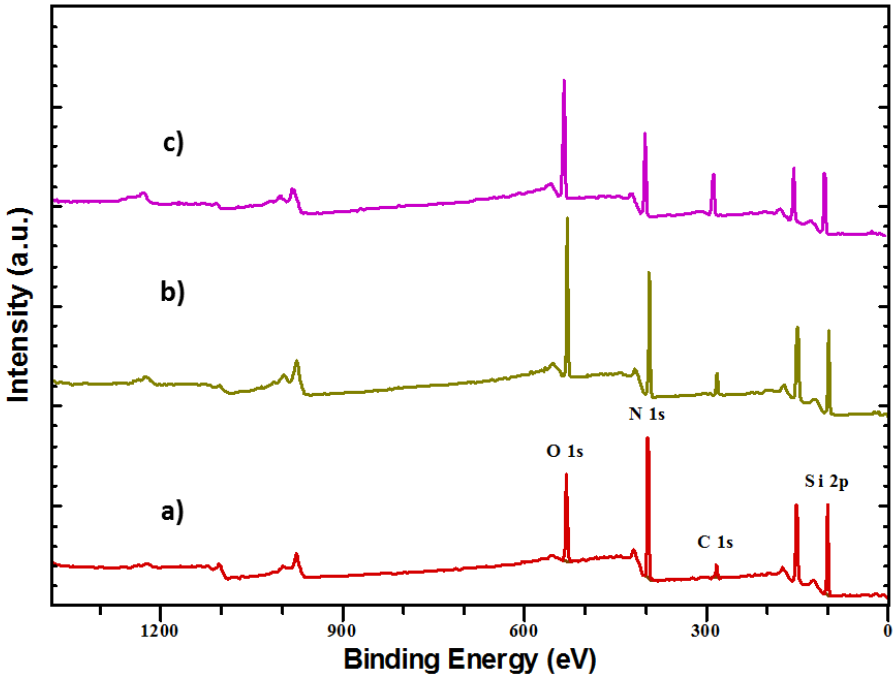

Fig.3.11. XPS survey spectra of: a) silicon nitride, b) silicon nitride coated with PEG-silane and c) antibody coated silicon nitride functionalized with PEG-silane.

The element analysis indicates a remarkable increase of carbon content after immobilization. Carbon increased from 6.2% (silicon nitride) to 20.7% on an antibody coated surface and nitrogen levels are lower on the surface of the sample with PEG-silane and antibody solution (table 5).

Table 5. Elemental composition of Si_3N_4 before and after surface modification with PEG-silane and antibody

sample	Elemental composition (at %)			
	C	N	O	Si
Si_3N_4	6.26	33.62	14.59	45.53
PEG-silane	10.15	26.68	21.86	41.31
Antibody	23.32	22.37	20.7	33

The high-resolution C 1s spectra (Fig. 3.12) show that the C 1s photoelectron peaks are much broader after the sample is immobilised with antibodied. The C 1s

peaks were deconvoluted according to binding energies of carbons in antibody. The first peak was centred at 284.7 (Fig. 3.12Aa) and related to aliphatic carbon (C-C). The second peak at 286.5 eV corresponds to carbon bonded to oxygen group (C-O) (Fig. 3.12Ab) which evidence the PEG-silane presence, and the antibody attachment by the component around 287.5 eV, corresponding to –C (-O)-NH_2 peptide carbon (Fig. 3.12Ac) [123, 124].

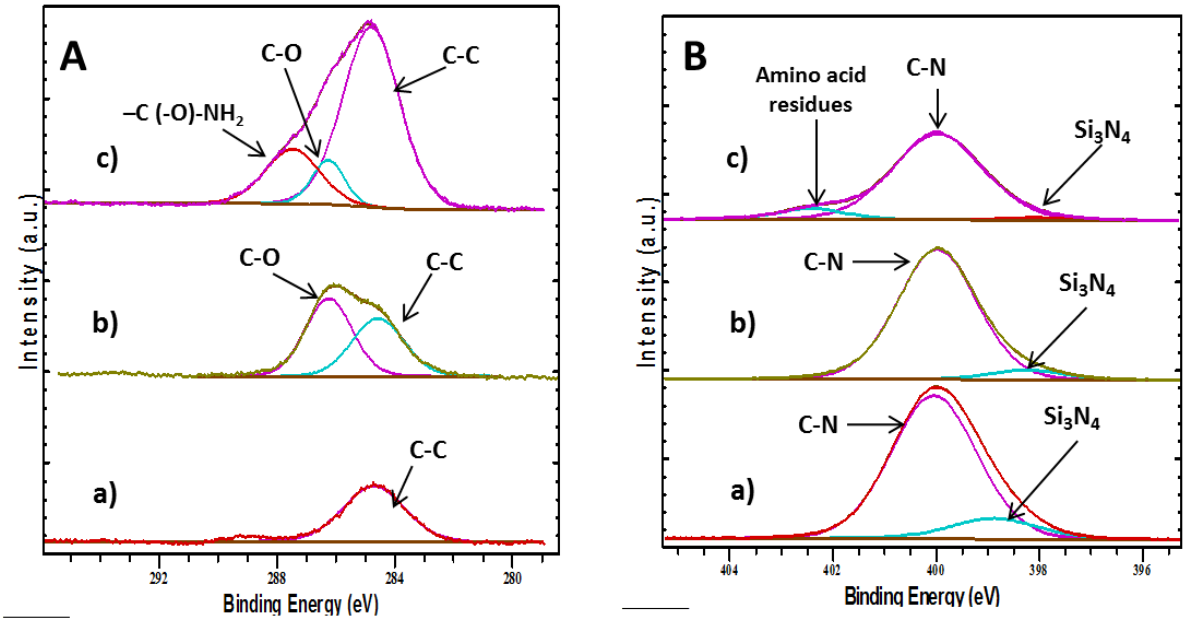

Fig.3.12. XPS high resolution spectra of: A) C 1s, B) N 1s. a) Untreated silicon nitride, b) PEG-silane and c) antibody.

The binding energies of N 1s detected on the samples (close to 400 eV) are typical for organic matrices and are related to C-N bonds [125, 126], at 398.2 eV corresponding to Si_3N_4 (Fig. 3.12Ba). At the same time, the amount of nitrogen decreased on the surface coated with PEG-silane and protein due to complete coverage of the silicon nitride (Fig. 3.12Bb and Fig. 3.12Bc). The component around

402 eV peak was assigned to imide-N, found on the amino acid proteins (Fig. 3.12Bc) [127].

Analysis of bacterial adhesion onto silicon nitride

The nonspecific adsorption of bacteria over the silicon nitride sensor surface coated with PEG-silane was evaluated with *S. aureus, E. coli* and *P. aeruginosa* as representative models of Gram-positive and Gram-negative microorganisms, respectively, since they are common pathogens often identified in nosocomial infections. For this study, Si_3N_4 surfaces treated with PEG_{600}-silane were incubated with a fixed concentration of bacteria (see Chapter 2 for further information). Image acquisitions were performed with FE-SEM. SEM images demonstrated that silicon nitride sensor surface treated with PEG_{600}-silane prevented the bacterial adhesion (Fig. 3.13). The images also showed the unspecific adsorption of bacteria over untreated silicon nitride, where the major adhesion was observed for *S. aureus* (Gram-positive) and a very low adhesion for *P. aeruginosa* (Gram-negative).

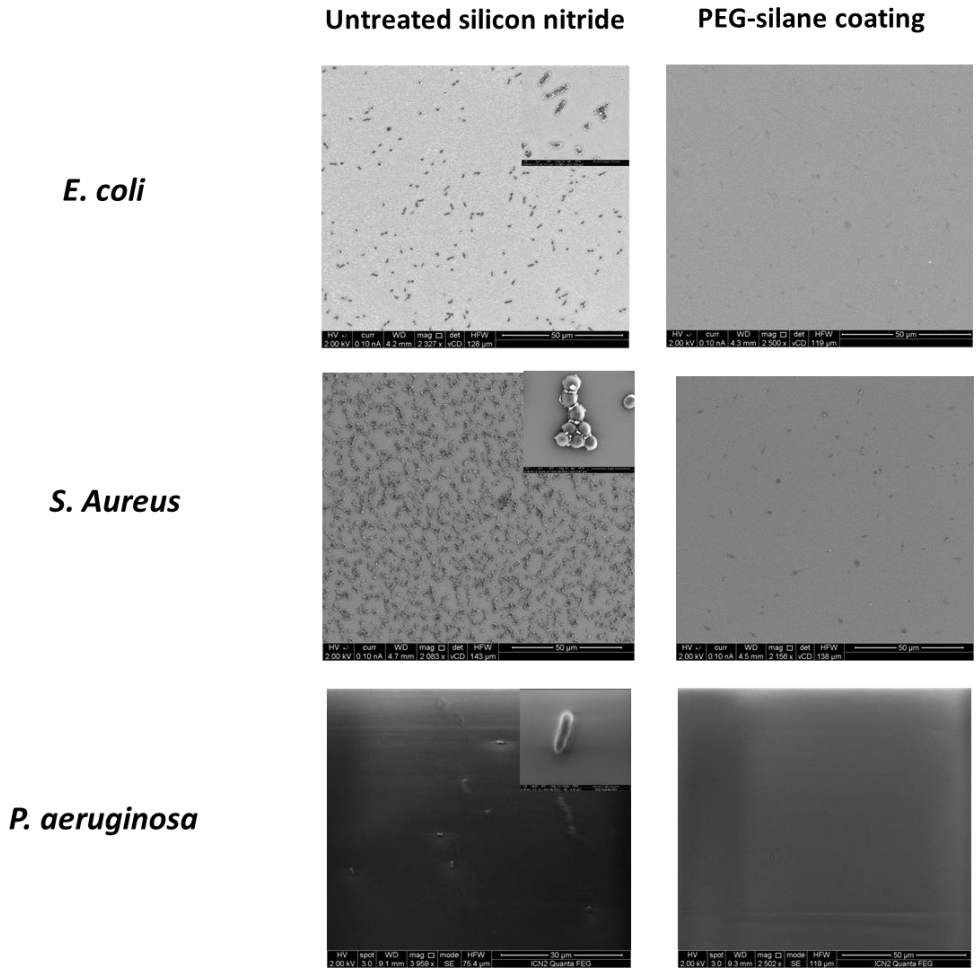

Fig. 3.13. SEM images of the bacterial adhesion in untreated silicon nitride surfaces and treated with PEG-silane

3.1. Conclusions

The BiMW biosensors developed using the CTES and APTES silanization for the immobilization of specific antibodies for hGH 22KDa were evaluated. In the case of the CTES silane, the resulting functionalized surfaces show high performance for antibody coupling. The CTES surface is stable to allow reusability to up to eight detection cycles. Moreover, CTES silanization combined with BiMW sensor showed one of the best LOD reported for a label-free bioassay. However, CTES silanization does not allow to perform direct immunoassays in a complex matrix as urine due to the high nonspecific adsorption of molecules. On the other side, the performance of the BiMW biosensor using APTES silanization for the detection of the hGH hormone

at clinically relevant levels in urine samples has been demonstrated. The results indicate that the BiMW biosensor allows an extreme sensitive evaluation of hGH in pure urine samples in a label-free way. To our knowledge, the established detection limit is the lowest ever reported for a label-free immunoassay in a complex matrix. We then have demonstrated that when combined with a high-quality bioreactor and an appropriate immobilization chemistry, the BiMW device became a high-efficient bioanalytical tool able to perform direct, rapid and cost-effective clinical diagnosis.

Moreover, an overpressured PEG-silane was employed to immobilize the antibodies in silicon nitride sensor surface. The nonspecific bacterial adsorption was successfully eliminated without requiring additional blocking steps. The PEG-silane surface was evaluated using XPS, AFM and SEM to check its performance and its antimicrobial capabilities.

The different biofunctionalizations employed in this Chapter have showed in general good performances in the immobilization of biomolecules. However, these strategies have also some limitations which are summarized in Table 6.

Table 6. Advantages and limitations of the employed biofunctionalization strategies

Functionalization	Advantages	Limitations
CTES	• Water-soluble • Real-time monitoring of the immobilization • Longevity • Good LOD • Easy-to-prepare	• No stable in complex matrices • Need blocking agent (BSA, Gelatin, Casein…) • Random antibody immobilization • Unstable after regeneration process
APTES	• Stable in complex matrices • High surface density • Uniform immobilization surface • Compatible with various functional groups • Good LOD	• Need blocking agents to reduce non-specific adsorptions • Ex-situ immobilization • Low stability • toxic
PEG-silane	• Non-toxic • Longevity • Stable in complex matrices • Not need of blocking steps • Antimicrobial properties • Real-time monitoring of the immobilization • Easy-to-prepare • Stable monolayer	• low surface density of biomolecules • Random antibodies immobilization • No water-soluble

Chapter 4

Rapid identification of nosocomial infections with a bimodal waveguide interferometer biosensor

Abstract: In this chapter, we report the application of the BiMW biosensor for the rapid and label-free detection of bacteria related to nosocomial infections by a direct immunoassay. We demonstrate the quantitative detection with relevant sensitivities of *Bacillus cereus* and *Pseudomonas aeruginosa* in buffer medium and *Escherichia coli* and *Pseudomonas aeruginosa* in real undiluted ascitic human fluid.

4. Rapid identification of nosocomial infection with a bimodal waveguide interferometer biosensor

We studied the unique capabilities of the BiMW sensor to capture frequent nosocomial bacteria in a label-free and high sensitive way. For that, we developed a direct immunoassay in which specific antibodies were immobilized on the sensor area of the device. The first step was the initial evaluation of the biosensor sensitivity for microorganism detection by the recognition of the *Bacillus cereus* (*B. cereus*) in buffer medium as a proof-of-concept. The second step was to check if the sample manipulation before the biosensor analysis influenced in the bacterial lysis. We also investigated if the possible lysis of the bacteria could enhance the sensitivity of the biosensor; samples were mechanically lysed and the detection was compared with the one from non-lysed bacteria. The third step was the evaluation of the BiMW biosensor for bacterial detection in pure human ascitic fluids. For this, we employed *Escherichia coli* (*E. coli*) in real ascites samples, as this is one of the most common bacteria related to ascitic infections. Finally, we studied a PEG_{600}silane layer which enables the covalent immobilization of the bioreceptors and the evaluation of the BiMW sensitivity for *Pseudomonas aeruginosa* detection.

4.1. Detection of Bacillus cereus in buffer solution using CTES silanization

Bacillus cereus is a spore-forming Gram-positive bacillus that exists in soil, marine environments, vegetables and human skin [128-132]. This bacterium is a common pathogen in food poison [133]. Bacteraemia for B. cereus, eye infection, central nervous system, and soft tissue infections [134-140] have been reported in hospital settings. Despite the *Bacillus cereus* is one of the pathogens causing nosocomial bloodstream infections, few works have studied its antimicrobial susceptibility and clinical characteristics [141].

To develop a BiMW biosensor for detecting this bacterium in buffer medium, the transducer surface was biofunctionalized employing the silane CTES which provides the surface with a stable layer of carboxylic groups [142]. The silanized sensor chip was then placed on the experimental set-up where the activation of the carboxylic groups and the subsequent amide biofunctionalization were carried out in-flow, as previously explained. After, PBST was flowed over the sensor surface at a constant flow rate until a stable baseline was reached. The flow rate was 20 $\mu L.min^{-1}$ for the detection of the different concentrations of bacteria. Bacterial samples were introduced into a 250 µL loop and flowed over the sensor surface from low to high concentrations.

Suspensions of *B. cereus* ranging from 70 to 7×10^5 $cfu.mL^{-1}$ were prepared in triplicate in PBST and were sequentially flowed through the sensor. Fig. 4.1 shows the calibration curve corresponding to triplicate measurements for each logarithmic concentration. The lowest concentration of *B. cereus* detected was **70 $cfu.mL^{-1}$** which produced a phase variation of 0.031 × 2π rad. The highest concentration

detected was 7 × 10^5 cfu·mL^{-1} obtaining a phase variation of 1.13 × 2π rad. The specificity of the detection was evaluated by flowing a non-specific bacterium (*E. Coli*) at concentrations of 1×10^3 and 1×10^4 cfu·mL^{-1}. No significant binding was observed for any *E. Coli* concentration, confirming that the signal contribution had come only from specific detection of *B. cereus* bacteria. The theoretical LOD for *B. cereus* detection was calculated from the linear fitting of the representation of the phase variation *vs.* bacteria concentration (inset of Fig. 4.1) obtaining a value of **12 cfu.mL^{-1}**.

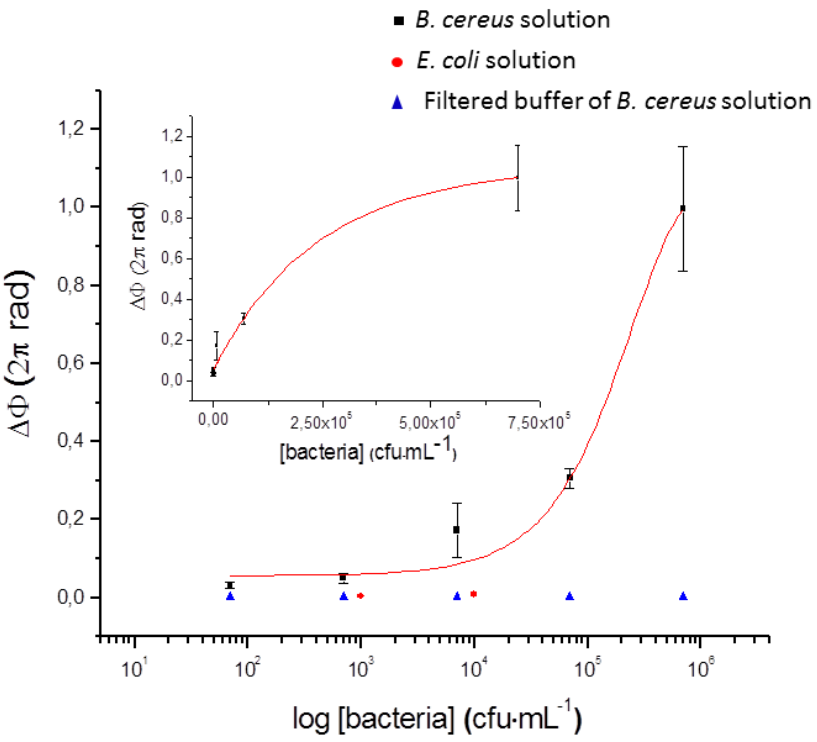

Fig. 4.1. Calibration curve for the detection of triplicate concentrations of *B. cereus* bacteria (*black, squares*) ranging from 70 to 7×10^5 cfu·mL^{-1} in comparison with non-specific bacteria *E. Coli* (*red, circles*) at concentrations of 1×10^3 cfu·mL^{-1} and 1×10^4 cfu·mL^{-1} and concentrations of filtered buffer from *B. Cereus* solutions (*blue, triangles*) ranging from 70 to 7×10^5 cfu·mL^{-1}. In the inset: linear representation of the data for the *B. Cereus* detection.

The pretreatment employed for the purification of bacteria (ultracentrifugation and mixing process explained in Chapter 2) could have lysed the bacteria and liberated antigens from the bacteria membrane that would have erroneously enhance the sensor signal (false positive). In order to check the contribution of this effect, different *B. Cereus* concentrations ranging from 70 to 7×10^5 cfu·mL^{-1} were filtered and each filtered buffer was sequentially injected into the sensor. In Fig. 4.2, it can be observed that the filtered bacterial solutions gave a negligible signal. The results were confirmed by the evaluation of the samples by a nanophotometer (operating at 280 nm) in which absorbance of these solutions was negligible, indicating that the buffer was free of bacteria antigens. These experiments validated our procedure for sample preparation, ensuring that we have only entire bacteria after the purification process.

Representative signals of specific *B. cereus* detection (7×10^3 cfu·mL^{-1}), non-specific *E. coli* (1×10^4 cfu·mL^{-1}) and filtered buffer of a *B. cereus* solution (7×10^3 cfu·mL^{-1}) are shown in Fig. 4.2b. These signals show a phase variation of 0.27 × 2π rad for the detection of 7×10^3 cfu·mL^{-1} of *B. cereus* and a negligible phase variation for the detection of 1×10^4 cfu·mL^{-1} of *E. coli,* which indicated the specificity of the immunoassay.

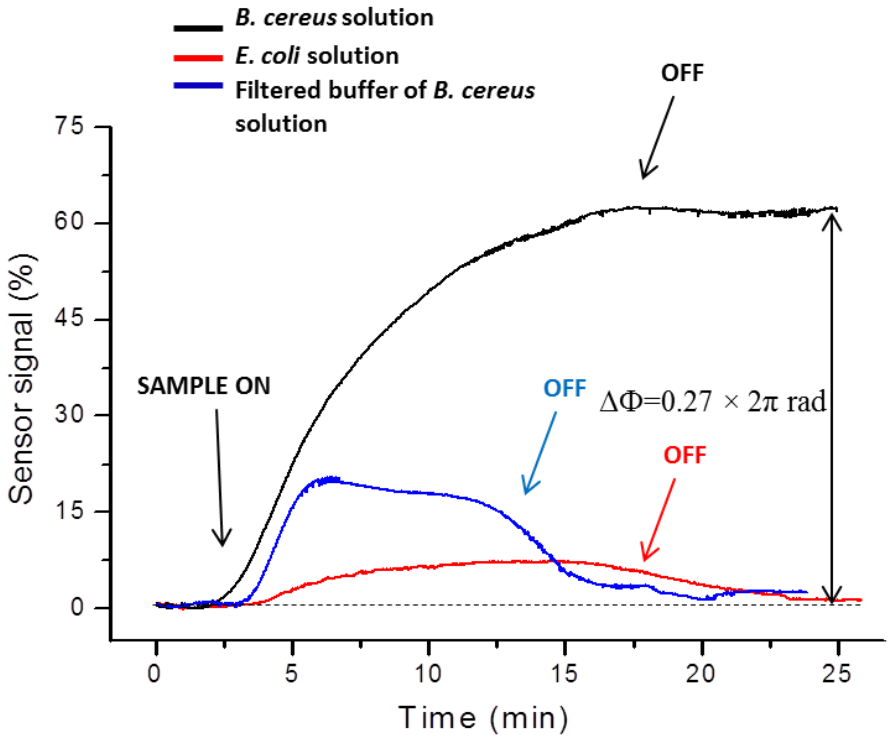

Fig. 4.2. Real-time detection of specific *B. cereus* solution at a concentration of 7×10^3 cfu·mL^{-1} (*black line*), non-specific *E. coli* solution at a concentration of 1×10^4 cfu·mL^{-1} (*red line*) and filtered buffer from *B. cereus* solution at a concentration of 7×10^3 cfu·mL^{-1} (*blue line*) by a direct immunoassay in PBST buffer.

Regeneration cycles (i.e. removal with acid conditions) are commonly employed to reuse the sensor surface in case this might be necessary, either to lengthen the surface life-time, to save costs or to study the reproducibility and optimization of the immunoassay protocols. In our study, after trying different regeneration solutions, the complete removal of the target bacteria was achieved by flowing HCl 100 mM without altering the amount of antibody on the surface, as explained in Chapter 3. As can be seen in Fig. 4.3a, after a regeneration step, the baseline for *B. cereus*, which had been previously detected at a concentration of 7×10^4 cfu·mL^{-1}, was recovered. Under these conditions, stability of the bioreceptor layer was maintained up to 6 cycles due to the limited stability of antibodies after aggressive acid medium treatments. Fig. 4.3b shows the triplicate measurements for the concentrations of 7×10^2 and 7×10^3 cfu·mL^{-1} of *B. cereus*, respectively.

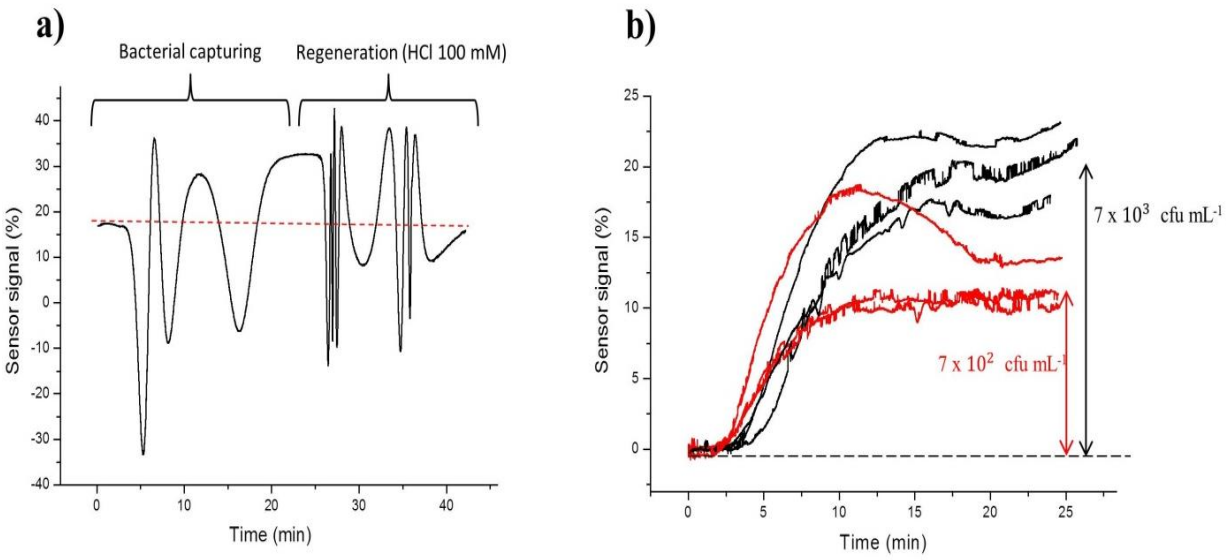

Fig. 4.3. (a) Real-time evaluation of a concentration of 7×10^4 cfu·mL^{-1} of *B. cereus*, followed by regeneration using HCl 100 mM. The dash lines indicate the recovering of the baseline after the regeneration and (b) real-time triplicate measurements of 7×10^2 and 7×10^3 cfu·mL^{-1} of *B. cereus.*

As explained above, the fragmentation of the bacteria can enhance the signal for a determined concentration since dispersion of the bacterial membrane along the medium increases the probability of capturing the antigen targets. We investigated the increase of the sensitivity when bacterial samples were mechanically lysed with sonication treatment before injecting in the biosensor. The lysis of the bacteria was confirmed by evaluating the optical density of the bacterial solutions. The value obtained for non-treated samples at a concentration of 7×10^5 cfu.mL^{-1} was of 0.704, whereas for a lysed bacterial sample of the same concentration the value was an O.D. of 0.221, indicating that the major part of the bacteria in the sample was fragmented. The calibration curve for logarithmic concentrations of lysed bacteria in comparison to the one for whole bacteria is shown in Fig. 4.4. It can be calculated that the sensitivity (in terms of discrimination between different concentrations) is 6% higher for lysed bacteria than for whole bacteria.

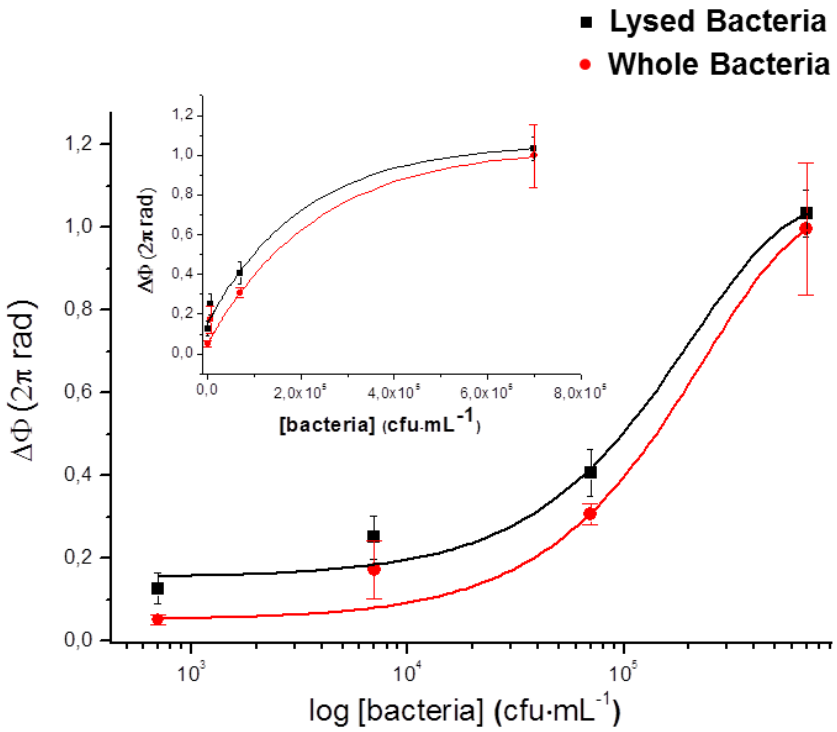

Fig. 4.4. Calibration curves for the concentrations of lysed *B. cereus* solutions ranging from 7×10^2 to 7×10^5 cfu·mL^{-1} in PBST buffer in comparison with the same concentration solutions of whole bacteria. In the inset: linear representation of the data for lysed *B. Cereus* detection and for whole *B. Cereus* detection.

Fig. 4.6 shows a comparison of real-time signals corresponding to the concentrations of 7×10^2 and 7×10^3 cfu·mL^{-1} for lysed and whole bacteria, respectively. The increase in the signal due to the lysis pretreatment was around 35% and 30% for 7×10^2 and 7×10^3 cfu·mL^{-1}, respectively. It is worth mentioning that the sonication treatment is time-consuming, thus the advantage in the increase of the signal must be significant (more than 100%) in order to consider its implementation in this type of analysis. From these findings, it can be concluded that the response increase obtained by sonicating the samples did not justify the incorporation of a pretreatment step which could have delayed the result of the analysis by more than one hour.

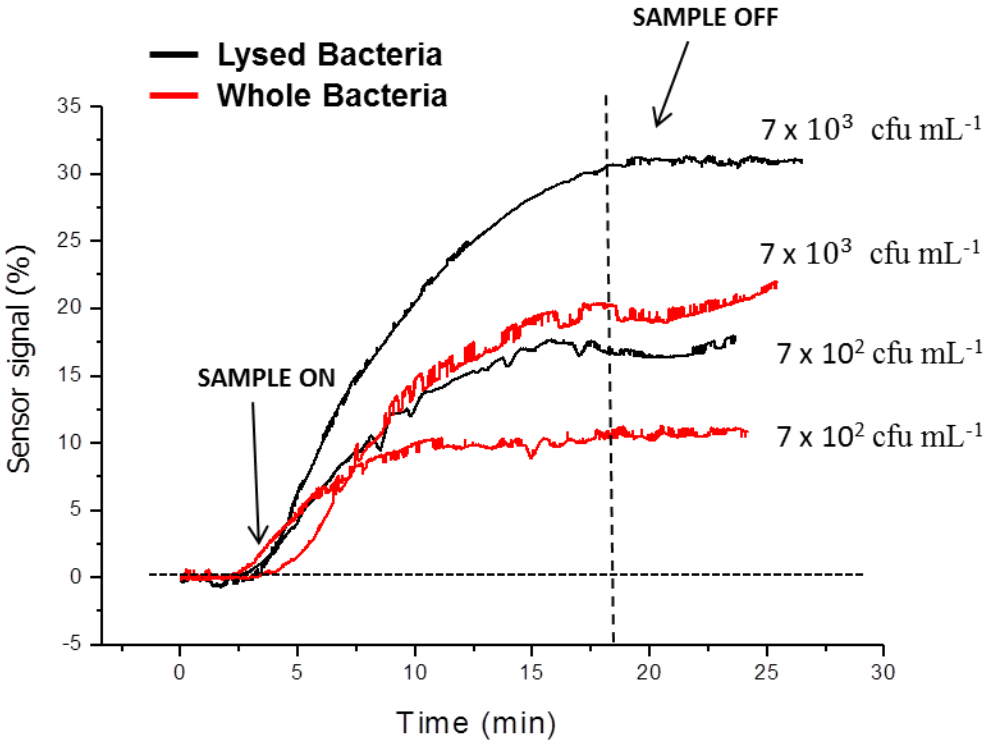

Fig. 4.5. Sensorgram for whole and lysed bacteria in buffer solution for 7×10^2 and 7×10^3 cfu·mL^{-1}.

4.2. BiMW immunosensor for rapid diagnosis of Escherichia coli infections in ascitic fluid.

For the detection of bacterial infections in ascitic fluid, we selected *E. coli* since it is highly common in spontaneous bacterial peritonitis and it is related to nosocomial infections in hospitals [143]. *E. coli* has a size of 2 μm in length and 0.5-1 μm in width and it is a gram-negative, facultative anaerobic and rod-shaped bacterium. The following stage of this study concerned the direct and label-free bacterial detection in 100% human ascitic fluid using the BiMW biosensor. As previously described, this analysis can become especially complex due to interferences and undesired non-specific adsorption of matrix components present in the ascitic fluid. As listed in Chapter 2, the ascitic fluid employed in this work contained concentrations of proteins in the same range (20 mg·mL^{-1}) as serum or plasma (60-80 mg·mL^{-1}). In addition, the high cell content of ascitic fluid (1.3×10^5

cell·mL^{-1}) represented another source of potential non-specific adsorptions. Therefore, it is clear that the detection of bacteria in undiluted ascitic fluid samples is a complex challenge not solved before for optical label-free immunosensors.

E. coli concentrations ranging from 40 cfu.mL^{-1} to 4 × 10^4 cfu.mL^{-1} were prepared in triplicate by spiking the ascitic fluid with different amounts of the stock solution. PBST was employed as running buffer and different concentrations of spiked ascitic fluid were flowed through the channel of the biosensor with a flow rate of 10 µL·min^{-1} for the detection of the different concentrations of *E. coli*. The sensor surface was then regenerated by injecting HCl 100 mM in order to break the bacteria-antibody interaction at 30 µL.min^{-1}, to be able to reuse the biosensor. Assays with PBST as running buffer resulted in good repeatability until the seventh cycle.

The calibration curve for triplicate measurements of each concentration is shown in Fig. 4.5. The phase variation for the highest concentration evaluated (4 × 10^4 cfu·mL^{-1}) was 2.5 × 2π rad and for the lowest concentration (40 cfu·mL^{-1}) was 0.21 × 2π rad. The LOD calculated from the fitting of the linear representation of *E. coli* detection (in the inset) was only **4 cfu·mL^{-1}**.

To evaluate the contribution of the sample matrix to the signal, pure ascitic fluid was injected into the biosensor. Injection of undiluted ascitic fluid in triplicate resulted in small and constant background signals (0.10, 0.15 and 0.13 × 2π rad). After each evaluation of the ascitic fluid non-specific adsorptions, bioreceptor surface was cleaned by injecting the regeneration solution before a new injection. Fig. 4.5 shows the specific calibration curve compared to the average of the phase variation (0.13 ±

0.02 × 2π rad) obtained for the pure ascitic fluid detection. As can be observed, the signal due to the non-specific adsorption of the ascitic fluid matrix was negligible when comparing with the specific *E. coli* signal.

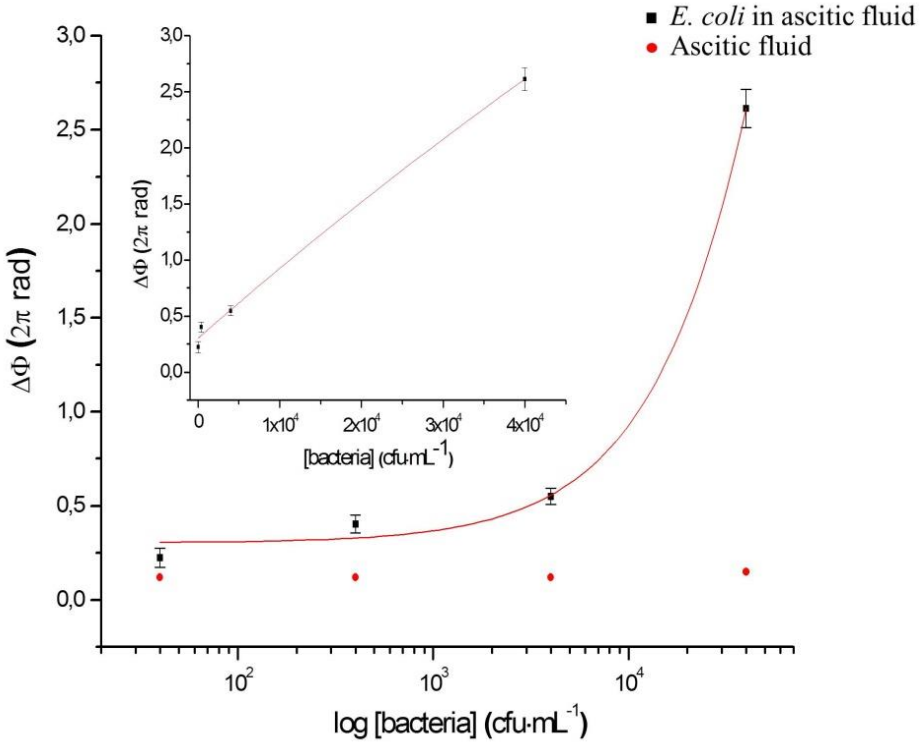

Fig. 4.6. Calibration curve for triplicate spiked concentrations of *E. coli* ranging from 40 and 4 ×10^4 cfu·mL^{-1} in ascitic fluid (*black, squares*) and unspecific detection of pure ascitic fluid. In the inset: linear representation of the data for *E. coli* detection.

Fig. 4.6a shows a representative real-time signal for the detection of a spiked concentration of *E. coli* of 4 ×10^3 cfu·mL^{-1} in human ascitic fluid. The real-time measurement of pure ascitic fluid is shown in Fig. 4.6b. An increase of the resulting phase variation for the *E. coli* spiked sample can be observed, indicating specific detection of the bacteria. In this experiment, the signal is not only due to the specific bacteria detection but to the homogeneous refractive index variation caused by the ascitic fluid. It must be noted that signals are not starting in the same point of the

transmission curve; while the signal due to the ascitic fluid itself is starting close to the quadrature point (maximum sensitivity point for a BiMW sensor), the signal due to the spiked ascitic fluid is starting close to the maximum of the transmission curve (minimum sensitivity point for a BiMW sensor). It is likely caused by the regular tolerances of the different processes as the transducer fabrication at Clean Room facilities and the biofunctionalization protocol.

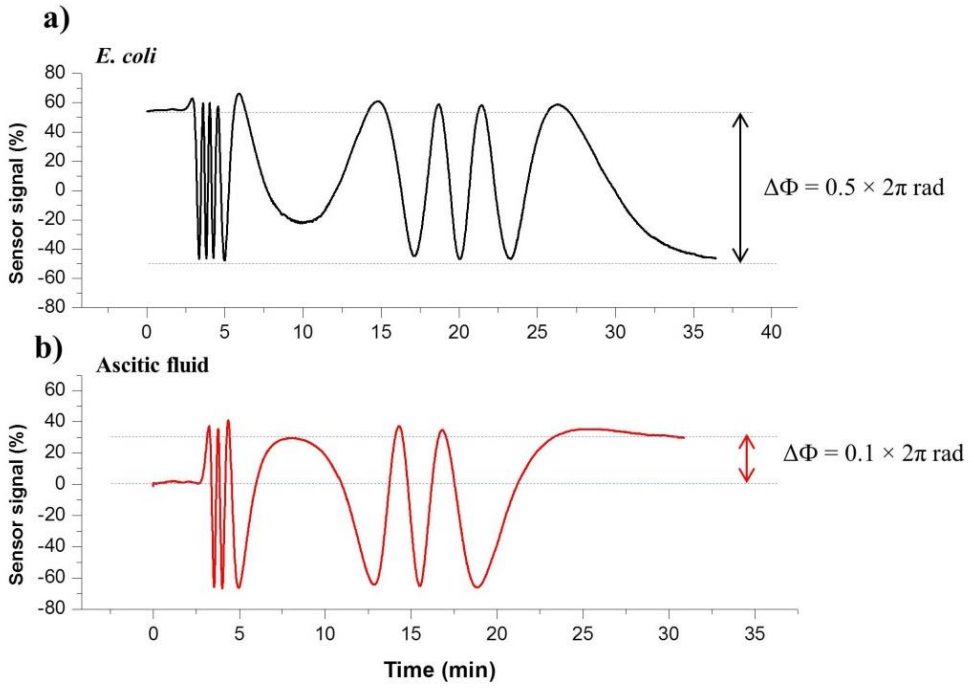

Fig. 4.7. Real-time measurements of ascitic fluid: a) spiked with *E. coli* at a concentration of 4 ×10^3 cfu.mL^{-1} and b) pure ascitic fluid.

4.3. Immunoassay for the detection of *Pseudomonas aeruginosa*

Pseudomonas aeruginosa contributes to 11% of all nosocomial infections resulting in high mortality and morbidity rates. It is a non-fermenter Gram-negative organism which affects especially immune-compromised individuals. The sites of colonization are kidney, urinary tract and upper respiratory tract. It is a cause of

surgical and wound infections, UTI, cystic fibrosis and bacteraemia. *P. aeruginosa* is a rod-shaped 1.5-3 µm in size that poses serious treatment issues because of the high intrinsic resistance level due to the very poor permeability of this bacillus (*P. aeruginosa* has most of its pores closed) and to the reduction of an external membrane protein expression that reduces the alternatives of drug treatment [10]. The modes of transmission of *P. aeruginosa* are common reservoirs including breast pump, incubators, sinks and hands of hospital staff and hand soaps.

The BiMW sensor was biofunctionalized using PEG-silane with the optimal conditions obtained by AFM and XPS characterization (see Chapter 3). The functionalized chip with PEG-silane was located in the experimental set-up. Then, the carboxyl groups of the PEG-silane surface were activated with a solution of 0.2 M EDC/0.05 M sulfo-NHS in MES buffer. Next, a polyclonal antibody against *P. aeruginosa* solution in 10 mM PBST at a concentration of 50 $\mu g.mL^{-1}$ was injected over the freshly activated surface (see Fig.4.7). The antibody immobilization produces a phase variation of 7.7 x 2π rad, which is almost similar to the one obtained with the CTES silanization. PBST was circulated over the sensor surface at a constant flow. Bacterial samples were placed into a 150 µL loop and flowed over the sensor from low to high concentrations at a flow rate of 20 $\mu L.min^{-1}$.

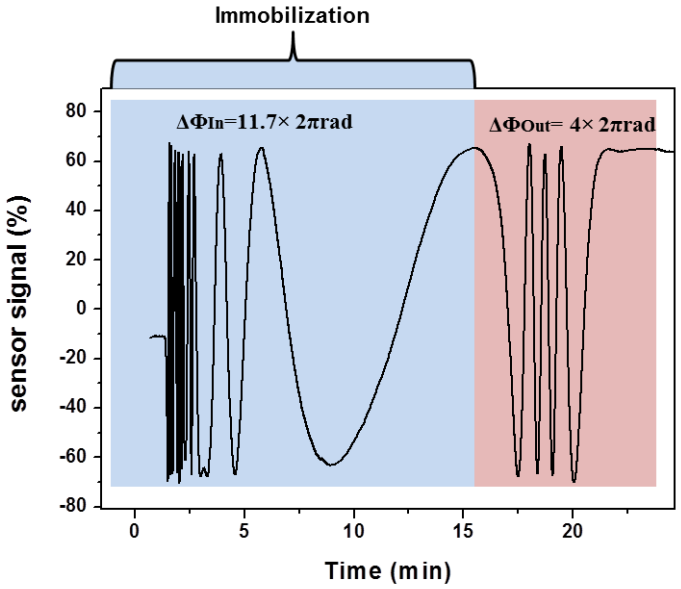

Fig. 4.8. Real-time immobilization of *Pseudomonas* antibody onto the sensor surface

P. aeruginosa samples were flowed through the sensor in a range from 800 to $1x10^7$ cfu.mL^{-1} in buffer running (PBST). The calibration curve corresponding to triplicate measurements for each concentration was performed, where the lowest concentration produced a phase variation of 0.074 x 2 πrad and the highest concentration gave a phase variation of 1.6 x 2 πrad (see Fig.4.8). The LOD obtained from the fitting of the linear regression of *P. aeruginosa* detection (inset Fig.4.8) was **170 cfu.mL^{-1}**. This LOD obtained in this immunoassay is higher than the obtained in the methodology where we employed APTES silanization. This may be due to low surface density of biomolecules. But, the LOD is relevant for the levels of detection required in a bacterial infection. Moreover, this LOD has the value required for ideal bacterial biosensor.

The specificity of the immunoassay was evaluated by flowing *E. coli* at concentrations from 1 x 10^5 to 1 x 10^7 cfu.mL^{-1}. No signal was observed for any

concentration, confirming that the signal contribution was coming only from the specific detection of *P. aeruginosa*.

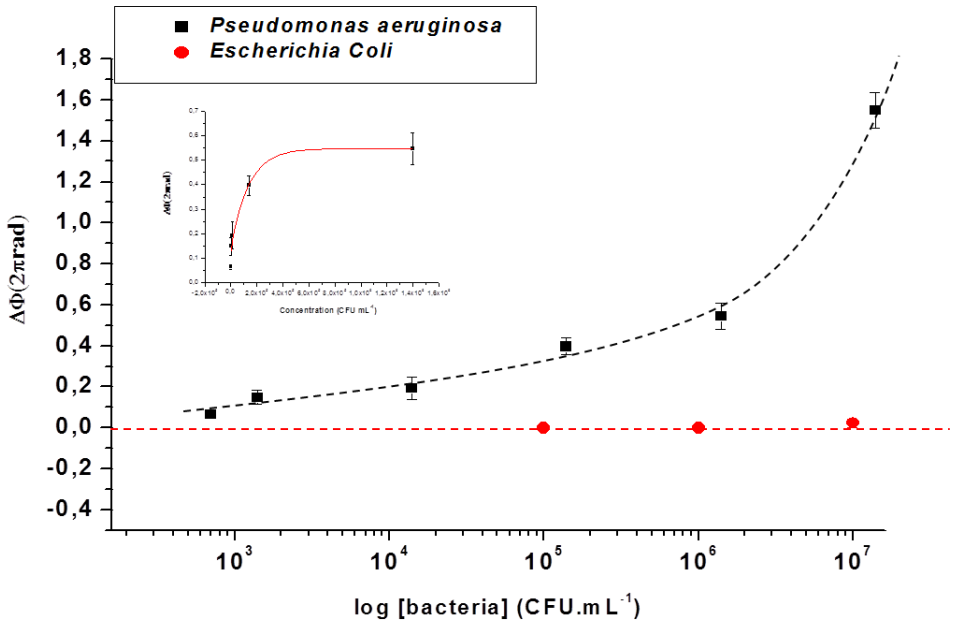

Fig.4.9. Calibration curve from triplicate concentrations of *P. aerugionosa* (*black squares*) and unspecific bacteria *E. coli* (*red circles*). In the inset: linear representation with exponential fitting of the *P. aeruginosa* detection.

Representative signals of specific *P. aeruginosa* detection (1.6 x 10^5 cfu.mL^{-1}) and non-specific *E. coli* (1 x 10^5 cfu.mL^{-1}) are shown in Fig.4.9a. These signals show a phase variation of 0.4 x 2π rad for the detection of *P. aeruginosa* and an insignificant signal from the *E. coli* sample, indicating the specificity of the immunoassay. Furthermore, we demonstrate that the interaction between the antibodies and the captured bacteria can be interrupted (see sensorgram in Fig.4.9b) by the simple injection of 100 mM HCl for 1 minute, making the biosensor reusable up to 6 cycles using the same bioreceptor layer.

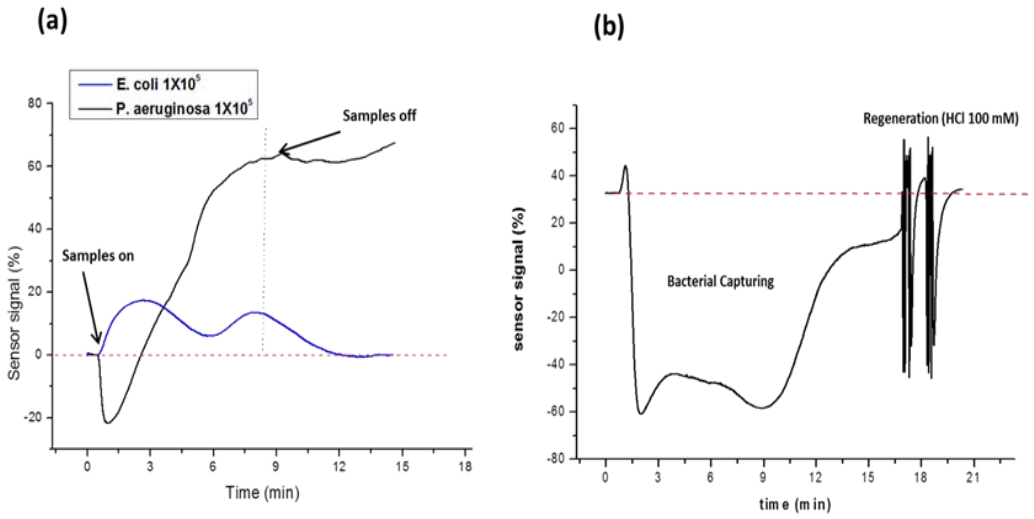

Fig. 4.10. (a) Real time evaluation of *P. aeruginosa* and *E. coli* (negative control) and (b) sensorgram of *Pseudomona* detection, followed by regeneration using HCl 100 mM (1 min) (*dash lines indicate the baseline*).

Figure 4.10 shows the assessment of the stability of the biosurface after the regeneration cycles. The signal for the specific detection significantly decreases when HCl 100 mM is injected for three times. However, the signal is recovered if HCl 100 mM is replaced by NaOH 50 mM as regeneration buffer. The decreasing of the signal due to a residual bacteria build-up and a change in buffer conditions, for instance, adding more salt or change the pH can remove these residues, and recover the baseline. This regeneration buffer must be stringent enough to remove the analyte but the mild enough to keep the biorecognition molecule intact.

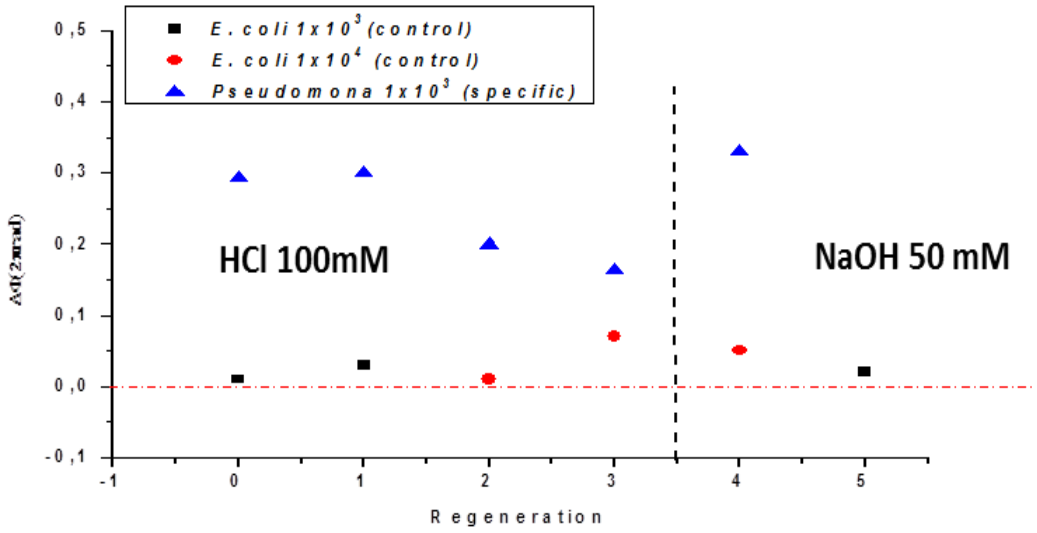

Fig. 4.11. Response of 1×10^3 cfu mL^{-1} specific *Pseudomonas* (*blue triangles*) in comparison with different concentration of unspecific of *E. coli* (*black squares and red circles*) after regeneration with HCl 100 mM and NaOH 50 mM.

4.3.1. Proof of concept of *Pseudomonas aeruginosa* detection in ascitic fluid using a PEG_{600}-silane sensor surface

For the direct detection of Pseudomonas in ascitic fluid using the BiMW biosensor combined with a PEG_{600}silane surface, solutions ranging from 7×10^2 cfu.mL^{-1} to 1×10^6 cfu.mL^{-1} were prepared by spiking the ascitic fluid with different amounts of the stock solution. PBST was employed as running buffer and different concentrations of spiked ascitic fluid were flowed through the microfluidic system. The sensor surface was then regenerated by injecting HCl 100 mM. The calibration curve for measurements of each concentration is shown in Fig. 4.11. The phase variation for the highest concentration evaluated (1×10^6 cfu.mL^{-1}) was 0.86× 2π rad and for the lowest concentration (700 cfu.mL^{-1}) was 0.68 × 2π rad. *Escherichia coli* (red circle) was employed as negative control. The specific detection of *Pseudomonas* showed a 65% of signal increased when compared with the signal

obtained for the same concentration of unspecific *E. coli*. Unspecific signal for the *E. coli* sample was related to same degree of cross-reactivity with the employed antibody. The limit of quantification showed the potential of this biosensor for detecting a concentration of 700 cfu.mL^{-1}. This limit quantification is the most high to found with the BiMW devices and is due to low surface density and some effect caused by the ascitic fluid. But the minimum concentration of bacteria detected is in the levels required in order to bacterial detection in a nosocomial infection.

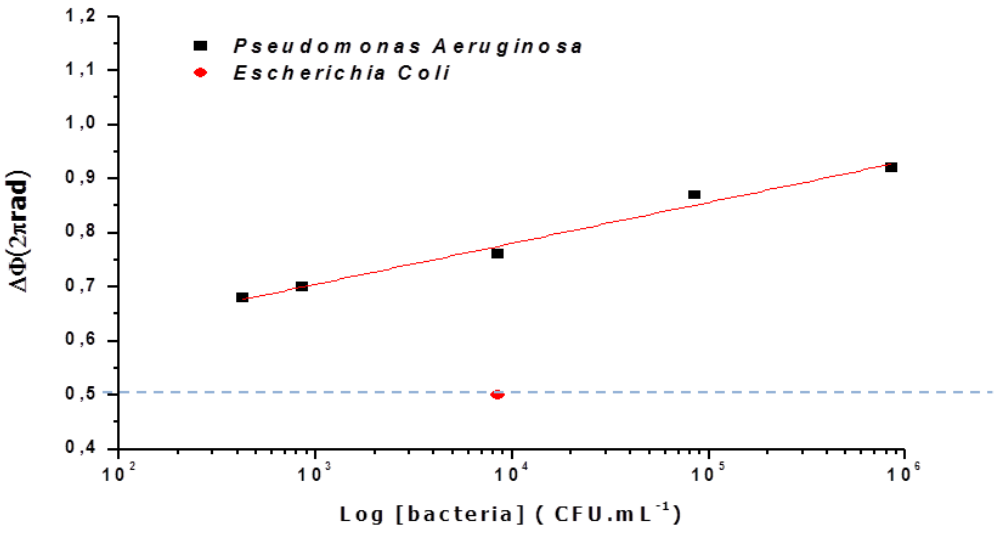

Fig. 4.12. Calibration curve of the specific detection of *Pseudomonas aeruginosa* (*black squares*) in comparison with the unspecific detection of *E. coli* (*red circles*) both in ascitic fluid.

Fig. 4.12a shows representative real-time responses for the detection of a spiked concentration of *Pseudomonas* of 1 ×10^5 cfu.mL^{-1} in human ascitic fluid. The real-time evaluation of *E. coli* in pure ascitic fluid is shown in Fig. 4.12b. An increase of the resulting phase variation for the *Pseudomonas* spiked sample can be observed, indicating the specific recognition of these bacteria. In this experiment (as in the case of *E. coli* detection), the signal is not only due to the specific bacteria

recognition but to the homogeneous refractive index variation caused by the ascitic fluid. It must be noted that signals are not starting in the same point of the transmission curve; while the signal due to the *E. coli* sample is starting close to the quadrature point, the signal due to the *Pseudomonas* sample is starting close to the maximum of the transmission curve.

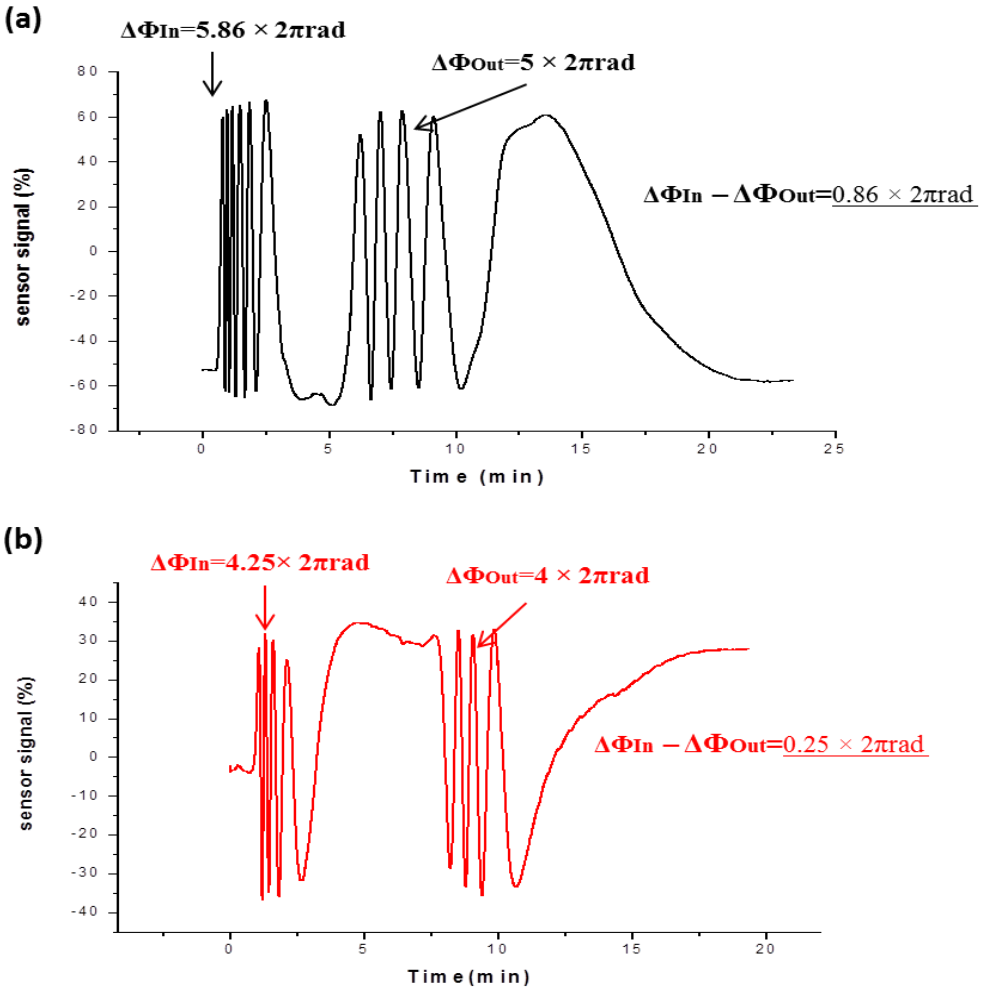

Fig. 4.13. Real-time measurements of ascitic fluid (a) spiked with *Pseudomonas* at a concentration of 1×10^5 cfu·mL^{-1} and (b) spiked with *E. coli* at 1×10^4 cfu·mL^{-1}.

4.4. Conclusions

In this chapter we have demonstrated a BiMW biosensor for the rapid and label-free detection of nosocomial pathogens. We are able to detect extremely low bacterial concentration in a label-free and fast way. The superior sensitivity of the BiMW device when comparing with other label-free biosensors can be attributed to the long interaction length (15000 μm) of the propagating light in the sensor area of the waveguide, where the biorecognition event is taking place together with the interferometric detection. It must be highlighted that, despite the high content of proteins and cells in the ascitic fluid, exceptional LOD was 4 cfu.mL^{-1} obtained for the detection of *E. coli*, reaching the criteria to directly evaluate this type of bacterium in ascites samples (from 10 to 10^4 cfu.mL^{-1})

For *Pseudomonas* detection, we present a high sensitive BiMW biosensor able to identify bacteria causing nosocomial infections due to the employment of a surface based on PEG-silane with excellent antimicrobial activity. With this biofunctionalization strategy based on PEG-silane the non-specific bacteria adsorption was successfully eliminated, avoiding extra blocking steps. Then, a *P. aeruginosa* BiMW immunosensor was fabricated based on this antimicrobial surface and the resulting BiMW biosensor showed a high specificity and selectivity with a good LOD of 170 cfu·mL^{-1}. It is expected that this strategy for fabricating antimicrobial surface using overpressure curing can be employed in a general way when developing silicon photonic biosensors.

Also, the results presented in this work show the great potential of the BiMW technology in combination with a PEG_{600}-silane interface to provide a label-free, rapid, stable, reusable, selective and specific sensor for the identification of

nosocomial pathogens.The BiMW technology could be employed for the label-free and cost-effective identification of the most frequent bacteria present in ascitic fluid. Moreover, this technology could be easily used in clinical settings to facilitate early bacterial diagnostics thereby improving patient prognosis and reducing the costs associated with medical complications in hospitalized patients.

Chapter 5

Rapid detection of multidrug-resistant bacteria using a bimodal waveguide biosensor

Abstract: In this chapter, we used the bimodal waveguide interferometer biosensor for the detection of genes and proteins associated to multidrug resistances. The strategy has been evaluated for an aptamer specific for MRSA bacteria, allowing their direct and rapid identification, and the discrimination between bacteria of the same species. Besides, we have employed the BiMW sensor for the evaluation of multi resistant genes by detecting directly the genomic bacteria DNA without PCR amplification.

5. Rapid detection of multidrug-resistant bacteria using bimodal waveguide biosensor

Various mechanisms exist for bacteria to acquire and spread resistance. Bacteria acquire resistance by exchanging genes or genetic elements with other bacteria of the same species. It is possible that bacteria transfer these resistance genes to other species, and this shuffling of genes takes places within a particular specie of bacteria; but the transfer between different species has brought multi-drug-resistant strains of bacteria. Indeed, the use of broadband antibiotic in hospitals was intended to enforce a germ-free environment but, sadly, the widespread misuse of drugs has increased the number of multiresistant bacteria [144].

These superbugs include methicillin resistant *S. aureus* which has resulted in an increase in infections caused by Staphylococci [145, 146]. Another threat is *Escherichia coli;* this superbug is genetically resistant to a last-resort antibiotic. Moreover, the gene responsible for this resistance could be transferred to other species of bacteria, including *Pseudomonas* and *Klebsiella*. These bacteria carry multiple resistance elements, including extended-spectrum beta-lactamases or carbapenemases that confer resistance to broad-spectrum cephalosporins and carbapenems [147, 148]. As a consequence, treatment of these infections can be extremely difficult, and there may be associated a high mortality. As the evolution of

new strains of superbugs that are resistant to multidrug continues, a biosensor approach able to directly detect and understand the interactions between them, could help in the rapidly resistance identification in order to provide the correct treatment and can also help in the development of new antibiotics.

5.1. An aptasensor for the detection of methicillin-resistant *Staphylococcus aureus* (MRSA)

Methicillin-resistant *Staph* is a leading pathogen associated with serious hospital diseases [149-152]. MRSA causes a range of illnesses, from skin and wound infections to pneumonia and bloodstream infections that can cause sepsis and death. MRSA has recently been found to be the main cause of HAI which in 2011 caused 85,461 invasive infections leading to mortality in 15% of those infected [3]. MRSA is resistance to methicillin and related antibiotics (e.g. nafcillin, oxacillin) and resistance to cephalosporins are of concern. Rapid detection of MRSA infection in humans is critical to implement a suitable treatment to reduce morbidity and mortality [151].

Prevalence in MRSA infection underlies in its resistance mechanism. Primarily, acquisition of *mecA* gene confers resistance in *S. aureus* to methicillin. This gene encodes for the production of a reduced-affinity penicillin-binding protein 2a (PBP2a) [153-155]. The low binding affinity of PBP2a to beta-lactams enables peptidoglycan cell wall synthesis in MRSA, despite the presence of lethal concentration of methicillin [13, 156].

Chapter V

We have studied the unique capabilities of the BiMW biosensor to capture MRSA bacteria using an aptamer in order to discriminate between multidrug-resistant *Staphylococcus aureus* and susceptible *Staphylococcus aureus.*

We have employed aptamers, which are single-strand DNA or RNA molecules artificially built by SELEX method (see Chapter 1) which work as a randomized library of molecules by following three simple steps: complex formation, separation and amplification (Fig. 5.1). Aptamers can be generated against a broad range of targets, from small metal ions to whole cells. They And have several advantages over antibodies, such as that are easy to prepare, have no batch variation, are easy to modify, are stable, and most important, they are non-immunogenic [157-159]. Of course, aptamers are not without their disadvantages. Their structure depends on solution conditions, few aptamers have a good selectivity, and they are easily degraded in complex media as blood or serum.

For our study we have employed an aptamer with 70 nucleotides that was selected from a randomized 32-mer library against PBP2a MRSA protein.

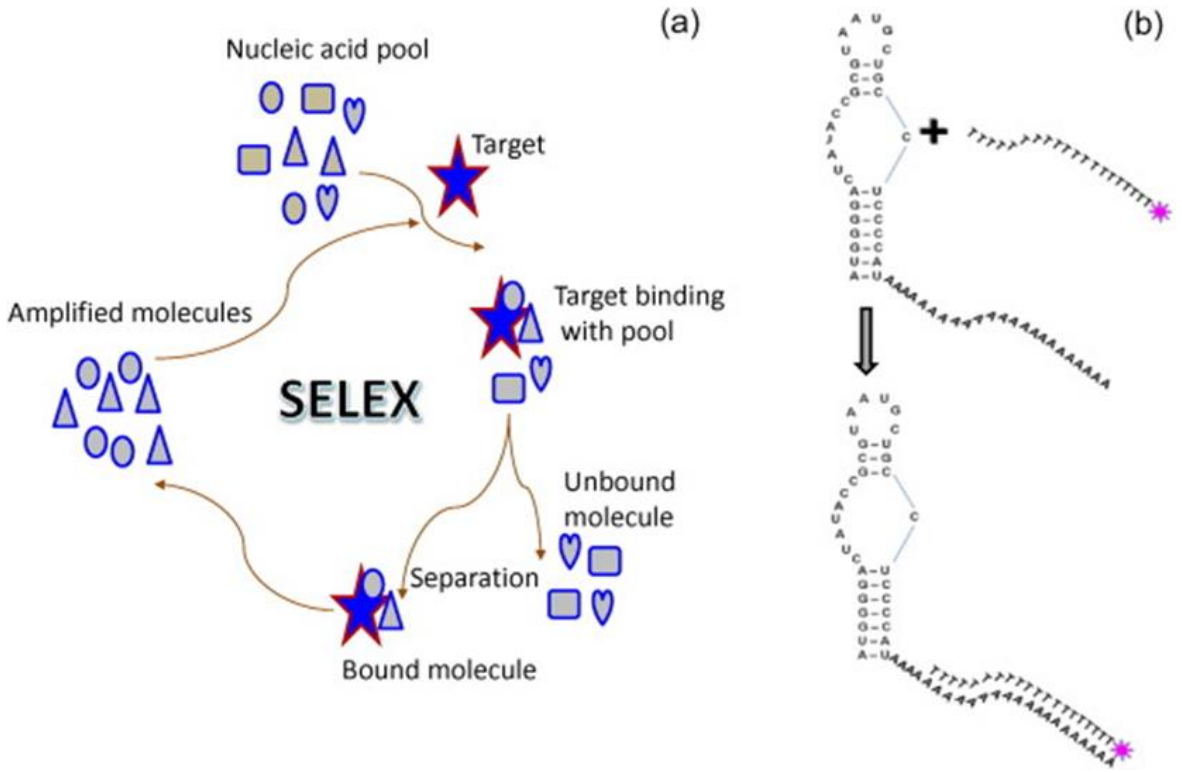

Fig. 5.1. (a) SELEX involves three steps including complex formation, partition and amplification. (b) Aptamer structure [157].

For the MRSA detection, an ex-situ immobilization using PEG-silane surface was employed. First, the carboxyl groups on the sensor surface were activated with a solution of 0.4 M EDC/0.1 M sulfo-NHS in MES buffer for 3 hours. Aptamer against *MRSA* was resuspended and folded by manufacturer's indication for an optimal binding. An aptamer solution in 1mM $MgCl_2$, 10 PBS at a concentration of 2 µM was incubated over the surface sensor overnight at room temperature. Finally, the chip was washed with PBS and water, and dried with a nitrogen stream. PBS was circulated over the sensor surface at a constant rate. Bacterial samples were placed into a 150 µL loop and flowed over the sensor from low to high concentrations with a flow rate of 20 µL min^{-1}. The interaction of MRSA with the aptamer was broken by flowing a dissolution of 0.025 M HCl for 1 min, making probes available for consecutive measurements.

In order to evaluate the non-specific binding of other proteins and the specific binding of the PBP2a protein to the aptamer, the bimodal waveguide chip was covalently biofunctionalized with the aptamer using the same PEG-silane protocol described in Chapter 2. The capability of the aptamer to detect PBP2a protein was evaluated by using two different concentrations: 500 ng.mL^{-1} and 100 ng.mL^{-1}. As negative control we employed a protein of the cell wall corresponding to the tuberculosis bacteria at 500 ng.mL^{-1} and 5 µg.mL^{-1} in buffer solution (Fig 5.2). These concentrations were used because are ten times higher than the employed with the specific PBP2a protein and it was a qualitative experiment in order to demonstrate the specificity of the aptamer.

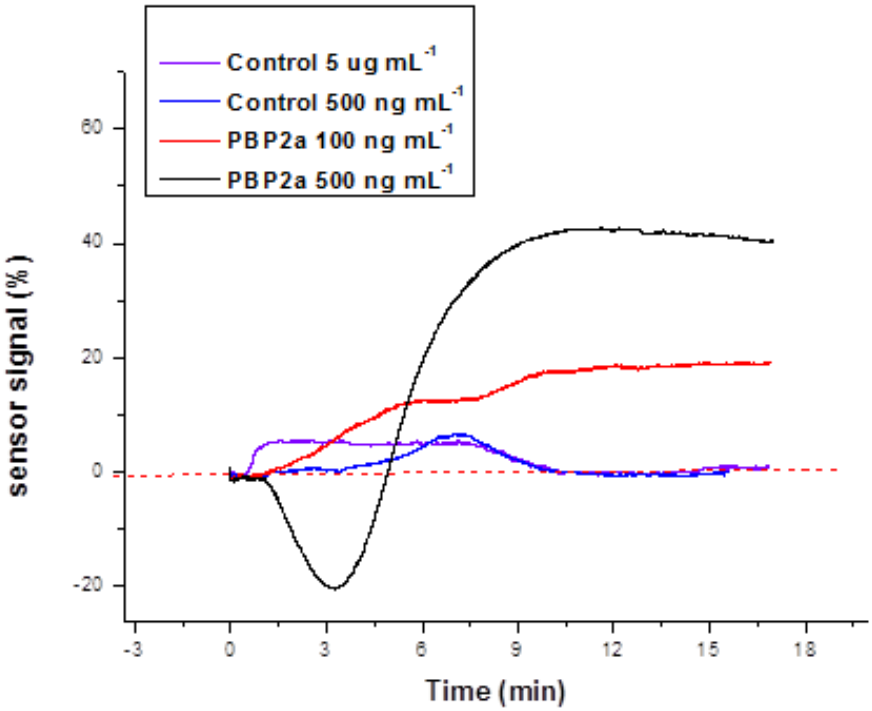

Fig. 5.2. Real-time measurements of PBP2a protein specific for MRSA aptamer and negative control.

For the detection of the whole bacteria using the BiMW aptasensor, solutions ranging from 800 to 1×10^{7} cfu.mL^{-1} were prepared in triplicate. PBS was used as

running buffer and different concentrations of bacteria were injected through the microfluidic cell over the biosensor. A calibration curve with triplicate measurements is shown in Fig 5.3. The phase variation for the highest concentration (1×10^7 cf. mL^{-1}) was 0.49 × 2πrad and for the lowest (800 $cfu.mL^{-1}$) was 0.04 × 2π rad. The LOD evaluated from the fitting of the linear regression of MRSA detection (inset Fig. 5.3) was **100 $cfu.mL^{-1}$**. The good LOD obtained in this bacterial detection is ten times lower than the minimum required for an ideal bacterial. In spite of the MRSA size which is little compare with rod bacteria.

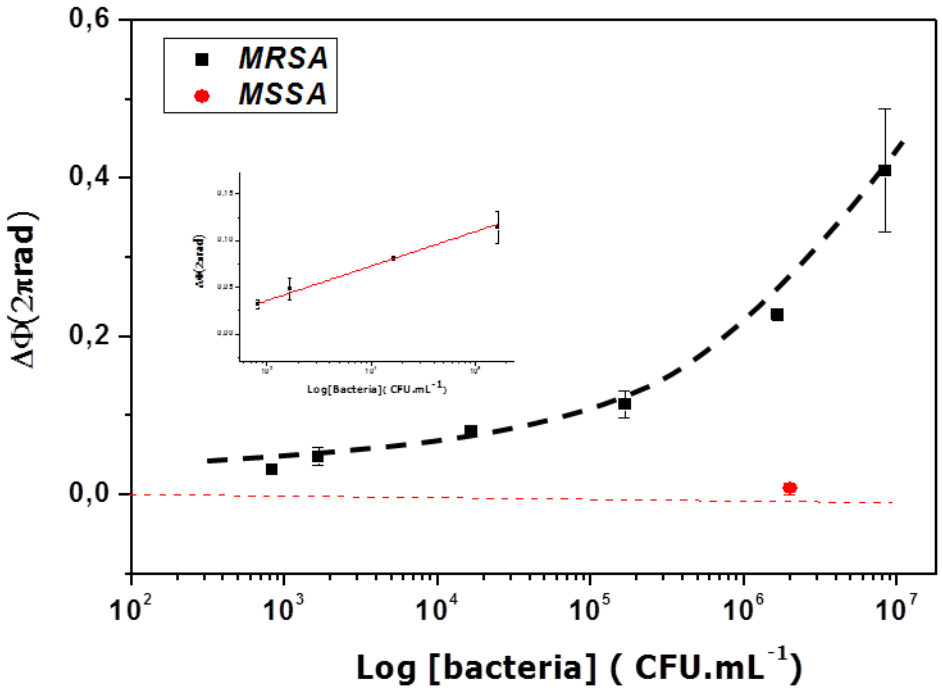

Fig. 5.3. Calibration for the detection of MRSA concentrations ranging from 800 to 1×10^7 $cfu.mL^{-1}$ in comparison with unspecific MSSA; (inset: linearization of the calibration plot).

The specificity of the detection was evaluated by flowing a *Methicillin-Susceptible Staphylococcus aureus* (MSSA) at concentrations of 1×10^6 $cfu.mL^{-1}$ (Fig 5.4). The MSSA concentration of 1×10^6 $cfu.mL^{-1}$ was used due to is the highest

employed with specific MRSA bacteria. No response was observed for any sample of MSSA, confirming that the aptamer is fully specific for *S aureus* which produce the PBP2a protein.

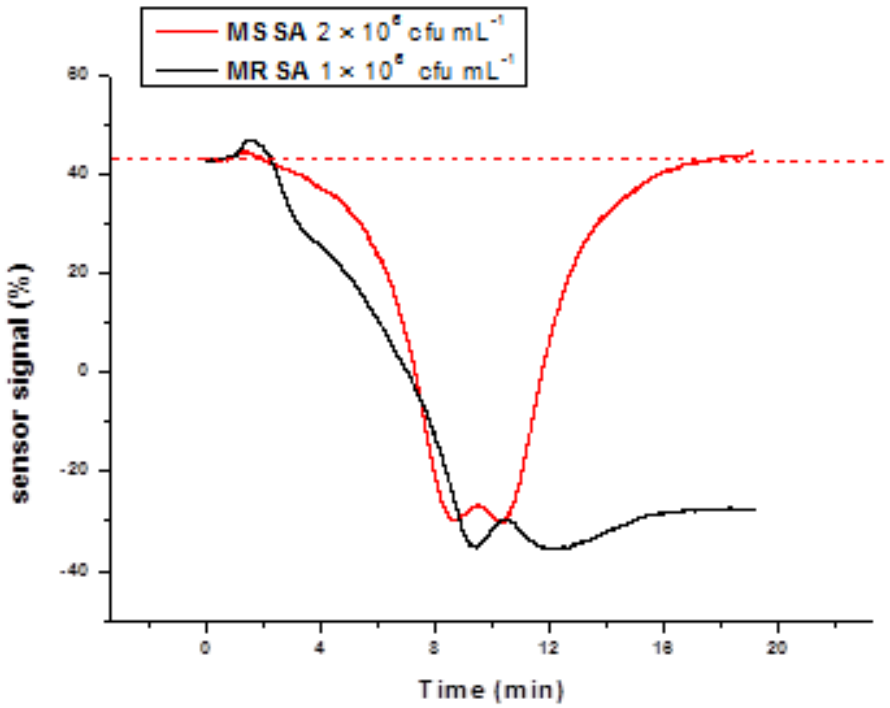

Fig. 5.4. Real time measurements of MRSA (*black line*) versus MSSA measurement (*Red line*).

In Figure 5.5, we demonstrate that the interaction between the aptamer and the captured bacteria can be interrupted by the simple injection of 0.025 M HCl for 1 minute. After the regeneration step, the baseline of the signal was recovered. Using these conditions, the biolayer was reused up to 12 cycles. This result demonstrates that that aptamer is more efficient and stable than antibodies in this particular case.

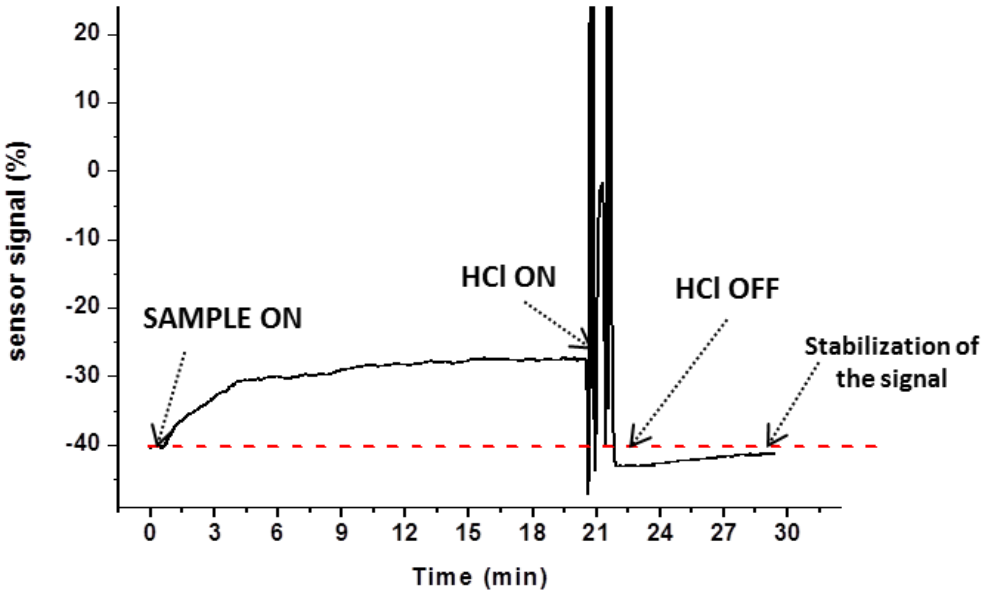

Fig. 5.5. Sensorgram of the MRSA detection, followed by regeneration step. (*dash lines indicate the baseline*).

The specificity of the aptamer and its capability to capture whole bacteria were confirmed using an inspection by SEM. Fig.5.6a and Fig. 5.6b show a silicon nitride surface coated with PEG-silane while in Fig. 5.6c and Fig. 5.6d the sensors were biofunctionalized with the MRSA aptamer. The sensors of Fig. 5.6a and Fig. 5.6c were incubated with MSSA and the ones of Fig. 5.6b and Fig. 5.6d were incubated with MRSA. All samples were incubated for 1 hour in PBS. The PBS buffer was replaced with a fixation buffer (glutaraldehyde 5% in HEPES buffer) and incubated for 1 hour. The presence of *S. aureus* was only observed in the sample that had been incubated with MRSA (Fig. 5.6d). These images confirm the specificity and capability to detect whole bacteria with MRSA aptamer.

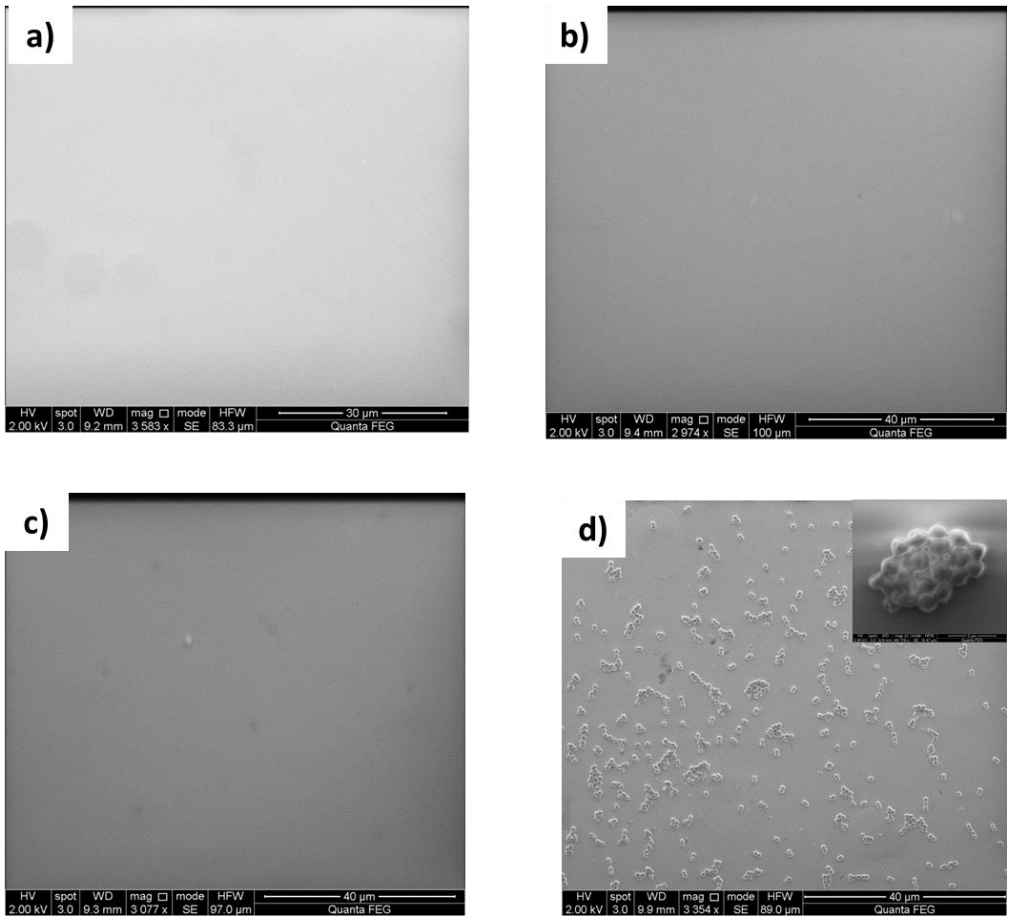

Fig. 5.6. SEM images for the validation of the specificity of the MRSA aptamer bioreceptor. a) MSSA on PEG-silane surface, a) MRSA on PEG-silane surface, c) MSSA on a surface with previously MRSA aptamer immobilized and d) MRSA on a surface with previously MRSA aptamer immobilized. In this image, we can clearly appreciate the whole bacteria captured by the aptamer.

5.2. Direct detection of multidrug-resistant *Escherichia coli* genes by the bimodal waveguide biosensor

We aimed to detect the extended-spectrum β-lactamases (ESBLs) secreted by strains of *Escherichia coli*. B-lactams, the antibiotics most frequently used against bacterial infection diseases are becoming less useful [160]. The principal cause of this decrease in efficacy is the production of β-lactamase by these bacteria. Our specific objective was to use the bimodal waveguide sensor to directly detect, without amplification, the genes encoding the β-lactamase enzymes because these

genes are resistant to a panel of antibiotics. This strategy would allow clinicians to be able to quickly determine the most effective antibiotic for each infected patient.

The detection of the unamplified genomic DNA directly extracted from samples, bypassing the standard PCR amplification and with high sensitivity, selectivity, and in a fast and cost-effective way is a big challenge [161]..In conventional techniques some pre-analytical steps are used in genomic DNA detection, such as DNA fragmentation, extraction, and denaturation. In any case, the extracted DNA is a double helix, in which the complementary strand is hidden and need to be exposed to the DNA probe. Hence, after the fragmentation step, the double-strand DNA is opened by thermal treatment in order to allow the DNA target to match with the probe sequence. With our new strategy we could reduce the drawbacks of a possible probe contamination due to all those steps [162].

We have applied the BiMW biosensor for the $bla_{\text{CTX-M-15}}$ and New Delhi metallo-β-lactamase 5 ($bla_{\text{NDM-5}}$) detections because these genes have been commonly found in patients at Vall d'Hebron hospital (Barcelona, Spain). For evaluating the DNA sample, several steps were considered, such as the most suitable silanization, the DNA fragmentation, and the DNA denaturation by thermal treatment. Pre-treatment optimization, reagents, methods and the electrophoresis study were described in Chapter 2. Figure 5.7 shows the bioassay scheme we have followed to develop the BiMW biosensor for whole DNA detection without PCR amplification.

A computer-assisted approach was applied to design probes for the detection of the gene sequences $bla_{\text{CTX-M-15}}$ (876 bp) and $bla_{\text{NDM-5}}$ (813 bp) over BiMW biosensors. The gene probes were designed with length between 18 and 20 mer and

modified with amine group for react with carboxyl group of PEG-silane (see Chapter 2), to assure a high degree of specificity within *Enterobacteriaceae* family.

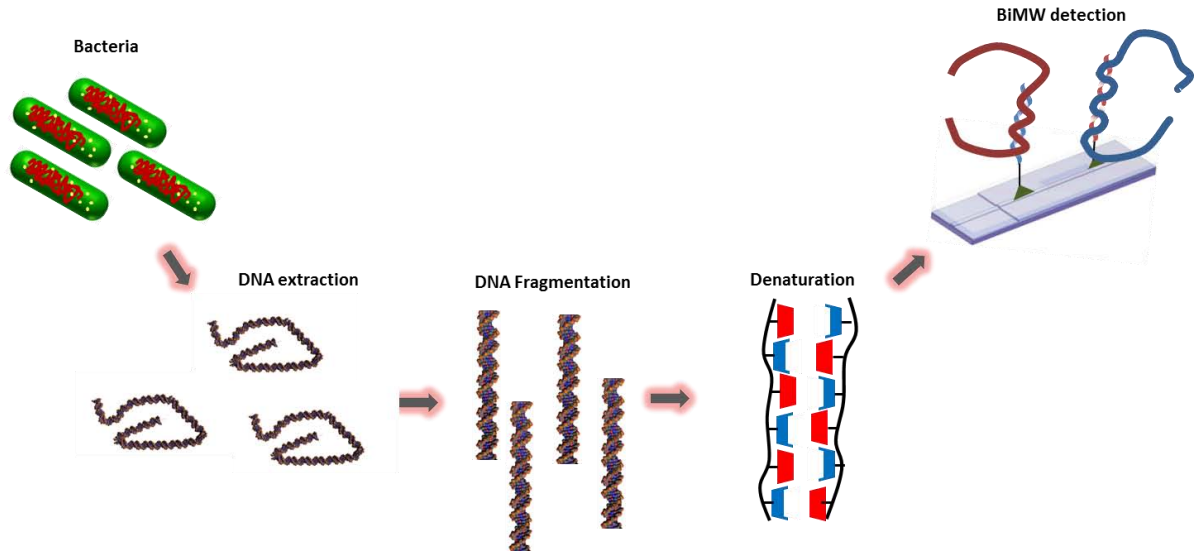

Fig. 5.7. Schematic of the implemented bioassay procedure. DNA is extracted from the bacteria, the DNA is fragmented, denaturation is done by thermal treatment, and the sequences are analyzed by the BiMW biosensor.

Once selected the sequence *bla*$_{\text{CTX-M-15}}$, the corresponding probe was immobilized onto the BiMW chip by using the PEG-silane chemistry, and its performance for binding the complementary synthetic target (88 mer) was tested within the range of concentration from 0.1 to10 nM (Fig. 5.8a). We ranged these concentrations due to 10 nM ten times higher than reported with the minimum reported with label-free SPR and the high LOD of BiMW biosensor. The specificity of the probe was evaluated by flowing a negative control target at a concentration of 10 nM (Fig 5.8b).

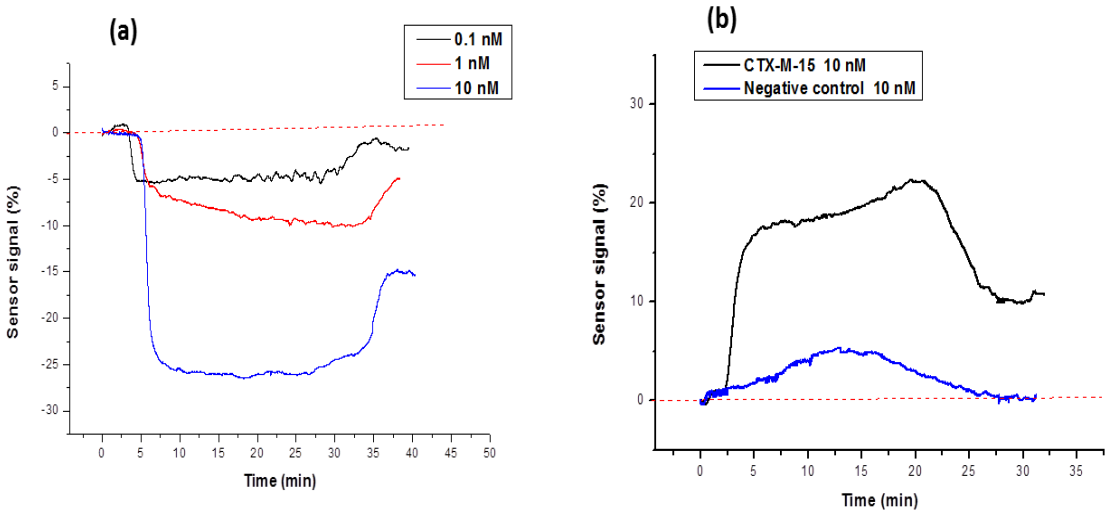

Fig. 5.8. (a) Sensorgram of the hybridization of the synthetic target (88 bp) to *bla*$_{CTX-M-15}$ probe and (b) sensorgram of 10 nM target binding to the *bla*$_{CTX-M-15}$ probe (*black line*) and negative control (*blue line*)

We confirmed the specificity of the *bla*$_{CTM-X-15}$ probe with a (10 nM) synthetic negative control. The response for the synthetic *bla*$_{NDM-5}$ target (10 nM) was 0.08 ×2π rad and for the synthetic target control (10 nM) was 0.0013 ×2π rad. (see figure 5.9). These concentrations were employed only with the purpose of determine the specificity of the probes as compared to a synthetic control with the same concentration.

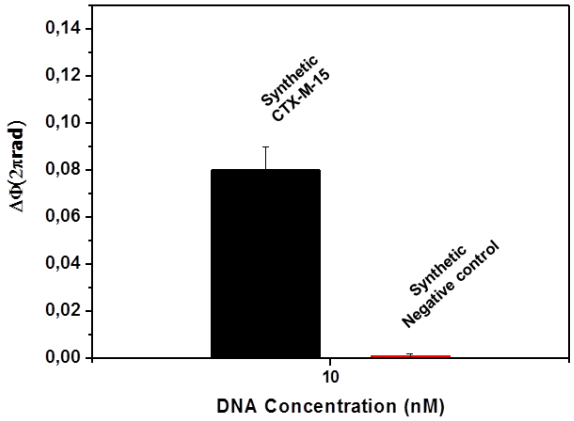

Fig. 5.9 Comparison of the signal of synthetic *bla*$_{CTX-M-15}$ DNA target (10 nM) *versus* synthetic control target (10 nM). The measurements were performed in triplicate and the data are showed as means ± SD.

The bacterial DNA was extracted with the most rapid commercial kit extraction with high yields and high-quality of purification. Then, the whole DNA extracted was fragmented using an ultrasonic fragmentation [163], which is required for the detection of unamplified DNA. The generation of fragments (~10000/20000 bp) of the bacterial DNA carrying the sequence of interest, provided a detectable phase variation also at very low molar concentration (0.45 fM), much lower than that was obtained for the synthetic target. Although, the hybridization of long fragments to probes can be deficient due to steric hindrance at the surface or due to a lower number of strands captured by the probes, the phase variation can be higher due to the large dimension of DNA molecule which match to the probes and the high sensitivity of the BiMW devices.

In the case of the $bla_{\text{CTX-M-15}}$ gene, we first immobilized the two probes (forward and reverse) as is used in PCR techniques and achieve the hybridization with the two strands of the gene, and increase the possibility to detect huge DNA strands. After thermal denaturation, DNA fragments were tested at concentrations of 0.45, 0.75, 1.5, 2.25 and 4.5 fM. The experiments revealed that the limit of detection was **~5.8 attomolar**. The data were fitted, showing a good coefficient of determination (R^2=0.994).

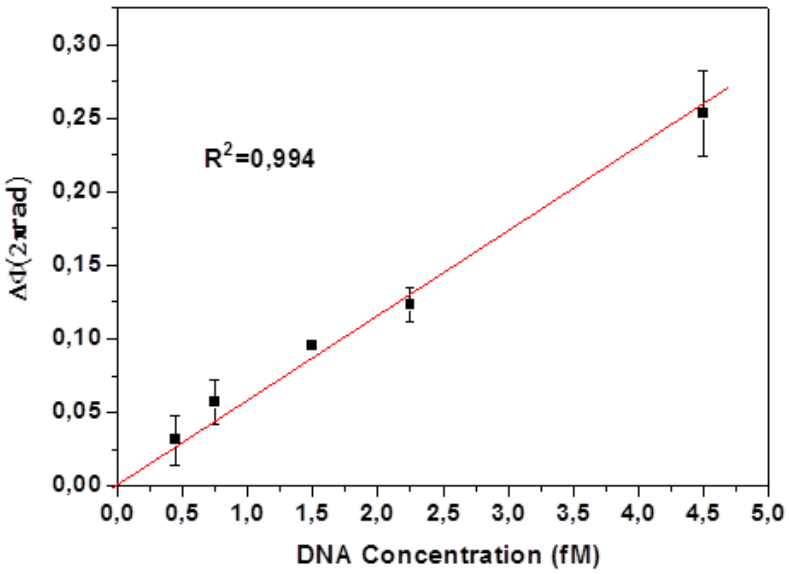

Fig. 5.10. Calibration curve for the detection of serial dilutions of the pre-treated DNA flowing onto the BiMW surface (0.5M NaCl/TE at 5 µL min^{-1}, 150 µL injected), the limit of detection was ~5.8 attomolar.

The specificity of the *bla*$_{CTX\text{-}M\text{-}15}$ probes was evaluated by injecting a non-specific target DNA from *Pseudomonas aeruginosa* at a concentration of 3.4 fM and a target from *E. coli* without *bla*$_{CTX\text{-}M\text{-}15}$ gene at a concentration of 2.9 fM (Fig. 5.11A). These concentrations of the negative controls were chosen because they are the similar concentrations after twenty dilutions from master DNA sample compare with positive control. No signal was observed for any control sample, confirming that the signal contribution had come exclusively from the *bla*$_{CTX\text{-}M\text{-}15}$ target. Figure 5.11B shows the results for all concentrations of the *bla*$_{CTX\text{-}M\text{-}15}$ target.

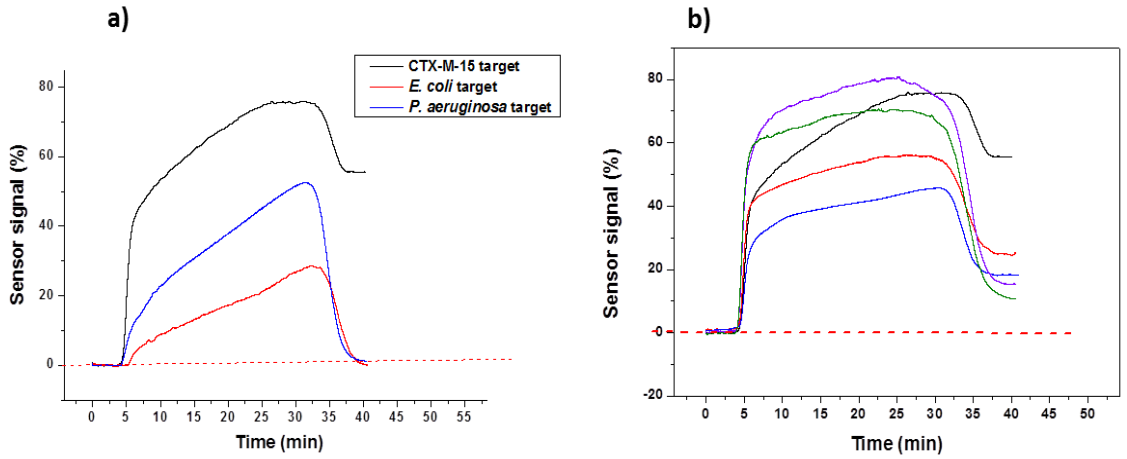

Fig. 5.11. a) Real-time detection of *bla*$_{CTX-M-15}$ gene solution at 4.5 fM (*black line*), non-specific *Pseudomonas aeruginosa* target at 3.4 fM (blue line), and *Escherichia coli* target without *bla*$_{CTX-M-15}$ gene at 2.9 fM (red line). b) Real-time signals of 0.45-4.5 fM concentrations used in these experiments.

We next adapted the assay for the *bla*$_{NDM-5}$ gene detection in another BiMW device. We employed the same strategy than for the ultrasensitive detection of the unamplified *bla*$_{NDM-5}$ DNA using with a probe with polyT (10 mer) vertical spacer. This vertical spacer is used to improve the mobility of immobilized probes and their accessibility to the complementary target molecule.

The *bla*$_{NDM-5}$ gene assay was compared using two different BiMW devices in order to assess the efficiency among sensors. *bla*$_{NDM-5}$ DNA target dilutions ranging from 0.6 to 3 fM were prepared in triplicates in 0.5 M NaCl/TE buffer due to the concentration final of master sample was 0.9 pM in 100 µL of sample. Then, the target was pre-treated (fragmentation and denaturation), and flowed through the sensor. Fig. 5.12a and 5.12b show the calibration plots corresponding to triplicate measurements for each BiMW sensor chips. The lowest concentration (0.6 fM) produced a phase variation of 0.041×2π rad (BiMW 1) and of 0.035×2π rad (BiMW 2) and the highest concentration (3 fM) produced a phase variation of 0.23×2π rad (BiMW 1) and 0.20×2π rad (BiMW 2), respectively. The calibration plots revealed

theoretical limits of detection of **~5.6 attomolar** (BiMW 1) and **~4.6 attomolar** (BiMW 2) with good correlation coefficients (R^2=0.998 for BiMW 1 and R^2=0.996 for BiMW 2), as reported in the upper part of Figure 5.12a and 5.12b. Also, we show a comparison of the real-time evaluation for the concentration of 0.6-3 fM for BiMW 1 and BiMW 2 biosensors.

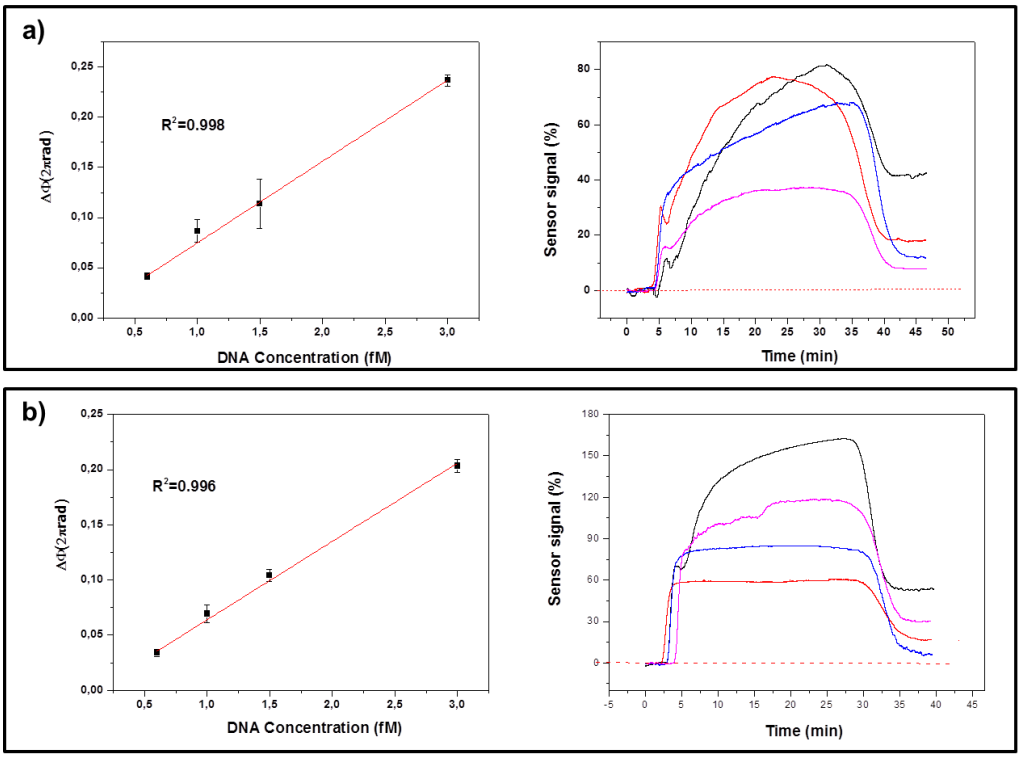

Fig. 5.12. Detection of *bla*$_{NDM-5}$ gene using the BIMW-DNA biosensor**.** A) Calibration plot. Samples with different concentration (0.6-3 fM) were prepared through serial dilutions. The limit of detection was ~5.6 aM. Sensorgrams of 0.6-3 fM for the hybridization between the *bla*$_{NDM-5}$ probe and the *bla*$_{NDM-5}$ DNA target were monitored in real-time. B) The assay was adapted in another BiMW-DNA biosensor to show the reproducibility of the bioassay with different devices. The limit of detection in the BiMW 2 was 4.6 aM and also a sensorgram of the measurements is shown. All measurements (BiMW 1 & BiMW 2) were performed in triplicate and the plots are displayed as means ± SD.

We confirmed the specificity of the *bla*$_{NDM-5}$ probe with *Pseudomonas* DNA target (3.4 fM) in both devices. The designed probe showed high specificity for DNA-5 and a negligible signal for the negative controls. For the BiMW1, the signal for *bla*$_{NDM-5}$ target (3 fM) was 0.24 ×2π rad and for the *Pseudomonas* DNA target control

(3.4) was 0.001 ×2π rad. Finally, for the BiMW2 sensor, the response for the NDM-5 was 0.21 ×2π rad and for the negative control was 0.004 ×2π rad (see figure 5.13)

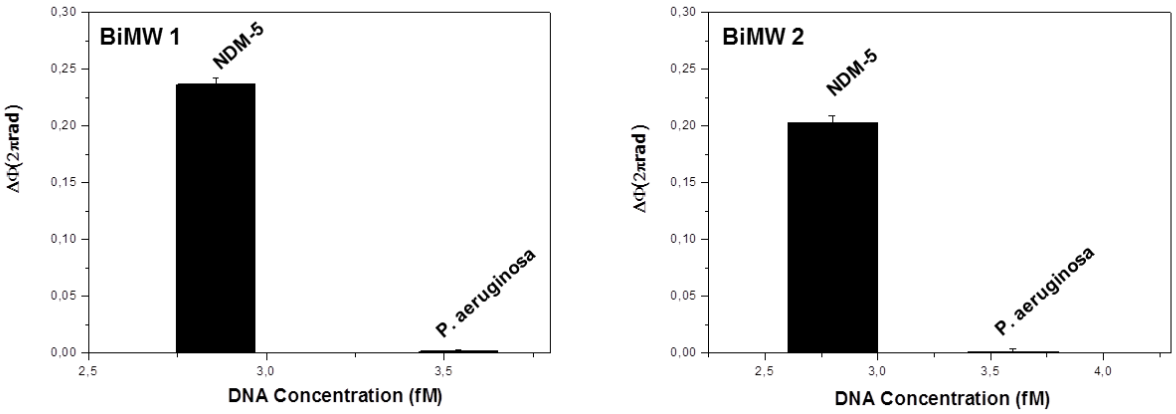

Fig.5.13. Comparison of the signal of *bla*$_{NDM-5}$ DNA target (3 fM) *versus P. aeruginosa* DNA target (3.4 fM) in 0.5 M NaCl/TE buffer for two different BiMW chips. All the measurements were performed in triplicate and the data are showed as means ± SD.

We also validated the gene presence in the samples by agarose electrophoretic gel. PCR was performed as previously described (chapter 2). Fig. 5.14 shows the electrophoretic analysis with clear bands, where L2 is the PCR product of *bla*$_{NDM-5}$ (813 bp), L3 sample is for *bla*$_{CTX-M-15}$ gene (876 bp) and lane L1, and L4 show 50 bp DNA ladder. Thereby, we demonstrate that the genes are present in the samples which we have used during these experiments.

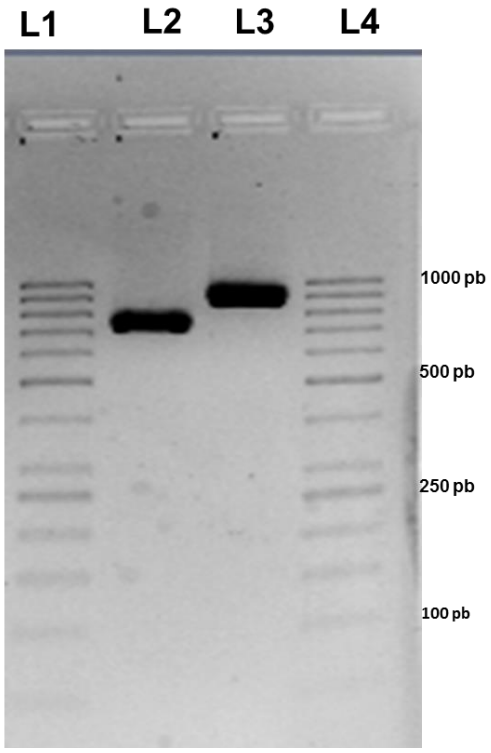

Fig. 5.14. Validation of *bla*$_{CTX\text{-}M\text{-}15}$ and *bla*$_{NDM\text{-}5}$ genes. 0.5% gel agarose electrophoresis of bacterial DNA samples. 50 bp DNA ladder is used as markers (L1 and L4). Lane L1 is *bla*$_{NDM\text{-}5}$ DNA sample and Lane L3 is *bla*$_{CTX\text{-}M\text{-}15}$ DNA sample that show the presence of the genes in the samples.

As a conclusion, the obtained limit of detection show the great potential of the BiMW biosensor for the identification of *E. coli* superbug genes. These limits of detection are superior of the ones obtained with several DNA-detection optical biosensors which have detected DNA without PCR amplification but most of them required of amplification steps. (See Table 6 for a comparison).

Table 7. Examples of Optical Biosensor for the detection of unamplified nucleic acids

Surface	Receptor	Analyte	Target	Signal amplification method	Sensing Approach	Assay time	Limit of detection (LOD)	Refs
Gold	PNA	GMO	GMO	Biotin	SPRi	40 min	41 zM	[164]
Gold	DNA probe	ABCB1 human gene	Human lymphocytes	Gold-nanostar	SPRi	70 min	6.9 aM	[165]
Gold	PNA	Beta-thalassemia	Homozygous	AuNP	SPRi	33 min	2.6 aM	[166]
Silicon nitride	**DNA probe**	***Bla*$_{CTX-M-15}$ and *Bla*$_{NDM-5}$ genes**	***E. coli***	**Label-free**	**BiMW**	**30 min**	**5 aM**	**this work**
Gold	µRNA	*BCL-X* gene	*Hela cell*	Label-free	SPR	17 min	0.15 nM	[167]
Gold	DNA probe	*Hippuricase gene*	*Campylobacter jejuni*	DNA scaffold	dotLab	17 min	2.5 nM	[168]

5.3. Conclusion

We have developed a label-free, rapid, stable, reusable, selective and specific biosensor capable of detecting superbugs. The combination between BiMW interferometer as sensor and the aptamer against MRSA as bioreceptor is an excellent alternative in order to difference among resistant and susceptible *Staphylococcus* at a concentration of only 100 cfu.mL^{-1}. Furthermore, the detection can be performed in only 15 min.

Moreover, we have shown that BiMW technology affords the label-free ultrasensitive detection of unamplified DNA solution. Our BiMW biosensor can detect *bla*$_{CTX-M-15}$ and *bla*$_{NDM-5}$ genes at attomolar levels. The detection time was 30 min for each sample.

In view of the high sensitivity exhibited by the BiMW biosensor, it could potentially be used for the early detection of infections caused by multidrug resistant genes of different pathogens and determine the most effective treatment for the patients directly at hospitals in a fast way.

General Conclusions

This thesis employs our exclusive BiMW biosensor technology for the rapid, direct and accurate analysis of pathogens, revealing its high potential for the testing of nosocomial infections in clinical settings. The BiMW biosensor consists of a bimodal waveguide interferometer as sensor platform and selective biomolecules as biorecognition elements. The optimization and assessment of the most suitable functionalization strategies and biodetection methodologies have allowed the reliable monitoring at sensitive levels comparable to conventional methods much as cell cultures and PCR. Moreover, the detection of bacteria in complex medium has demonstrated the viability of the biosensor for its use for near-patients point-of-care settings

The main general conclusions that can be extracted from this Doctoral Thesis are the following:

- Different functionalization strategies were studied for the silicon nitride ended surface of the BIMW devices for the direct detection of protein and bacteria. According to that, a carboxylic-terminated silane (CTES) and a 3-aminopropyltriethoxysilane were employed as the chemical modification to immobilized the required antibodies and to achieve the evaluation of the corresponding analytes in complex matrices as urine or ascetic fluid. Finally a carboxylic poly(ethylene glycol) silane were also employed for biofunctionalization in order characterized to immobilize different biomolecules (antibody, aptamer or DNA strands), and analyse the antimicrobial properties of the generated bioreceptor surface.

- The optical characterization to obtained the lowest limit of detection of 5×10^{-8} RIU which is very low, comparable with the most sensitive interferometer sensors reported up to date. We employed the BiMW for the detection of the human growth hormone (hGH) using a monoclonal antibody as biorecognition element and CTES as silanization strategy. The LOD obtained was 0.3 $pg.mL^{-1}$, which is the reached by a label-free biosensor in a direct approach (without any further amplification). For the detection of this hormone in complex matrix as urine, we used an APTES silanization to obtain a LOD of 3 $pg.mL^{-1}$ in urine. The detection time was 15 min, which is faster than the regular clinical analysis.
- The BiMW device was used for the determination of bacteria in real-time using a direct immunoassay with antibodies as bioreceptors. The first bacterial detection was done for the detection of whole *Bacillus cereus* using CTES silanization with BSA as blocking agent, and obtaining a LOD of 12 $cfu.mL^{-1}$. Furthermore, the specificity of the biosensor was analyzed using *Escherichia coli* as negative control. Moreover, we have demonstrated the capability to detect *Escherichia coli* in ascitic fluid and reaching a LOD of only 4 $cfu.mL^{-1}$. Finally, we evaluated the same methodology for the real-time detection of *Pseudomonas aeruginosa* using a PEG-silano strategy obtaining a LOD of 170 $cfu.mL^{-1}$. The LOD obtained with PEG-silanization was higher that the APTES and CTES silanization, but this is still an excellent result for the clinical requirements. The implementation of a BiMW biosensor may solve the health-care associated infections and would allow the clinicians to determinate the most effective treatment for the patients in a faster way.

- We have proposed a biosensor methodology based on DNA-aptamer for real-time determination of the well-known pathogenic bacterium methicillin-resistant *Staphylococcus aureus (*MRSA). The use of this bioreceptor allows discriminating between a susceptible Staph and a MRSA due to a protein (PBP2a) which is expressed in the MRSA cell wall and protects the bacterium against antibiotics and the aptamer is specific for this protein. The LOD obtained with this methodology was 100 $CFU.mL^{-1}$with an analysis time of 15 min which is very competitive as compared to the ones achieved by the conventional methods.
- We have developed an alternative and ultra-sensitive methodology for the detection of genes associated with multidrug resistance found in Gram-negative bacteria as *E. coli.* The methodology has been optimized using the BiMW biosensor to ensure selective detection of $bla_{CTX\text{-}M\text{-}15}$ and $bla_{NDM\text{-}5}$ without PCR amplification. The use of steps as DNA extraction, fragmentation and denaturation let us to detect these genes in a time of 30 min. The methodology reached in this case a LOD of 5 aM, which represents the most sensitive DNA detection without amplification or labeling steps reported up to date. The implementation of the BiMW biosensor may improve not only the fast diagnosis of nosocomial infection but can also determinate the proper antibiotic treatment for each patient in a short time.

This Thesis work has exposed the extraordinary performance of the BiMW biosensor in comparison with conventional test due to its high sensitivity demonstrated for different applications. The limits of detections achieved are in the $pg.mL^{-1}$ range in protein detection, less than 100 $CFU.mL^{-1}$ in bacterial detection,

both in complex matrices (urine and ascitic fluid), and a LOD in the range of aM for genomic DNA detection.

The demonstration of simple and rapid methodology for the identification of nosocomial infections and their resistance to antibiotic opens the road for the achievement of an efficient diagnostic and determination of the proper antibiotic treatment, preventing disease spread, and allowing the identification of infections source in hospitals, homes, and other field settings.

Publications

Articles in peer-reviewed international journals

- **J. Maldonado**, A. B. González-Guerrero, C. Domínguez and L. M. Lechuga. *Label-free bimodal waveguide immunosensor for rapid diagnosis of bacterial infections in cirrhotic patients***,** *Biosensors & Bioelectronic*, **85**, 2016, 310-316 - **DOI:** DOI:10.1016/j.bios.2016.04.095.
- A. B. González-Guerrero, **J. Maldonado**, S. Dante, D. Grajales, and L. M. Lechuga. *Direct and label-free detection of the human growth hormone in urine by an ultrasensitive bimodal Waveguide biosensor*, Journal of Biophotonics, 10, 1, 2017, 123-136 – DOI: 10.1515/nanoph-2016-010.
- A. B. González-Guerrero, **J. Maldonado**, S. Herranz and L. M. Lechuga. *Trends in photonic lab-on-a-chip in interferometric biosensor for point-of-care diagnostics*, Analytical Methods, 8, 2016, 8380-8394-DOI: 10.1039/c6ay02972h.
- **J. Maldonado**, A. B. González-Guerrero, A. Fernández Gavela, J. J. González-López, C. Domínguez and L. M. Lechuga. *An antimicrobial biosensor for the detection of Methicillin-resistant Staphylococcus aureus and Pseudomonas aeruginosa by bimodal waveguide interferometry*. Submitted.
- **J. Maldonado**, A. B. González-Guerrero, A. Fernández Gavela, J. J. González-López, C. Domínguez and L. M. Lechuga. *Bimodal waveguide biosensor for the ultrasensitive detection of unamplified genes encoding β-lactamase in Escherichia coli.* In preparation.

Proceedings

- D. Duval, A. B. González-Guerrero, S. Dante, C. Sanchez Huertas, **J. Maldonado** and L. M. Lechuga. *Point-of-care diagnostics using integrated optical-based interferometric nanobiosensors,* OSA, 2014. Optical sensor, DOI: 10.1364/SENSORS.2014.Seth3B.4.

Conference participation

- **J. Maldonado**, A. B. González-Guerrero, J. J. Gonzalez-López, C. Domínguez and L. M. Lechuga. *Development of an immunosensor for the detection of Pseudomonas Aeruginosa in ascitic fluid by bimodal waveguide interferometry.* XIII Conference on Optical Chemical Sensors and Biosensors. Graz (Austria), 2016. (oral)

- A. B. González-Guerrero, P. Ramírez, **J. Maldonado** and L. M. Lechuga. *Direct quantification of exosomes from tumor cell cultures by bimodal waveguide interferometry*, XIII Conference on Optical Chemical Sensors and Biosensors. Graz Austria, 2016. (poster)

Bibliography

1. McFee, R.B., *Nosocomial or Hospital-acquired Infections: An Overview.* Disease-a-Month, 2009. **55**(7): p. 422-438.
2. Brusaferro, S., et al., *Harmonizing and supporting infection control training in Europe.* Journal of Hospital Infection, 2015. **89**(4): p. 351-356.
3. Prevention, C.f.D.C.a., *Antinbiotic Resistance threats in the United States*, in *US Deparment of health and human services, Atlanta, Georgia.* 2013.
4. Zimlichman, E., et al., *Health care–associated infections: A meta-analysis of costs and financial impact on the us health care system.* JAMA Internal Medicine, 2013. **173**(22): p. 2039-2046.
5. Raka, L., et al., *Prevalence of Nosocomial Infections in High-Risk Units in the University Clinical Center of Kosova.* Infection Control & Hospital Epidemiology, 2016. **27**(4): p. 421-423.
6. Canbaz, S., et al., *Antibiotic prescribing and urinary tract infection.* International Journal of Antimicrobial Agents, 2002. **20**(6): p. 407-411.
7. Horan, T.C., M. Andrus, and M.A. Dudeck, *CDC/NHSN surveillance definition of health care–associated infection and criteria for specific types of infections in the acute care setting.* American Journal of Infection Control, 2008. **36**(5): p. 309-332.
8. Lausch, K.R., et al., *Colonisation with multi-resistant Enterobacteriaceae in hospitalised Danish patients with a history of recent travel: A cross-sectional study.* Travel Medicine and Infectious Disease, 2013. **11**(5): p. 320-323.
9. Al Laham, N., et al., *MRSA clonal complex 22 strains harboring toxic shock syndrome toxin (TSST-1) are endemic in the primary hospital in Gaza, Palestine.* PLoS One, 2015. **10**(3): p. e0120008.
10. Balasoiu, M., et al., *Pseudomonas aeruginosa resistance phenotypes and phenotypic highlighting methods.* Curr Health Sci J, 2014. **40**(2): p. 85-92.
11. Fernández, J. and T. Gustot, *Management of bacterial infections in cirrhosis.* J Hepatol, 2012. **56, Supplement 1**(0): p. S1-S12.
12. Gordon, R.J. and F.D. Lowy, *Pathogenesis of Methicillin-Resistant Staphylococcus aureus Infection.* Clinical infectious diseases : an official

publication of the Infectious Diseases Society of America, 2008. **46**(Suppl 5): p. S350-S359.

13. Santiago, C., et al., *Inhibition of penicillin-binding protein 2a (PBP2a) in methicillin resistant Staphylococcus aureus (MRSA) by combination of ampicillin and a bioactive fraction from Duabanga grandiflora.* BMC Complementary and Alternative Medicine, 2015. **15**(1): p. 178.
14. Klein, E., D.L. Smith, and R. Laxminarayan, *Hospitalizations and Deaths Caused by Methicillin-Resistant Staphylococcus aureus, United States, 1999–2005.* Emerging Infectious Diseases, 2007. **13**(12): p. 1840-1846.
15. Card, R., et al., *Evaluation of an expanded microarray for detecting antibiotic resistance genes in a broad range of gram-negative bacterial pathogens.* Antimicrob Agents Chemother, 2013. **57**(1): p. 458-65.
16. Ahmed, A., et al., *Biosensors for Whole-Cell Bacterial Detection.* Clinical Microbiology Reviews, 2014. **27**(3): p. 631-646.
17. Gooding, J.J., *Biosensor Technology for Detecting Biological Warfare Agents: Recent Progress and Future Trends.* Analytica Chimica Acta 559(2):137-151, 2006.
18. Xihong Zhao, C.-W.L., Jun Wang, Deog Hwan Oh, *Advances in Rapid Detection Methods for Foodborne Pathogens.* Journal of Microbiology and Biotechnology, 2014.
19. *http://www.biomerieux.com/.*
20. *https://www.beckmancoulter.com/wsrportal/wsr/diagnostics/clinical-products/microbiology/index.htm.*
21. Alexander, T.W., et al., *Conventional and real-time polymerase chain reaction assessment of the fate of transgenic DNA in sheep fed Roundup Ready® rapeseed meal.* British Journal of Nutrition, 2006. **96**(6): p. 997-1005.
22. Law, J.W.-F., et al., *Rapid methods for the detection of foodborne bacterial pathogens: principles, applications, advantages and limitations.* Frontiers in Microbiology, 2014. **5**: p. 770.
23. Vogelstein, B. and K.W. Kinzler, *Digital PCR.* Proceedings of the National Academy of Sciences, 1999. **96**(16): p. 9236-9241.
24. Lind, K., et al., *Combining sequence-specific probes and DNA binding dyes in real-time PCR for specific nucleic acid quantification and melting curve analysis.* Biotechniques, 2006. **40**(3): p. 315-9.

25. Liu, J., M. Enzelberger, and S. Quake, *A nanoliter rotary device for polymerase chain reaction.* ELECTROPHORESIS, 2002. **23**(10): p. 1531-1536.
26. Ma K., D.Y., Bai Y., Xu D., Chen E., Wu H., , *Rapid and simultaneous detection of Salmonella, Shigella, and Staphylococcus aureus in fresh pork using a multiplex real-time PCR assay based on immunomagnetic separation.* . Food Cont, 2014.
27. Silva, D.S.P., et al., *Multiplex PCR for the simultaneous detection of Salmonella spp. and Salmonella Enteritidis in food.* International Journal of Food Science & Technology, 2011. **46**(7): p. 1502-1507.
28. Gore, H.M., et al., *Real-time molecular beacon NASBA reveals hblC expression from Bacillus spp. in milk.* Biochemical and Biophysical Research Communications, 2003. **311**(2): p. 386-390.
29. Ramalingam, N., et al., *Real-time PCR-based microfluidic array chip for simultaneous detection of multiple waterborne pathogens.* Sensors and Actuators B: Chemical, 2010. **145**(1): p. 543-552.
30. Severgnini, M., et al., *Advances in DNA Microarray Technology for the Detection of Foodborne Pathogens.* Food and Bioprocess Technology, 2011. **4**(6): p. 936-953.
31. Lauri, A. and P.O. Mariani, *Potentials and limitations of molecular diagnostic methods in food safety.* Genes & Nutrition, 2009. **4**(1): p. 1-12.
32. Li, Y., et al., *Development of a Serotype-Specific DNA Microarray for Identification of Some Shigella and Pathogenic Escherichia coli Strains.* Journal of Clinical Microbiology, 2006. **44**(12): p. 4376-4383.
33. Zhou, B., et al., *Simultaneous detection of six food-borne pathogens by multiplex PCR with a GeXP analyzer.* Food Control, 2013. **32**(1): p. 198-204.
34. Spindel, S. and K.E. Sapsford, *Evaluation of Optical Detection Platforms for Multiplexed Detection of Proteins and the Need for Point-of-Care Biosensors for Clinical Use.* Sensors (Basel, Switzerland), 2014. **14**(12): p. 22313-22341.
35. Ivnitski, D., et al., *Biosensors for detection of pathogenic bacteria.* Biosensors and Bioelectronics, 1999. **14**(7): p. 599-624.
36. Chang, T.M.S., *Biomedical Applications of Immobilized Enzymes and Proteins.* Springer, 2013. **1**.

37. Anderson, M.J., H.R. Miller, and E.C. Alocilja, *PCR-less DNA co-polymerization detection of Shiga like toxin 1 (stx1) in Escherichia coli O157:H7.* Biosensors and Bioelectronics, 2013. **42**: p. 581-585.
38. Paniel, N. and J. Baudart, *Colorimetric and electrochemical genosensors for the detection of Escherichia coli DNA without amplification in seawater.* Talanta, 2013. **115**: p. 133-142.
39. Gerasimova, Y.V. and D.M. Kolpashchikov, *Detection of bacterial 16S rRNA using a molecular beacon-based X sensor.* Biosensors and Bioelectronics, 2013. **41**: p. 386-390.
40. Foudeh, A.M., et al., *Sub-femtomole detection of 16s rRNA from Legionella pneumophila using surface plasmon resonance imaging.* Biosensors and Bioelectronics, 2014. **52**: p. 129-135.
41. Miranda, O.R., et al., *Colorimetric Bacteria Sensing Using a Supramolecular Enzyme–Nanoparticle Biosensor.* Journal of the American Chemical Society, 2011. **133**(25): p. 9650-9653.
42. Farrow, B., et al., *A Chemically Synthesized Capture Agent Enables the Selective, Sensitive, and Robust Electrochemical Detection of Anthrax Protective Antigen.* ACS Nano, 2013. **7**(10): p. 9452-9460.
43. Daniel Thevenot, K.T., Richard Durst, George Wilson, *Electrochemical biosensors: recommended definitions and classification.* Pure and Applied Chemistry, 1999. **71**: p. 2333 - 2348.
44. Ronkainen, N.J., H.B. Halsall, and W.R. Heineman, *Electrochemical biosensors.* Chem Soc Rev, 2010. **39**(5): p. 1747-63.
45. Privett, B.J., J.H. Shin, and M.H. Schoenfisch, *Electrochemical nitric oxide sensors for physiological measurements.* Chem Soc Rev, 2010. **39**(6): p. 1925-35.
46. Grieshaber, D., et al., *Electrochemical Biosensors - Sensor Principles and Architectures.* Sensors, 2008. **8**(3): p. 1400.
47. Mongra, A.C., Kaur, A., Bansal, R.K., *Review study on electrochemical-based biosensors.* J. Res. Appl. Agric. Eng, 2003. **2**: p. 743-749.
48. Esteban-Fernández de Ávila, B., et al., *Sensitive and rapid amperometric magnetoimmunosensor for the determination of Staphylococcus aureus.* Analytical and Bioanalytical Chemistry, 2012. **403**(4): p. 917-925.

49. Tlili, C., et al., *Bacteria Screening, Viability, And Confirmation Assays Using Bacteriophage-Impedimetric/Loop-Mediated Isothermal Amplification Dual-Response Biosensors.* Analytical Chemistry, 2013. **85**(10): p. 4893-4901.
50. Perrotta, P.R., et al., *Development of a very sensitive electrochemical magneto immunosensor for the direct determination of ochratoxin A in red wine.* Sensors and Actuators B: Chemical, 2012. **162**(1): p. 327-333.
51. Rhouati, A., et al., *Development of an automated flow-based electrochemical aptasensor for on-line detection of Ochratoxin A.* Sensors and Actuators B: Chemical, 2013. **176**: p. 1160-1166.
52. Jiang, X., et al., *Evaluation of different micro/nanobeads used as amplifiers in QCM immunosensor for more sensitive detection of E. coli O157:H7.* Biosensors and Bioelectronics, 2011. **29**(1): p. 23-28.
53. Guo, X., et al., *A piezoelectric immunosensor for specific capture and enrichment of viable pathogens by quartz crystal microbalance sensor, followed by detection with antibody-functionalized gold nanoparticles.* Biosensors and Bioelectronics, 2012. **38**(1): p. 177-183.
54. Salam, F., Y. Uludag, and I.E. Tothill, *Real-time and sensitive detection of Salmonella Typhimurium using an automated quartz crystal microbalance (QCM) instrument with nanoparticles amplification.* Talanta, 2013. **115**: p. 761-767.
55. Hao, R., et al., *Rapid detection of Bacillus anthracis using monoclonal antibody functionalized QCM sensor.* Biosensors and Bioelectronics, 2009. **24**(5): p. 1330-1335.
56. Cooper, M.A., *Optical biosensors in drug discovery.* Nat Rev Drug Discov, 2002. **1**(7): p. 515-528.
57. Pires, N., et al., *Recent Developments in Optical Detection Technologies in Lab-on-a-Chip Devices for Biosensing Applications.* Sensors, 2014. **14**(8): p. 15458.
58. Torun, Ö., et al., *Comparison of sensing strategies in SPR biosensor for rapid and sensitive enumeration of bacteria.* Biosensors and Bioelectronics, 2012. **37**(1): p. 53-60.
59. Tokel, O., F. Inci, and U. Demirci, *Advances in Plasmonic Technologies for Point of Care Applications.* Chemical Reviews, 2014. **114**(11): p. 5728-5752.

60. Yoo, S.M. and S.Y. Lee, *Optical Biosensors for the Detection of Pathogenic Microorganisms.* Trends in Biotechnology. **34**(1): p. 7-25.
61. Yoo, S.M., D.K. Kim, and S.Y. Lee, *Aptamer-functionalized localized surface plasmon resonance sensor for the multiplexed detection of different bacterial species.* Talanta, 2015. **132**: p. 112-7.
62. Wang, Y., W. Knoll, and J. Dostalek, *Bacterial pathogen surface plasmon resonance biosensor advanced by long range surface plasmons and magnetic nanoparticle assays.* Anal Chem, 2012. **84**(19): p. 8345-50.
63. Nordin, A.N., *Optical-resonator-based biosensing systems: current status and future prospects.* Nanobiosensors in Disease Diagnosis, 2016. **5**: p. 41-50.
64. Ramachandran, A., et al., *A universal biosensing platform based on optical micro-ring resonators.* Biosensors and Bioelectronics, 2008. **23**(7): p. 939-944.
65. Dante, S., et al., *All-optical phase modulation for integrated interferometric biosensors.* Optics Express, 2012. **20**(7): p. 7195-7205.
66. Hartman, N.F., J. Cobb, and J.G. Edwards. Proceedings of SPIE - the International Society for Optical Engineering. 1999: SPIE - The International Society for Optical Engineering.
67. Ymeti, A., et al., *Integration of microfluidics with a four-channel integrated optical Young interferometer immunosensor.* Biosensors and Bioelectronics, 2005. **20**(7): p. 1417-1421.
68. Swann, M.J., et al., *Dual-polarization interferometry: an analytical technique to measure changes in protein structure in real time, to determine the stoichiometry of binding events, and to differentiate between specific and nonspecific interactions.* Anal Biochem, 2004. **329**(2): p. 190-8.
69. Schneider, B.H., J.G. Edwards, and N.F. Hartman, *Hartman interferometer: versatile integrated optic sensor for label-free, real-time quantification of nucleic acids, proteins, and pathogens.* Clin Chem, 1997. **43**(9): p. 1757-63.
70. Nagel, T., et al., *Direct detection of tuberculosis infection in blood serum using three optical label-free approaches.* Sensors and Actuators B: Chemical, 2008. **129**(2): p. 934-940.
71. Mathesz, A., et al., *Integrated optical biosensor for rapid detection of bacteria*, in *Optofluidics, Microfluidics and Nanofluidics*. 2015. p. 15.

72. Bouguelia, S., et al., *On-chip microbial culture for the specific detection of very low levels of bacteria.* Lab on a Chip, 2013. **13**(20): p. 4024-4032.
73. Mondani, L., et al., *Simultaneous enrichment and optical detection of low levels of stressed Escherichia coli O157:H7 in food matrices.* Journal of Applied Microbiology, 2014. **117**(2): p. 537-546.
74. Tuerk, C. and L. Gold, *Systematic evolution of ligands by exponential enrichment: RNA ligands to bacteriophage T4 DNA polymerase.* Science, 1990. **249**(4968): p. 505-510.
75. Cao, X., et al., *Combining use of a panel of ssDNA aptamers in the detection of Staphylococcus aureus.* Nucleic Acids Research, 2009. **37**(14): p. 4621-4628.
76. Zelada-Guillén, G.A., et al., *Immediate Detection of Living Bacteria at Ultralow Concentrations Using a Carbon Nanotube Based Potentiometric Aptasensor.* Angewandte Chemie International Edition, 2009. **48**(40): p. 7334-7337.
77. Zelada-Guillén, G.A., et al., *Label-free detection of Staphylococcus aureus in skin using real-time potentiometric biosensors based on carbon nanotubes and aptamers.* Biosensors and Bioelectronics, 2012. **31**(1): p. 226-232.
78. Yoo, S.M., D.-K. Kim, and S.Y. Lee, *Aptamer-functionalized localized surface plasmon resonance sensor for the multiplexed detection of different bacterial species.* Talanta, 2015. **132**: p. 112-117.
79. Gervais, L., et al., *Immobilization of biotinylated bacteriophages on biosensor surfaces.* Sensors and Actuators B: Chemical, 2007. **125**(2): p. 615-621.
80. Arya, S.K., et al., *Chemically immobilized T4-bacteriophage for specific Escherichia coli detection using surface plasmon resonance.* Analyst, 2011. **136**(3): p. 486-492.
81. Tawil, N., et al., *Surface plasmon resonance detection of E. coli and methicillin-resistant S. aureus using bacteriophages.* Biosensors and Bioelectronics, 2012. **37**(1): p. 24-29.
82. Templier, V., et al., *Ligands for label-free detection of whole bacteria on biosensors: A review.* TrAC Trends in Analytical Chemistry, 2016. **79**: p. 71-79.
83. Gill, D., et al., *The Roles of Antimicrobial Peptides in Innate Host Defense.* Current Pharmaceutical Design, 2009. **15**(21): p. 2377-2392.

84. Nguyen, L.T., E.F. Haney, and H.J. Vogel, *The expanding scope of antimicrobial peptide structures and their modes of action.* Trends in Biotechnology, 2011. **29**(9): p. 464-472.
85. Mannoor, M.S., et al., *Electrical detection of pathogenic bacteria via immobilized antimicrobial peptides.* Proceedings of the National Academy of Sciences, 2010. **107**(45): p. 19207-19212.
86. Rotem, S., et al., *Bacterial Capture by Peptide-Mimetic Oligoacyllysine Surfaces.* Applied and Environmental Microbiology, 2010. **76**(10): p. 3301-3307.
87. Nakanishi, K., T. Sakiyama, and K. Imamura, *On the adsorption of proteins on solid surfaces, a common but very complicated phenomenon.* J Biosci Bioeng, 2001. **91**(3): p. 233-44.
88. Awsiuk, K., et al., *Protein adsorption and covalent bonding to silicon nitride surfaces modified with organo-silanes: comparison using AFM, angle-resolved XPS and multivariate ToF-SIMS analysis.* Colloids Surf B Biointerfaces, 2013. **110**: p. 217-24.
89. Vashist, S.K., et al., *Immobilization of Antibodies and Enzymes on 3-Aminopropyltriethoxysilane-Functionalized Bioanalytical Platforms for Biosensors and Diagnostics.* Chemical Reviews, 2014. **114**(21): p. 11083-11130.
90. Escorihuela, J., et al., *DNA microarrays on silicon surfaces through thiol-ene chemistry.* Chemical Communications, 2012. **48**(15): p. 2116-2118.
91. Trilling, A.K., J. Beekwilder, and H. Zuilhof, *Antibody orientation on biosensor surfaces: a minireview.* Analyst, 2013. **138**(6): p. 1619-27.
92. Wong, L.S., F. Khan, and J. Micklefield, *Selective covalent protein immobilization: strategies and applications.* Chem Rev, 2009. **109**(9): p. 4025-53.
93. Frasconi, M., F. Mazzei, and T. Ferri, *Protein immobilization at gold-thiol surfaces and potential for biosensing.* Anal Bioanal Chem, 2010. **398**(4): p. 1545-64.
94. Samanta, D. and A. Sarkar, *Immobilization of bio-macromolecules on self-assembled monolayers: methods and sensor applications.* Chemical Society Reviews, 2011. **40**(5): p. 2567-2592.

95. Castello, J.G., et al., *Real-time observation of antigen-antibody association using a low-cost biosensing system based on photonic bandgap structures.* Opt Lett, 2012. **37**(17): p. 3684-6.
96. Zinoviev, K.E., et al., *Integrated Bimodal Waveguide Interferometric Biosensor for Label-Free Analysis.* Journal of Lightwave Technology, 2011. **29**(13): p. 1926-1930.
97. Coelho, A., et al., *Spread of Escherichia coli O25b:H4-B2-ST131 producing CTX-M-15 and SHV-12 with high virulence gene content in Barcelona (Spain).* J Antimicrob Chemother, 2011. **66**(3): p. 517-26.
98. González-López, J.J., et al., *ESBL-Producing Salmonella enterica Serovar Typhi in Traveler Returning from Guatemala to Spain.* Emerging Infectious Diseases, 2014. **20**(11): p. 1918-1920.
99. Chen, X., et al., *Prevalence of qnr, aac(6')-Ib-cr, qepA, and oqxAB in Escherichia coli isolates from humans, animals, and the environment.* Antimicrob Agents Chemother, 2012. **56**(6): p. 3423-7.
100. Lavilla, S., et al., *Prevalence of qnr genes among extended-spectrum beta-lactamase-producing enterobacterial isolates in Barcelona, Spain.* J Antimicrob Chemother, 2008. **61**(2): p. 291-5.
101. González-Guerrero, A.B., et al., *A comparative study of in-flow and micro-patterning biofunctionalization protocols for nanophotonic silicon-based biosensors.* Journal of Colloid and Interface Science, 2013. **393**: p. 402-410.
102. Lee, S., et al., *Label-free optical biosensing using a horizontal air-slot SiNx microdisk resonator.* Optics Express, 2010. **18**(20): p. 20638-20644.
103. Ksendzov, A. and Y. Lin, *Integrated optics ring-resonator sensors for protein detection.* Optics Letters, 2005. **30**(24): p. 3344-3346.
104. Hunt, H.K., C. Soteropulos, and A.M. Armani, *Bioconjugation Strategies for Microtoroidal Optical Resonators.* Sensors, 2010. **10**(10): p. 9317-9336.
105. Turner, J.N., et al., *Cerebral Astrocyte Response to Micromachined Silicon Implants.* Experimental Neurology, 1999. **156**(1): p. 33-49.
106. Edell, D.J., et al., *Factors influencing the biocompatibility of insertable silicon microshafts in cerebral cortex.* IEEE Transactions on Biomedical Engineering, 1992. **39**(6): p. 635-643.

107. Schmidt, S., K. Horch, and R. Normann, *Biocompatibility of silicon-based electrode arrays implanted in feline cortical tissue.* Journal of Biomedical Materials Research, 1993. **27**(11): p. 1393-1399.
108. Hermanson, G.T., *Chapter 3 - The Reactions of Bioconjugation*, in *Bioconjugate Techniques (Third edition)*, G.T. Hermanson, Editor. 2013, Academic Press: Boston. p. 229-258.
109. Banuls, M.J., R. Puchades, and A. Maquieira, *Chemical surface modifications for the development of silicon-based label-free integrated optical (IO) biosensors: A review.* Analytica Chimica Acta, 2013. **777**: p. 1-16.
110. Gonzalez-Guerrero, A.B., et al., *A comparative study of in-flow and micro-patterning biofunctionalization protocols for nanophotonic silicon-based biosensors.* Journal of Colloid and Interface Science, 2013. **393**: p. 402-410.
111. Schneider, B.H., et al., *Highly sensitive optical chip immunoassays in human serum.* Biosensors and Bioelectronics, 2000. **15**(1–2): p. 13-22.
112. De Vos, K., et al., *SOI optical microring resonator with poly(ethylene glycol) polymer brush for label-free biosensor applications.* Biosensors and Bioelectronics, 2009. **24**(8): p. 2528-2533.
113. García-Rupérez, J., et al., *Label-free antibody detection using band edge fringes in SOI planar photonic crystal waveguides in the slow-light regime.* Optics Express, 2010. **18**(23): p. 24276-24286.
114. Escorihuela, J., et al., *Chemical silicon surface modification and bioreceptor attachment to develop competitive integrated photonic biosensors.* Anal Bioanal Chem, 2012. **404**(10): p. 2831-2840.
115. Sepúlveda, B., et al., *Optical biosensor microsystems based on the integration of highly sensitive Mach–Zehnder interferometer devices.* Journal of Optics A: Pure and Applied Optics, 2006. **8**(7): p. S561.
116. Gandhiraman, R.P., et al., *Deposition of chemically reactive and repellent sites on biosensor chips for reduced non-specific binding.* Colloids and Surfaces B: Biointerfaces, 2010. **79**(1): p. 270-275.
117. Dugas, V., A. Elaissari, and Y. Chevalier, *Surface Sensitization Techniques and Recognition Receptors Immobilization on Biosensors and Microarrays*, in *Recognition Receptors in Biosensors*, M. Zourob, Editor. 2010, Springer New York. p. 47-134.

118. Hartwell, L., et al., *Cancer biomarkers: a systems approach.* Nat Biotech, 2006. **24**(8): p. 905-908.
119. Popii, V. and G. Baumann, *Laboratory measurement of growth hormone.* Clin Chim Acta, 2004. **350**(1-2): p. 1-16.
120. Ionescu, M. and L.A. Frohman, *Pulsatile secretion of growth hormone (GH) persists during continuous stimulation by CJC-1295, a long-acting GH-releasing hormone analog.* J Clin Endocrinol Metab, 2006. **91**(12): p. 4792-7.
121. de Juan-Franco, E., et al., *Implementation of a SPR immunosensor for the simultaneous detection of the 22K and 20K hGH isoforms in human serum samples.* Talanta, 2013. **114**: p. 268-275.
122. Michel, R., et al., *Influence of PEG architecture on protein adsorption and conformation.* Langmuir, 2005. **21**(26): p. 12327-32.
123. Lebugle, A., M. Subirade, and J. Gueguen, *Structural characteristics of a globular protein investigated by X-ray photoelectron spectroscopy: comparison between a legumin film and a powdered legumin.* Biochim Biophys Acta, 1995. **1248**(2): p. 107-14.
124. Sharma, S., R.W. Johnson, and T.A. Desai, *XPS and AFM analysis of antifouling PEG interfaces for microfabricated silicon biosensors.* Biosens Bioelectron, 2004. **20**(2): p. 227-39.
125. Serro, A.P., et al., *Adsorption of albumin on prosthetic materials: implication for tribological behavior.* J Biomed Mater Res A, 2006. **78**(3): p. 581-9.
126. Vanea, E., et al., *Synthesis and characterisation of a new composite aluminosilicate bioceramic.* Journal of Non-Crystalline Solids, 2011. **357**(22–23): p. 3791-3796.
127. Chen, R., et al., *Antimicrobial peptide melimine coating for titanium and its in vivo antibacterial activity in rodent subcutaneous infection models.* Biomaterials, 2016. **85**: p. 142-51.
128. Kotiranta, A., K. Lounatmaa, and M. Haapasalo, *Epidemiology and pathogenesis of Bacillus cereus infections.* Microbes and Infection, 2000. **2**(2): p. 189-198.
129. Pirttijärvi, T.S.M., et al., *Evaluation of Methods for Recognising Strains of the Bacillus cereus Group with Food Poisoning Potential Among Industrial and Environmental Contaminants.* Systematic and Applied Microbiology, 1999. **22**(1): p. 133-144.

130. Slaten, D.D., R.I. Oropeza, and S.B. Werner, *An outbreak of Bacillus cereus food poisoning - Are caterers supervised sufficiently?* Public Health Reports, 1992. **107**(4): p. 477-480.
131. Kamat, A.S., D.P. Nerkar, and P.M. Nair, *BACILLUS CEREUS IN SOME INDIAN FOODS, INCIDENCE AND ANTIBIOTIC, HEAT AND RADIATION RESISTANCE.* Journal of Food Safety, 1989. **10**(1): p. 31-41.
132. Rusul, G. and N.H. Yaacob, *Prevalence of Bacillus cereus in selected foods and detection of enterotoxin using TECRA-VIA and BCET-RPLA.* International Journal of Food Microbiology, 1995. **25**(2): p. 131-139.
133. Dohmae, S., et al., *Bacillus cereus nosocomial infection from reused towels in Japan.* Journal of Hospital Infection, 2008. **69**(4): p. 361-367.
134. Bottone, E.J., *Bacillus cereus, a volatile human pathogen.* Clin Microbiol Rev, 2010. **23**(2): p. 382-98.
135. Avashia, S.B., et al., *Fatal pneumonia among metalworkers due to inhalation exposure to Bacillus cereus Containing Bacillus anthracis toxin genes.* Clin Infect Dis, 2007. **44**(3): p. 414-6.
136. Rishi, E., et al., *Acute postoperative Bacillus cereus endophthalmitis mimicking toxic anterior segment syndrome.* Ophthalmology, 2013. **120**(1): p. 181-185.
137. Gaur, A.H., et al., *Bacillus cereus Bacteremia and Meningitis in Immunocompromised Children.* Clinical Infectious Diseases, 2001. **32**(10): p. 1456-1462.
138. Hansford, J.R., et al., *Bacillus cereus bacteremia and multiple brain abscesses during acute lymphoblastic leukemia induction therapy.* J Pediatr Hematol Oncol, 2014. **36**(3): p. e197-201.
139. Meredith, F.T., et al., *Bacillus cereus necrotizing cellulitis mimicking clostridial myonecrosis: case report and review of the literature.* Scand J Infect Dis, 1997. **29**(5): p. 528-9.
140. Lee, Y.L., et al., *Fatal spontaneous bacterial peritonitis and necrotizing fasciitis with bacteraemia caused by Bacillus cereus in a patient with cirrhosis.* J Med Microbiol, 2010. **59**(Pt 2): p. 242-4.
141. Ikeda, M., et al., *Clinical characteristics and antimicrobial susceptibility of Bacillus cereus blood stream infections.* Annals of Clinical Microbiology and Antimicrobials, 2015. **14**: p. 43.

142. Chen, Y., et al., *Bio/chemical detection in liquid with self-sensing Pr-Oxi-Lever (piezo-resistive SiO2 cantilever) sensors.* Microelectronic Engineering, 2010. **87**(12): p. 2468-2474.
143. Lausch, K.R., et al., *Colonisation with multi-resistant Enterobacteriaceae in hospitalised Danish patients with a history of recent travel: a cross-sectional study.* Travel Med Infect Dis, 2013. **11**(5): p. 320-3.
144. Huber, F., H.P. Lang, and C. Gerber, *Biosensors: New leverage against superbugs.* Nat Nano, 2008. **3**(11): p. 645-646.
145. Cohen, M.L., *Changing patterns of infectious disease.* Nature, 2000. **406**(6797): p. 762-7.
146. Naaber, P., S. Kõljalg, and M. Maimets, *Antibiotic usage and resistance — trends in Estonian University Hospitals.* International Journal of Antimicrobial Agents. **16**(3): p. 309-315.
147. Freire-Moran, L., et al., *Critical shortage of new antibiotics in development against multidrug-resistant bacteria—Time to react is now.* Drug Resistance Updates, 2011. **14**(2): p. 118-124.
148. Hawkey, P.M. and A.M. Jones, *The changing epidemiology of resistance.* J Antimicrob Chemother, 2009. **64 Suppl 1**: p. i3-10.
149. Stefani, S., et al., *Meticillin-resistant Staphylococcus aureus (MRSA): global epidemiology and harmonisation of typing methods.* Int J Antimicrob Agents, 2012. **39**.
150. Lu, X., et al., *Detecting and tracking nosocomial methicillin-resistant Staphylococcus aureus using a microfluidic SERS biosensor.* Analytical chemistry, 2013. **85**(4): p. 2320-2327.
151. Harris, S.R., et al., *Evolution of MRSA during hospital transmission and intercontinental spread.* Science, 2010. **327**(5964): p. 469-74.
152. Kavanagh, K.T., L.E. Calderon, and D.M. Saman, *Viewpoint: a response to "Screening and isolation to control methicillin-resistant Staphylococcus aureus: sense, nonsense, and evidence".* Antimicrobial Resistance and Infection Control, 2015. **4**: p. 4.
153. Santiago, C., et al., *Inhibition of penicillin-binding protein 2a (PBP2a) in methicillin resistant Staphylococcus aureus (MRSA) by combination of ampicillin and a bioactive fraction from Duabanga grandiflora.* BMC Complement Altern Med, 2015. **15**: p. 178.

154. Lim, D. and N.C. Strynadka, *Structural basis for the beta lactam resistance of PBP2a from methicillin-resistant Staphylococcus aureus.* Nat Struct Biol, 2002. **9**(11): p. 870-6.
155. Ubukata, K., et al., *Expression and inducibility in Staphylococcus aureus of the mecA gene, which encodes a methicillin-resistant S. aureus-specific penicillin-binding protein.* Journal of Bacteriology, 1989. **171**(5): p. 2882-2885.
156. Hao, H., et al., *Key genetic elements and regulation systems in methicillin-resistant Staphylococcus aureus.* Future Microbiol, 2012. **7**(11): p. 1315-29.
157. Gopinath, S.C.B., et al., *Aptamer-based 'point-of-care testing'.* Biotechnology Advances, 2016. **34**(3): p. 198-208.
158. Rusconi, C.P., et al., *RNA aptamers as reversible antagonists of coagulation factor IXa.* Nature, 2002. **419**(6902): p. 90-94.
159. Conidi, A., V. van den Berghe, and D. Huylebroeck, *Aptamers and Their Potential to Selectively Target Aspects of EGF, Wnt/β-Catenin and TGFβ–Smad Family Signaling.* International Journal of Molecular Sciences, 2013. **14**(4): p. 6690.
160. Dia, M.L., et al., *Molecular detection of CTX-M-15-type β-lactamases in Escherichia coli strains from Senegal.* New Microbes and New Infections, 2016. **9**: p. 45-46.
161. Zanoli, L.M., R. D'Agata, and G. Spoto, *Functionalized gold nanoparticles for ultrasensitive DNA detection.* Analytical and Bioanalytical Chemistry, 2012. **402**(5): p. 1759-1771.
162. Shi, L., et al., *Reproducible and reliable microarray results through quality control: good laboratory proficiency and appropriate data analysis practices are essential.* Current Opinion in Biotechnology, 2008. **19**(1): p. 10-18.
163. Ermini, M.L., et al., *Direct detection of genomic DNA by surface plasmon resonance imaging: An optimized approach.* Biosensors and Bioelectronics, 2013. **40**(1): p. 193-199.
164. D'Agata, R., et al., *Ultrasensitive detection of non-amplified genomic DNA by nanoparticle-enhanced surface plasmon resonance imaging.* Biosensors and Bioelectronics, 2010. **25**(9): p. 2095-2100.
165. Mariani, S., et al., *A reusable optical biosensor for the ultrasensitive and selective detection of unamplified human genomic DNA with gold nanostars.* Biosensors and Bioelectronics, 2015. **74**: p. 981-988.

166. D'Agata, R., et al., *Direct Detection of Point Mutations in Nonamplified Human Genomic DNA.* Analytical Chemistry, 2011. **83**(22): p. 8711-8717.
167. Huertas, C.S., et al., *Quantitative evaluation of alternatively spliced mRNA isoforms by label-free real-time plasmonic sensing.* Biosensors and Bioelectronics, 2016. **78**: p. 118-125.
168. Gnanaprakasa, T.J., et al., *Tethered DNA scaffolds on optical sensor platforms for detection of hipO gene from Campylobacter jejuni.* Sensors and Actuators B: Chemical, 2011. **156**(1): p. 304-311.